REPORT DOCUMENTATION PAGE

AFRL-SR-AR-TR-05-

0457

1. REPORT DATE (DD-MM-YYYY)	2. REPORT TYPE	3. DATES COVERED (From - To)
30-09-2005	Final Technical Report	01/01/02 - 06/30/05

4. TITLE AND SUBTITLE
Impact of Structural Damping Nonlinearity in Transonic Limit Cycle Oscillations (LCO)

5a. CONTRACT NUMBER

5b. GRANT NUMBER
F49620-02-1-0066

5c. PROGRAM ELEMENT NUMBER

6. AUTHOR(S)
Danny D. Liu, Marc P. Mignolet

5d. PROJECT NUMBER

5e. TASK NUMBER

5f. WORK UNIT NUMBER

7. PERFORMING ORGANIZATION NAME(S) AND ADDRESS(ES)

Mechanical and Aerospace Engineering Department
Arizona State University
Tempe, AZ 85287-6106

ATTN: Capt. Clark Allred
Program Officer / NA

8. PERFORMING ORGANIZATION REPORT NUMBER
XAA 0122/TE

9. SPONSORING / MONITORING AGENCY NAME(S) AND ADDRESS(ES)
Air Force Office of Scientific Research / NA
875 North Randolph Street,
Suite 325, Room 3112,
Arlington, VA 22203-1768

10. SPONSOR/MONITOR'S ACRONYM(S)
AFOSR

11. SPONSOR/MONITOR'S REPORT NUMBER(S)

12. DISTRIBUTION / AVAILABILITY STATEMENT
APPROVED FOR PUBLIC RELEASE

13. SUPPLEMENTARY NOTES

14. ABSTRACT

The focus of this research has been on the assessment of the effects of internal friction on the response of aeroelastic systems exhibiting either explosive flutter or limit cycle oscillations to provide a confirmation of the potential of friction as a significant stabilizing factor in the limit cycle oscillations observed on several aircraft, e.g. F-16. The work performed in this regard can broadly be divided into three major efforts, two computational/theoretical and one experimental:

(1) the analysis of the effects of friction on a structural dynamic systems in which the effects of the aerodynamic forces have been modeled. The computational expediency of this simple model allowed to analyze and study a vast array of cases from which broad conclusions were derived the validity of which was later extended to the complex models of task (2).

(2) the analysis of the effects of friction on actual aeroelastic systems, i.e. airfoil and flat plate in a uniform flow, in which the aerodynamic forces are computed in time in parallel to the structural dynamic analysis in a tight coupling format.

(3) the experimental testing in the DLR- Göttingen (Germany) Transonic wind tunnel of a NLR7301 airfoil equipped with a friction device similar to the ones studied in tasks (1) and (2). This effort was followed by a data analysis that revealed mostly similarities, albeit a few differences, with the theoretical results of tasks (1) and (2) above.

15. SUBJECT TERMS
limit cycle oscillations, flutter, aeroelasticity, friction, nonlinear behavior

16. SECURITY CLASSIFICATION OF:			17. LIMITATION OF ABSTRACT	18. NUMBER OF PAGES	19a. NAME OF RESPONSIBLE PERSON
a. REPORT	b. ABSTRACT	c. THIS PAGE		198	Marc P. Mignolet
					19b. TELEPHONE NUMBER (include area code) (480) 965-1484

FINAL REPORT

EXECUTIVE SUMMARY

Focus of the Present Investigation

The focus of this research has been on the assessment of the effects of internal friction on the response of aeroelastic systems exhibiting either explosive flutter or limit cycle oscillations to provide a confirmation of the potential of friction as a significant stabilizing factor in the limit cycle oscillations observed on several aircraft, e.g. F-16. The work performed in this regard can broadly be divided into three major efforts, two computational/theoretical and one experimental:

(1) the analysis of the effects of friction on a structural dynamic systems in which the effects of the aerodynamic forces have been modeled. Specifically, a dashpot of negative constant was introduced to model the unstable linear aerodynamic effects, while an additional van der Pol restoring force was included to characterize possible stable nonlinear aerodynamic effects. Although approximate (because of the modeling of the aeroelastic forces), this system was shown to behave almost exactly as the aeroelastic systems of task (2). The computational expediency of this simple model allowed to analyze and study a vast array of cases from which broad conclusions were derived the validity of which was later extended to the complex models of task (2).

(2) the analysis of the effects of friction on actual aeroelastic systems, i.e. airfoil and flat plate in a uniform flow, in which the aerodynamic forces are computed in time in parallel to the structural dynamic analysis. A tight coupling between structural motions and flow field was achieved by proceeding iteratively at each time step until both sets of field equations (structural and aerodynamic) were satisfied.

(3) the experimental testing in the DLR- Göttingen (Germany) Transonic wind tunnel of a NLR7301 airfoil equipped with a friction device similar to the ones studied in tasks (1) and (2). This effort was followed by a data analysis that revealed mostly similarities, albeit a few differences, with the theoretical results of tasks (1) and (2) above.

The overall results of this study demonstrate that friction can indeed provide a stabilization of an impending flutter and can significantly decrease the amplitude of existing limit cycle oscillations of aeroelastic systems with an appropriate selection of the friction device parameters most notably natural frequency and coefficient of friction.

Participants and Publications

These efforts were carried out by the principal investigators, Prof. Danny D. Liu and Marc P. Mignolet from Arizona State University and the former graduate students Anthony M. Agelastos and Goang Gae Choi both of whom have successfully defended their M.S. thesis on this topic. The executive summary of results presented below highlights the findings discussed in details in their theses:

1. Agelastos, A.M., *Effects of Coulomb Friction on Flutter and Limit Cycle Oscillations According to a Structural Dynamic Model*, M.S., Arizona State University, May 2005.

2. Choi, G.G., *Effects of Coulomb Friction on Aeroelastic Systems*, M.S., Arizona State University, August 2005.

and which are included to this final report as Attachments. Several additional persons contributed very significantly to the experimental component of this project, most specifically Dr. Dallas Kingsbury from Arizona State University and the staff of the

DLR-Göttingen Institute for Aeroelasticity, in particular Dr. Guido Dietz and Dr. Günter Schewe.

In addition to the above theses, several conference papers have been published that describe the findings of this project:

1. Choi, G.G., Agelastos, A.M, Mignolet, M.P., and Liu, D.D., "On the Impact of Internal Friction on Flutter Onset and Limit Cycle Oscillations Amplitude," *International Forum on Aeroelasticity and Structural Dynamics 2005*, Munich, Germany, Jun. 28-Jul. 1, 2005. Paper IF-022.

2. Kingsbury, D.W., Agelastos, A.M., Dietz, G., Mignolet, M.P., Liu, D.D., and Schewe, G., "Limit Cycle Oscillations of Aeroelastic Systems with Internal Friction in the Transonic Domain - Experimental Results," *Proceedings of the 46th Structures, Structural Dynamics, and Materials Conference*, Austin, Texas, Apr. 18-21, 2005. AIAA Paper AIAA-2005-1914.

3. Choi, G.G., Agelastos, A.M., Mignolet, M.P., and Liu, D.D., "Effects of Internal Friction on the Dynamic Behavior of Aeroelastic Systems," *Proceedings of the 45th Structures, Structural Dynamics, and Materials Conference*, Palm Springs, California, Apr. 19-22, 2004. Paper AIAA-2004-1591.

4. Mignolet, M.P., Agelastos, A.M., and Liu, D.D., "Impact of Frictional Structural Nonlinearity in the Presence of Negative Aerodynamic Damping," *Proceedings of the 44th Structures, Structural Dynamics, and Materials Conference*, Norfolk, Virginia, Apr. 7-10, 2003. Paper AIAA-2003-1428.

Finally, the following three journal papers are in preparation:

1. Kingsbury, D.W., Agelastos, A.M., Dietz, G., Mignolet, M.P., Liu, D.D., and Schewe, G., "Measurements of Limit Cycle Oscillations of Aeroelastic Systems Induced by Internal Friction in the Transonic Domain - Experimental Results".

2. Agelastos, A.M., Choi, G.G., Mignolet, M.P., Liu, D.D., and Liao, Y., "Effects of Internal Friction on the Behavior of Aeroelastic Systems. Part I: Increased Stability and Limit Cycle Oscillations due to Friction only".

3. Choi, G.G., Agelastos, A.M., Mignolet, M.P., and Liu, D.D., "Effects of Internal Friction on the Behavior of Aeroelastic Systems. Part II: Reduction of Existing Limit Cycle Oscillations".

Summary of Findings

The findings of the three separate tasks (1)-(3) will be summarized in order. The structural dynamic model of task (1) was a two degree of freedom system in which the largest mass represented the wing while the smallest one would model the sliding component, e.g. a missile or store. The negative dashpot and the van der Pol force were assumed to act only on the largest mass (wing). Further, the sliding mass was assumed to be connected to the wing through a friction slider, a spring ($k_1 \geq 0$), and possibly a dashpot (positive viscous damping, $c_1 \geq 0$).

The system was analyzed first without a van der Pol term. Further, in the absence of elastic deformation during sliding, i.e., for $k_1 = 0$, it was shown that an exact procedure can be followed to transform the nonlinear equations of motion into a set of nonlinear algebraic equations and that a stabilization of the unstable aerodynamic forces was possible. The most negative damping that could be stabilized in this configuration was in fact shown to be $2r/\pi^2$ (for $r << 1$) where r denotes the ratio of the two masses

of the system. The system was found to exhibit periodic motions with possible stick phases. The introduction of a nonzero spring constant was shown to lead to an increased stabilization potential that is maximum in a "tuned damper" configuration, i.e. when the natural frequency of the primary component (the wing alone) closely matches the natural frequency of the secondary alone (sliding mass on spring k_1). In addition to this benefit, a broader set of motions was also observed. Besides periodic (referred to as single frequency here) solutions, multiple frequency motions were also found to exist, especially near the tuned damper configuration while the single frequency solutions were typically obtained near the stability border. Both continuous slip and stick slip multiple frequency motions were noted which were shown to be either aperiodic or chaotic. Further, the transition from single to multiple frequency was shown to be a Hopf bifurcation. It was finally observed that the maximum steady state response of the wing is typically minimum for the single frequency motions occurring just next to the bifurcation. A sharp increase in response level is obtained after bifurcation that results from the beating induced by the presence of multiple frequencies.

The inclusion of a van der Pol term did not significantly change the above findings with the noted exception that the system is always stable even in the absence of friction in which case it experiences a continuous slip single frequency motion. In fact, it was observed that the van der Pol term leads to a significant reduction of the large amplitude beating excursions obtained otherwise in connection with multiple frequency solutions and appears to postpone the Hopf bifurcation. In regards to stick slip vs. continuous slip, the decrease in response implied by the presence of the van der Pol term was found to increase the likelihood of stick slip motions which typically occur at lower

response levels than continuous slip solutions do. The effects of the coefficients of friction (the static and dynamic coefficients were assumed equal here) was studied next. It was first noted that the amplitude of continuous slip motions (single or multiple frequency) is linearly scaled by the coefficient of friction and this parameter plays no further role in these cases. When stick phases occur, a more complex dependency on the coefficient of friction is obtained. Next, it was found that 2 stable solutions can be obtained for low coefficients of friction. One such solution has a low amplitude and is dominated by friction effects alone with little influence of the van der Pol term. The reverse statement holds for the other solution, the amplitude is large with the stabilization dictated by the van der Pol force with little effect of friction. As the coefficient of friction increases, these two solutions become closer together and eventually merge. The amplitude of response then appears to increase monotonically with further increases of the coefficient of friction. The effects of a second, viscous damper in parallel to the friction element was finally considered. It was found that the two damping mechanisms do not necessarily reinforce each other and that the friction hinders the viscous dissipation when stick occurs. In fact, nonzero amplitude limit cycle oscillations were noted with friction in situations where the equilibrium (zero response) would in fact be stable without friction.

Two tightly coupled aeroelastic systems were considered in task (2):

(A) a flat-plate airfoil model supporting a torsional friction device composed of a disk flexibly connected to the plate by a torsional spring and squeezed between two rough surfaces, The behavior of this system is studied when placed in a uniform, inviscid and incompressible flow.

(B) a NACA0012 airfoil placed in a uniform inviscid and incompressible air flow and supporting either the same frictional device as the flat plate or a block sliding in a rough internal track.

The system A does not exhibit limit cycle oscillations in the absence of friction, it is either stable or displays an explosive flutter. The system B has been shown in some earlier studies to exhibit, in the absence of friction, aerodynamic-driven limit cycle oscillations near the flutter speed. The analysis of these two systems thus provide distinct perspectives on the role of friction, on systems exhibiting explosive flutter (system A) and those in which an aero-driven limit cycle oscillation occurs (system B).

The system A was analyzed first and a stability analysis of it was initially conducted with the disk in either continuous sticking or frictionless slipping modes to assess the expected stability domains. It was shown and justified that the system in slip mode exhibits instabilities at earlier flow velocities than its stuck counterpart. This property allows for the existence of both super- and subcritical limit cycle oscillations. While the subcritical limit cycles were observed to be unstable, a zone of stable supercritical limit cycle oscillations was found that extends about 3% past the flutter speed of the system without the friction device. This gain shows a good stabilization property since the moment of inertia of the selected friction device system is only 5% of the moment of inertia of the plate. The observed limit cycles exhibit either continuous slip or stick slip behaviors and are either single frequency (periodic) or multiple frequency (aperiodic or chaotic) with the latter ones appearing primarily at the highest flow speeds and for the highest frequencies of the torsional friction device. The above results were obtained by time marching the plate equations of motions with a rational

approximation of the Theodorsen function but a harmonic balance approach was also developed that led to very good approximations of the single frequency continuous slip limit cycle oscillations.

The system B was considered next with a friction component modeled by a block moving in an internal track. While limit cycle oscillations were observed, it was also shown that the block could become stuck at a position far from its original one and thus would create a change of inertia sufficiently large to stabilize the airfoil. This effect does not involve any dissipation due to friction and is thus not relevant to the present effort. Accordingly, this frictional model was not considered further and was replaced by its torsional counterpart (as in the flat plate analysis) which does not suffer from the same defect. The results of time marching computations demonstrate that friction can substantially decrease the level of the limit cycle oscillations, especially with a low coefficient of friction, but that increases in the response are also possible, depending on the selection of the natural frequency of the torsional friction device. As in the flat plate, continuous slip and stick slip solutions were observed most of which were single frequency (periodic).

The last task, i.e. (3), of this project focused on the design, fabrication, and testing of an actual friction device on an airfoil. The basic design of the system is a rotating disk connected to the airfoil by a torsional spring of natural frequency closely matching that of the airfoil to achieve the tuned damper arrangement discussed above. The spring was instrumented with strain gauges to measure the angle of torsion of the system. Finally, a complex system was designed to produce the required normal force to induce friction on the moving airfoil without transmitting any shear or moment. Preliminary shaker testing

in the ASU vibrations laboratory successfully validated the design: stuck, stick-slip, and continuous slip motions could be observed by varying the preload on the disk. Full blown testing in the DNW-TWG transonic wind tunnel at DLR led to the observation of the first recorded limit cycle oscillations with friction effects and relative motions of the disk and airfoil. Only single frequency motions were observed but both continuous slip and stick slip behaviors were found. The measurements demonstrate a slight effect of friction and the subcritical nature of the limit cycle oscillations. This behavior was explained by analyzing the natural frequencies of the stuck and slipping configurations as in task (2). Several findings are however still unexplained, e.g. the asymmetry of the sticking phase, the continuous slip to stick slip transition associated with an increase in response, and the near Mach independent amplitude of torsional response.

The overall results of this study demonstrate that friction can indeed provide a stabilization of an impending flutter and can significantly decrease the amplitude of existing limit cycle oscillations of aeroelastic systems with an appropriate selection of the friction device parameters most notably natural frequency and coefficient of friction.

REPORT DOCUMENTATION PAGE

Form Approved
OMB No. 0704-0188

1. REPORT DATE *(DD-MM-YYYY)*	2. REPORT TYPE	3. DATES COVERED *(From - To)*
30-09-2005	Final Technical Report	01/01/02 - 06/30/05

4. TITLE AND SUBTITLE
Impact of Structural Damping Nonlinearity in Transonic Limit Cycle Oscillations (LCO)

5a. CONTRACT NUMBER

5b. GRANT NUMBER
F49620-02-1-0066

5c. PROGRAM ELEMENT NUMBER

6. AUTHOR(S)
Danny D. Liu, Marc P. Mignolet

5d. PROJECT NUMBER

5e. TASK NUMBER

5f. WORK UNIT NUMBER

7. PERFORMING ORGANIZATION NAME(S) AND ADDRESS(ES)

Mechanical and Aerospace Engineering Department
Arizona State University
Tempe, AZ 85287-6106

ATTN: Capt. Clark Allred
Program Officer / NA

8. PERFORMING ORGANIZATION REPORT NUMBER
XAA 0122/TE

9. SPONSORING / MONITORING AGENCY NAME(S) AND ADDRESS(ES)
Air Force Office of Scientific Research / NA
875 North Randolph Street,
Suite 325, Room 3112,
Arlington, VA 22203-1768

10. SPONSOR/MONITOR'S ACRONYM(S)
AFOSR

11. SPONSOR/MONITOR'S REPORT NUMBER(S)

12. DISTRIBUTION / AVAILABILITY STATEMENT
APPROVED FOR PUBLIC RELEASE

13. SUPPLEMENTARY NOTES

14. ABSTRACT

The focus of this research has been on the assessment of the effects of internal friction on the response of aeroelastic systems exhibiting either explosive flutter or limit cycle oscillations to provide a confirmation of the potential of friction as a significant stabilizing factor in the limit cycle oscillations observed on several aircraft, e.g. F-16. The work performed in this regard can broadly be divided into three major efforts, two computational/theoretical and one experimental:

(1) the analysis of the effects of friction on a structural dynamic systems in which the effects of the aerodynamic forces have been modeled. The computational expediency of this simple model allowed to analyze and study a vast array of cases from which broad conclusions were derived the validity of which was later extended to the complex models of task (2).

(2) the analysis of the effects of friction on actual aeroelastic systems, i.e. airfoil and flat plate in a uniform flow, in which the aerodynamic forces are computed in time in parallel to the structural dynamic analysis in a tight coupling format.

(3) the experimental testing in the DLR- Göttingen (Germany) Transonic wind tunnel of a NLR7301 airfoil equipped with a friction device similar to the ones studied in tasks (1) and (2). This effort was followed by a data analysis that revealed mostly similarities, albeit a few differences, with the theoretical results of tasks (1) and (2) above.

15. SUBJECT TERMS
limit cycle oscillations, flutter, aeroelasticity, friction, nonlinear behavior

16. SECURITY CLASSIFICATION OF:			17. LIMITATION OF ABSTRACT	18. NUMBER OF PAGES	19a. NAME OF RESPONSIBLE PERSON
a. REPORT	b. ABSTRACT	c. THIS PAGE		198	Marc P. Mignolet
					19b. TELEPHONE NUMBER *(include area code)* (480) 965-1484

ATTACHMENT A:

THESIS OF ANTHONY M. AGELASTOS

EFFECTS OF COULOMB FRICTION ON FLUTTER AND LIMIT CYCLE OSCILLATIONS ACCORDING TO A STRUCTURAL DYNAMIC MODEL

by

Anthony Michael Agelastos

A Thesis Presented in Partial Fulfillment
of the Requirements for the Degree
Master of Science

ARIZONA STATE UNIVERSITY

May 2005

EFFECTS OF COULOMB FRICTION ON FLUTTER AND LIMIT CYCLE OSCILLATIONS ACCORDING TO A STRUCTURAL DYNAMIC MODEL

by

Anthony Michael Agelastos

has been approved

January 2005

APPROVED:

_____, Chair

_____

_____

Supervisory Committee

ACCEPTED:

_____

Department Chair

_____

Dean, Division of Graduate Studies

ABSTRACT

The appearance of limit cycle oscillations in aeroelastic systems has usually been associated with nonlinearity in the aerodynamics and/or in the structural restoring forces. It has however been recently suggested that nonlinearity in the damping mechanism, more notably friction between a small moving part (or many such parts) and the wing, may indeed be a source of post-flutter limit cycle oscillations. The present work provides a first validation of this expectation.

In the first part of this thesis, a two-degree-of-freedom structural dynamic model is considered in which the biggest mass, representing the wing, and the smaller one, modeling the sliding component, are connected by at least a friction element. The unstable aerodynamic effects are approximated by a dashpot of negative value acting on the wing alone. The response of this system is analyzed in a variety of situations, i.e. with an additional spring between masses, an additional positive damper between them, and/or with a van der Pol restoring force acting on the wing and modeling stabilizing nonlinear aerodynamic effects. It is indeed found that the friction can stabilize an otherwise unstable aeroelastic system, especially when the natural frequency of the wing and sliding masses considered alone are close together. Periodic, aperiodic, and chaotic motions of the wing are observed and discussed. The presence of continuous slip, stick-slip, and stuck motions is also demonstrated and analyzed. Finally, predictions from the harmonic balance method are shown to match well the amplitude of continuous slip, periodic motions.

This theoretical work was complemented by a series of tests conducted in the transonic wind tunnel of the Deutsches Zentrum für Luft und Raumfahrt (DLR) in

Göttingen, Germany. The design of the friction test article, its preliminary validation in the ASU vibrations laboratory, and the final wind tunnel testing are presented and discussed. The wind tunnel results demonstrated a slight stabilization effect of friction.

This thesis is dedicated to my loving wife, Michelle Ursula Marina Jaramillo-Agelastos, without whom none of this would have been possible.

ACKNOWLEDGEMENTS

I would like to begin this page by acknowledging the tremendous gift of knowledge and guidance from the Chair, Dr. Marc P. Mignolet. His patience and ability have both helped and positively molded me like no other mentor ever has, not only from the four classes and five years of research with him, but also from getting to know him. Thank you.

Committee-member Dr. Danny D. Liu has taught me everything I know about aerodynamics and aerodynamic-related subjects, and has given me an invaluable insight into the field of which I now join; he has always answered my questions and offered to help more than necessary. Thank you.

Committee-member Dr. Dallas W. Kingsbury, who has been an invaluable help with the experimental side of this endeavor, always managed to get the group through whatever experimental tragedy awaited us with patience, poise, and talent. Thank you.

Dr. Guido Dietz, who was willing to spend much of his own time assisting this project, has not only helped it succeed, but was the final piece in the puzzle allowing me to partake in the wind tunnel testing. Thank you.

Dr. Bruce Steele has always been an irreplaceable member of the team, and has made a tremendous impact in not only the vibration lab experiments, but the preparation for Germany as well. Thank you.

TABLE OF CONTENTS

LIST OF FIGURES

Figure Page

CHAPTER 1

INTRODUCTION

Several modern aircraft, most notably some fighters with external stores, have been found to exhibit Limit Cycle Oscillations (LCO), i.e. self-sustained vibrations. Clearly, these vibrations are undesirable from all perspectives: they affect the comfort of the pilot and/or passengers, they may negatively impact the accuracy in shooting, and generally produce fatigue in the aircraft structure. Accordingly, a series of investigations have focused on explaining the occurrence of these limit cycle oscillations in aircraft and it is generally recognized that these vibrations occur in the neighborhood of flutter. They further have been classified into supercritical (or hard) and subcritical (or soft) limit cycles oscillations with the critical point being flutter. Supercritical LCO's thus appear at flow/flight speeds larger than the flutter speed while their subcritical counterparts occur below flutter speed. Both supercritical and subcritical LCO's are the manifestation of a nonlinear aeroelastic system, as a linear damped aero-structure model can only exhibit a decay toward rest or an explosive, divergent behavior. Thus, paramount to LCO discussions is the origin, aerodynamic and/or structural, and nature of the nonlinearity present.

Nonlinear aerodynamic effects have often been invoked, e.g. the transonic shock separation mechanism[1,2] in the context of the F-16, but structural nonlinearities have also been discussed. Most often considered have been the large deformation stiffening (as in panel flutter[3]), and freeplay[4,5]. The work by Chen et al.[6] and Mignolet et al.[7] suggested however that a different mechanism, specifically friction, could qualitatively explain many of the LCO findings associated with the F-16. Interestingly, such an explanation is

also supported by studies performed on turbomachine blades[8,9] that demonstrated that friction can, in certain conditions, stabilize flutter and lead to supercritical LCO. A recent investigation has also shown the value of friction to damp out the effects of gust[10].

In this light, the focus of the present investigation and of a related one[11] is to conduct an in-depth study of the effects of friction on a class of aeroelastic systems exhibiting either explosive flutter or limit cycle oscillations. A distinguishing feature of the wing/wing-store system considered here is that the friction mechanism must be internal to the system, i.e. no rubbing takes place between components separately supported (e.g. between two blades of a rotor) but rather the components in relative slip must be mounted on the wing (or be the wing itself). In keeping with the phenomenological aspect of the present investigation, the analysis was conducted under the following structural simplifications.

(i) The friction effects will be assumed to originate from a single, rigid component moving relatively with respect to the wing and to be characterized by a preload N and coefficients of friction μ_S and μ_D.

(ii) The changes of external structural geometry that occur due to the relative sliding will be neglected. This assumption appears justified as all aircraft components are subjected to a large preload so that a large amount of energy can be dissipated with only small relative motions at the joints. Accordingly, there will be no direct effect of the moving component on the aerodynamics.

Combining the above two assumptions led to the introduction[11] of an airfoil model with internal friction, more specifically with a block sliding in a rough track, see

Fig. 1.1. While the behavior of this system was shown to exhibit several of the characteristics expected from friction, it was also found to be very sensitive to the change of inertia that occurs as the block is moving along the track. In fact, it was noted that a static displacement of the block in the track provided a significant stabilization property which rendered extremely difficult the assessment of the effects of friction. This situation was then remedied[12] by assuming that the rigid component of Fig. 1.1 is a disk that spins around its center of mass inside the airfoil, see Fig. 1.2. Note that this new model does satisfy, as well as its counterpart from Fig. 1.1, the simplifications (i) and (ii) above.

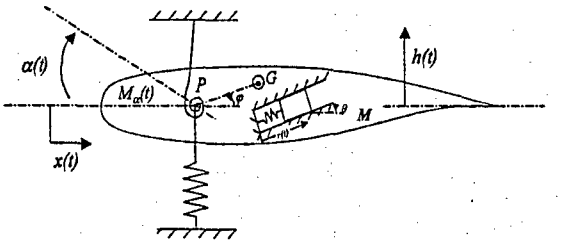

Fig. 1.1 Aeroelastic system with sliding block.

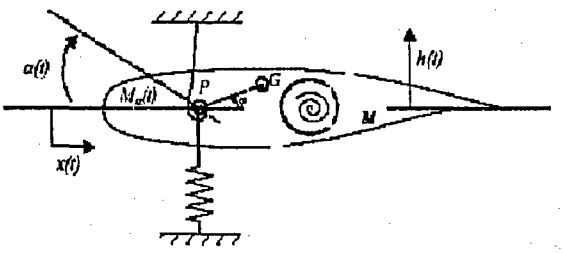

Fig. 1.2 Aeroelastic system with rotating disk.

In this overall context, the specific objectives of the present effort are twofold. First, a thorough analysis will be conducted on a purely structural dynamic model

representative of the aeroelastic systems of Fig. 1.2 to assess the potential of friction to stabilize an explosive flutter and reduce the amplitude of existing limit cycle oscillations. This study will also concentrate on the properties of the response of the system and on the influence of many of the parameters involved. The second objective is the design, fabrication, and testing of a friction device similar to the torsional spring and disk of Fig. 1.2. The preliminary testing of the device was successfully accomplished in shaker tests in the ASU Vibrations Laboratory. Then, its final testing took place in the DLR transonic wind tunnel mounted on a NLR 7301 airfoil undergoing limit cycle oscillations around Mach number 0.6.

CHAPTER 2

TWO-DEGREE-OF-FREEDOM DYNAMIC MODEL

The focus of this part of the investigation is on gaining a basic physical understanding of the effects of friction on the stability/response of aeroelastic systems. Given that very little is known about this topic and that friction inevitably brings out complex nonlinear characteristics, it was decided here to select the simplest dynamical model that would exhibit the features of the problem. Friction in aircraft must take place between two components of the aircraft, as opposed to, for example, the wing and the ground. A two-degree-of-freedom thus seemed the lowest order system to be considered. The components of a wing are well fastened together and thus one expects that a relative motion can only be of a small component. Thus, the "sliding" mass (M_2 below) must have a mass much less than the wing mass (M_1). It remains to discuss the "aeroelastic" modeling. In keeping with the novelty of the topic, it was decided to construct a mathematically simple aerodynamic model that would exhibit the noted explosive flutter and limit cycle oscillation behavior. These possible behaviors are included in the model through a dashpot of negative value in parallel with a van der Pol restoring force. The negative dashpot allows unstable motions to grow, as in a explosive flutter case, but the van der Pol force, if present, reinstates stability at sufficiently high levels of response. Finally, deformations of the components were allowed by the inclusion of springs. The general model to be considered here is thus represented in Fig. 2.1.

In a series of papers, Tondl[13-15] investigated a more complex version of Fig. 2.1 in which a structural damper also exists between the two masses. His approach, based on

harmonic balance (see section 2.4), presented only limited information and was restricted by the necessary assumptions of periodic and continuous slip motions. Unfortunately, as will be found in the ensuing sections, these assumptions are applicable only in an extremely limited set of cases so that the results of References 11-13 neither carry the generality nor the accuracy required here.

It should finally be noted that the structural components of the models of Figs 1.2 and 2.1 (i.e. without aerodynamics and without the dashpot c and van der Pol term δ) are in fact very much alike, they are identical if the plunging motion (vertical displacement) of the airfoil is neglected. In this case, the displacements x_1 and x_2 denote the pitching and disk angles, the masses M_1 and M_2 are in fact the corresponding inertias, and k_1 is the torsional spring stiffness.

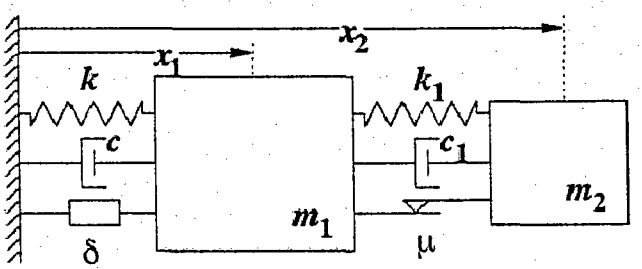

Fig. 2.1 2DOF system with full coupling

2.1 Computational Details

The system in Fig. 2.1 would be considered a linear system if it did not contain the Coulomb friction element. Friction adds significant complexity to the simulation of the system in that it can completely or partially inhibit the relative motion of the two masses and that it switches direction abruptly as the relative velocity changes sign. In

fact, during unidirectional (no velocity reversal) slip phases as well as stick phases, the equation of motion of the system are linear, so that the nonlinearity is wholly concentrated at the transitions. These observations emphasize the need to accurately capture the transition of states (stick-slip, slip-stick, slip-slip). To this end, the time step was reduced in the neighborhood of these transitions by a factor as large as 128 through successive halving. Further, the equations of motion were integrated numerically using the IMSL routine DIVPRK (Runge-Kutta of orders 4-5) with a low tolerance of 10^{-8} (both relative and absolute errors) and a time step typically smaller or equal to 0.01 s while the fundamental linear frequency is close to 1 radian per second.

2.2 Assessment of Friction on an Aeroelastic System Exhibiting Explosive Flutter

The analysis of the 2-degree-of-freedom system was conducted in two separate steps. It was first analyzed under the assumption $\delta = 0$ which implies that no nonlinear stabilizing aerodynamic effect exists. Accordingly, the linear system (without friction) exhibits only an unstable behavior typical of explosive flutter. The considerations of stabilizing nonlinear aerodynamics, i.e. $\delta \neq 0$, will be conducted in Section 2.3. Two separate cases were further considered with $\delta = 0$, i.e. k_1=0 or $k_1 \neq 0$. Under the first condition, the 2-degree-of-freedom system obtained in slip phases is classically damped (at the contrary of the situation $k_1 \neq 0$) and an exact formulation (EF) of the response can be derived without too much difficulty. This approach, as well as a direct numerical simulation, (NS), of the equations of motion were thus performed for k_1=0. In the second

step, nonzero values of k_1 were considered but only the numerical simulation was carried out.

2.2.1 *Primary-Secondary Coupling Through the Friction Element Only*

The system under consideration in this section is the 2-degree-of-freedom (2DOF) system shown in Fig. 2.2.

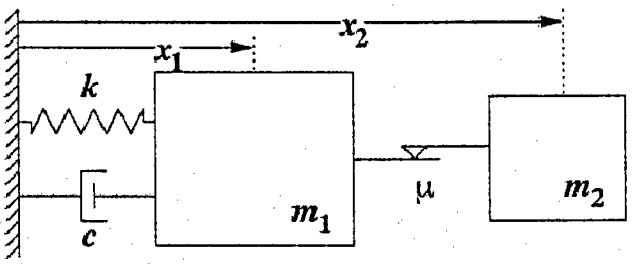

Fig. 2.2 2DOF system with friction coupling.

2.2.1.1 Exact Formulation

Following Den Hartog[16] (see also Pesheck and Pierre[17]), a periodic solution of the equations of motion can be obtained by marching the solution from unknown initial conditions at $t = 0$ to an unknown time T at which periodicity conditions are enforced. Such an approach can be used for continuous slip behavior as well as solutions with stick-slip but the number of stick-slip phases must be chosen a priori. This process transforms the solution of the nonlinear differential equations into the solution of a set of nonlinear algebraic equations for the unknown initial conditions, period (or half period T), and stuck times t_i if applicable. This process is exemplified below on the system of Fig. 2.2.

Since the equations of motion of the system of Fig. 2.2 are time invariant, the time $t = 0$ can be arbitrarily selected. Then, assume for convenience that this time corresponds to a stick-slip or slip-slip transition. Thus, the initial conditions were selected as

$$\dot{x}_1(0) = \dot{x}_2(0) = v_0;\ x_1(0) = x_{10} \text{ and } x_2(0) = x_{20}. \tag{2-1}$$

During the ensuing slip phase, it is assumed that $\dot{x}_1 > \dot{x}_2$ so that the response is described by the equations of motion

$$M_1\ddot{x}_1 + c\dot{x}_1 + kx_1 = F_{31} \text{ and } M_2\ddot{x}_2 = -F_{31} \tag{2-2}$$

where

$$F_{31} = \mu_D N \operatorname{sgn}(\dot{x}_2 - \dot{x}_1) \tag{2-3}$$

The response of the two blocks can thus be expressed as

$$x_1(t) = e^{-\zeta_2'\omega_2' t}\left[A_2 \cos\omega_{d2}' t + B_2 \sin\omega_{d2}' t\right] - \frac{\mu_D N}{k} \tag{2-4}$$

and

$$x_2(t) = \frac{\mu_D N}{2M_2} t^2 + v_0 t + x_{20} \tag{2-5}$$

where

$$\omega_2' = \sqrt{\frac{k}{M_1}};\ \zeta_2' = \frac{c/M_1}{2\omega_2'};\ \omega_{d2}' = \omega_2'\sqrt{1-\zeta_2'^2} \tag{2-6}$$

$$A_2 = x_{10} + \frac{\mu_D N}{k};\ B_2 = \frac{v_0 + \zeta_2'\omega_2' A_2}{\omega_{d2}'}. \tag{2-7}$$

If a continuous slip solution takes place, the unknown initial conditions in Eq. (2-1) and the half-cycle time T will be evaluated from the periodicity conditions

$$x_1(T) = -x_1(0) = -x_{10};\ \dot{x}_1(T) = -\dot{x}_1(0) = -v_0;\ \dot{x}_2(T) = -\dot{x}_2(0) = -v_0. \tag{2-8}$$

Enforcing these constraints leads to a nonlinear equation for the half-cycle time T and ensuing linear equations for the unknown initial conditions. Specifically, imposing the periodicity condition at T for $\dot{x}_2$ yields

$$\frac{\mu_D N}{M_2} T = -2v_0 . \tag{2-9}$$

The periodicity conditions for $\dot{x}_1$ and x_1, respectively, yield

$$A_2\left[\frac{\omega_2'^2}{\omega_{d2}'}\sin\omega_{d2}'T\right] = v_0\left[e^{\zeta_2'\omega_2'T} + \cos\omega_{d2}'T - \frac{\zeta_2'\omega_2'}{\omega_{d2}'}\sin\omega_{d2}'T\right] \tag{2-10}$$

and

$$A_2\left[e^{-\zeta_2'\omega_2'T}\left(\cos\omega_{d2}'T + \frac{\zeta_2'\omega_2'}{\omega_{d2}'}\sin\omega_{d2}'T\right)+1\right] + \frac{v_0}{\omega_{d2}'}e^{-\zeta_2'\omega_2'T}\sin\omega_{d2}'T = -\frac{2\mu_D N}{k}. \tag{2-11}$$

Combining Eq. 2-9-2-11 then results in the single nonlinear algebraic equation for the half-period T

$$2r\sin\omega_{d2}'T + \omega_{d2}'T\left[\cos\omega_{d2}'T + \cosh\zeta_2'\omega_2'T\right] = 0 . \tag{2-12}$$

A stick-slip solution was also obtained. The transition from slip to stick was assumed to take place at time $t = t_0$ such that the relative velocity of the two blocks vanishes, i.e.

$$\dot{x}_1(t_0) - \dot{x}_2(t_0) = 0 \tag{2-13}$$

or

$$e^{-\zeta_2'\omega_2't_0}\left[v_0\cos\omega_{d2}'t_0 - \left(\zeta_2'\omega_2'B_2 + A_2\omega_{d2}'\right)\sin\omega_{d2}'t_0\right] = \frac{\mu_D N}{M_2}t_0 + v_0 . \tag{2-14}$$

After the transition, the slider sticks and the system is governed by the equations of motion

$$(M_1 + M_2)\ddot{x}_1 + c\dot{x}_1 + kx_1 = 0 \text{ and } \dot{x}_1 = \dot{x}_2 \tag{2-15}$$

The corresponding response can thus be expressed as

$$x_1(t) = e^{-\zeta_1'\omega_1' t}\left[A_1 \cos\omega_{d1}' t + B_1 \sin\omega_{d1}' t\right] \tag{2-16}$$

where

$$\omega_1' = \sqrt{\frac{k}{M_1 + M_2}}$$

$$\zeta_1' = \frac{c/(M_1 + M_2)}{2\omega_1'};\ \omega_{d1}' = \omega_1'\sqrt{1-\zeta_1'^2};$$

$$A_1 = x_1(t_0) \text{ and } B_1 = \frac{\dot{x}_1(t_0) + \zeta_1'\omega_1' x_1(t_0)}{\omega_{d1}'}. \tag{2-17}$$

2.2.1.2 Numerical Results

A parametric study of the 2-degree-of-freedom system with $k_1 = 0$ has revealed that the internal friction mechanism stabilizes the unstable aerodynamics and leads to LCO for a broad range of negative damping ratios (see Fig. 2.3). Further, the response of the system was found to exhibit many of the features already observed in connection with the 1.5 degree-of-freedom system[6,7,17], e.g. at most one stable solution was observed in all cases considered, an upper-lower branch structure exists in the plot of amplitude versus damping, Fig. 2.4 (the lower branch is stable and denoted by S while the upper branch is unstable and denoted by U), and the solutions were both periodic and symmetric. However, at the contrary of that simpler system, the two-degree-of-freedom model with $k_1 = 0$ displays two types of LCO solutions: continuous slip (CS) and stick-slip (SS, a single stick phase per half-cycle).

While the unstable solutions were all characterized by a continuous slip behavior, the stable motions were primarily corresponding to a stick-slip behavior although a small zone of stable continuous slip responses were observed near the largest stabilizable damping ratio. The results obtained with the exact formulation matched very closely their numerical simulation counterparts even in a stick-slip motion[18].

The results shown in Fig. 2.3 and 2.4 were obtained for a typical friction setup ($\mu_S=\mu_D=0.25$, $N=1$, $k=1$) but for a rather large mass ratio, i.e. M_1=1, M_2=0.25. While the phenomenological features described above were found to also hold at much lower values of the secondary/sliding mass M_2, it was found that the largest stabilizable damping ratio is approximately proportional to the mass ratio, $r=M_2/M_1$. A relationship between the damping and mass ratios is now desired to fully understand Fig. 2.4. To this end, the condition of Eq. (2-12) was reconsidered and it was argued that the largest damping ratio is such that (see also Fig. 2.4)

$$\frac{\mathrm{d}T}{\mathrm{d}\zeta_2'}=\infty \text{ or } \frac{\mathrm{d}\zeta_2'}{\mathrm{d}T}=0. \tag{2-18}$$

Then, differentiating Eq. (2-12) with respect to T and using Eq. (2.18) leads to

$$\begin{aligned} 2r\cos\omega_{d2}'T+\cos\omega_{d2}'T+\cosh\left(\zeta_2'\omega_2'T\right) \\ +\omega_{d2}'T\left[-\sin\omega_{d2}'T+\zeta_2'\sinh\left(\zeta_2'\omega_{d2}'T\right)\right]=0. \end{aligned} \tag{2-19}$$

Equations (2-12) and (2-19) can be simplified as

$$2r\sin u+u\left[\cos u+\cosh\mu u\right]=0 \tag{2-20}$$

$$2r\cos u+\cos u+\cosh\eta u-u\sin u+\eta u\sinh\eta u=0 \tag{2-21}$$

where

$$u = \omega'_{d2} T \,,\ \zeta'_2 \omega'_2 T = \frac{\zeta'_2}{\sqrt{1-\zeta'^2_2}} u = \eta u \,. \tag{2-22}$$

It is then desired to solve Eq. (2-20) and (2-21) for the damping ratio and half-period, i.e. for u and η given r small. When the mass ratio goes to zero, it is expected that the maximum stabilizable damping is zero and thus that there exists a solution of Eq. (2-20) and (2-21) with $r = \eta = 0$. It is indeed the case and requires that $u = \pi$. For small but nonzero mass ratios, a perturbation analysis will be carried out with

$$u = \pi + \alpha \,. \tag{2-23}$$

In fact, it is found that

$$-2r\alpha + \frac{\pi}{2}\left(\alpha^2 + \eta^2 \pi^2\right) = 0 \,, \tag{2-24}$$

$$\alpha = \frac{2r}{\pi} \,. \tag{2-25}$$

In terms of the half-period and damping ratio, these results imply

$$T = \pi + \frac{2r}{\pi} \tag{2-26}$$

and

$$\left(\zeta'_2\right)_{\max} = \left(\frac{-c}{2\sqrt{kM_1}}\right)_{\max} \approx \frac{2r}{\pi^2} \ \text{ for } r \ll 1 \,. \tag{2-27}$$

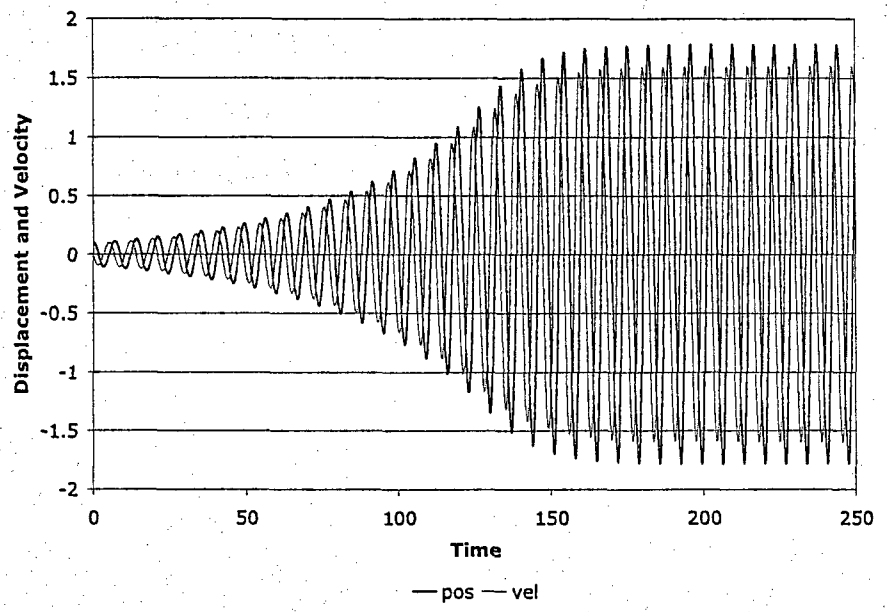

a) Time histories

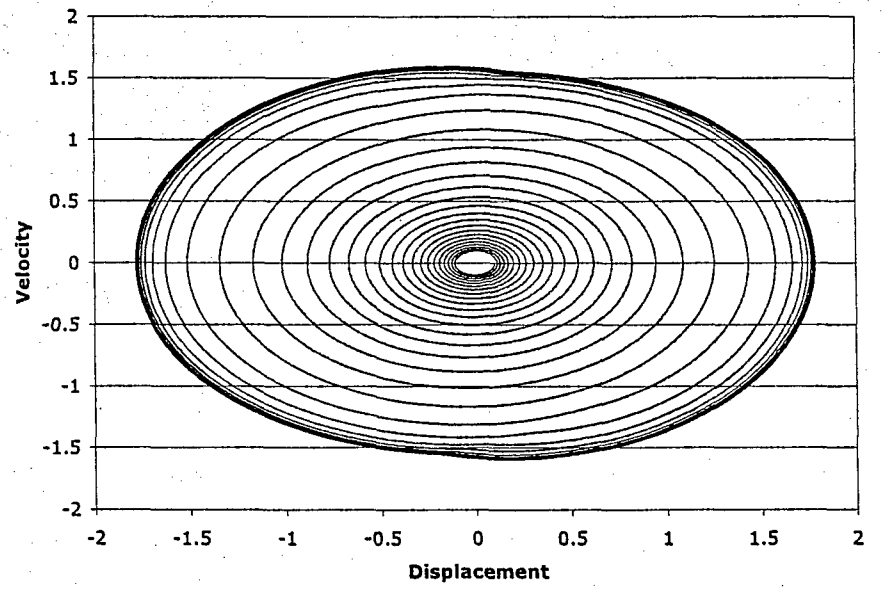

b) Phase plane plot

Fig. 2.3 Typical response of mass M_1 for $k_1 = 0$.

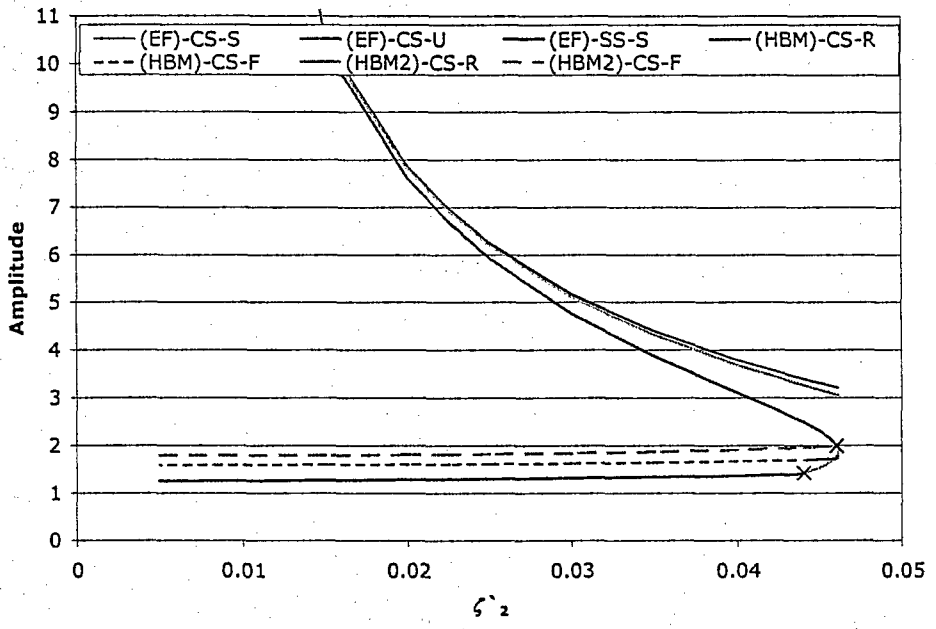

a) Amplitude vs. damping

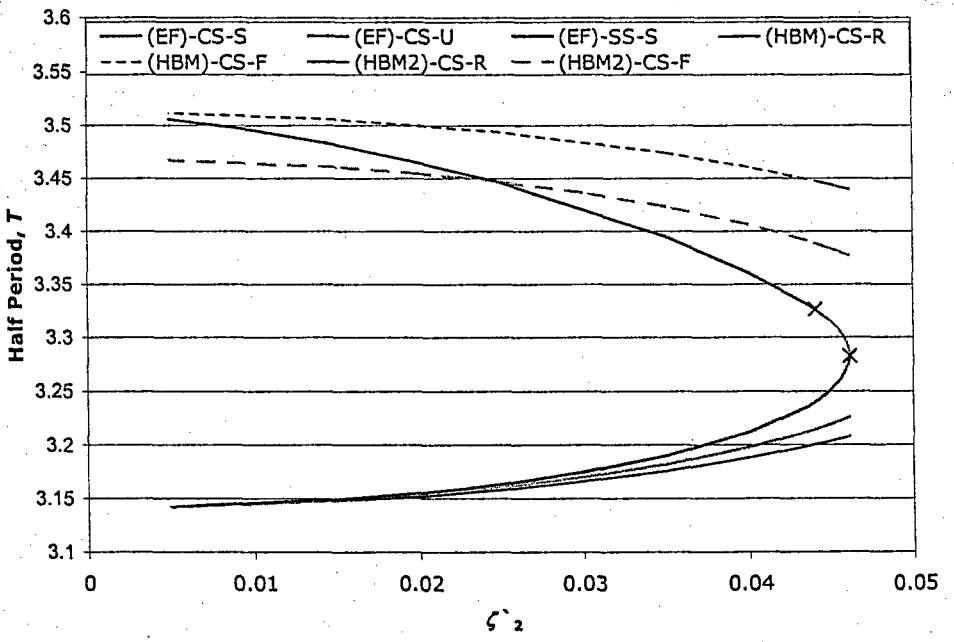

b) Half period vs. damping

Fig. 2.4 Amplitude of LCO and half-period of response vs. magnitude of negative aerodynamic damping for different solutions, $k_1 = 0$.

According to this relation, a 2% damping ratio stabilization would require a mass ratio r of at least 0.1, a larger value than would be expected to be typical of the F-16. A larger stabilization capacity of the two mass system of Fig. 2.2, and thus potentially a lower mass ratio, would require an increased relative response of the two masses. Such an increase can be achieved by increasing the transfer of energy between the two masses. In view of the primary-secondary nature of the system, it is expected that the difference in the natural frequencies of the primary ($\omega_1 = \sqrt{k/M_1}$) and the secondary (ω_2=0 for the system with k_1=0) will be the dominant parameter controlling the energy transfer. Further, a maximum transmission could be conjectured to occur when $\omega_1 \approx \omega_2$.

2.2.2. Primary-Secondary Coupling Through the Friction Element and a Spring

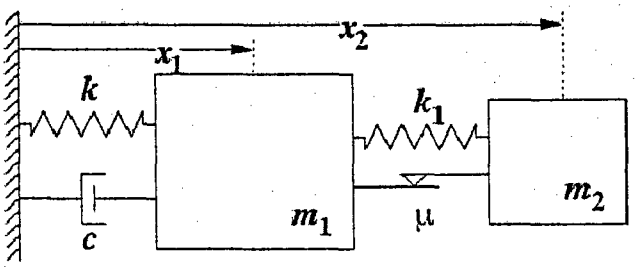

Fig. 2.5 2-degree-of-freedom system with friction and stiffness coupling.

In this section, the stiffness k_1 was varied from zero and the system response was obtained by numerical integration. A series of values of the stiffness k_1 and of the damping coefficient c were considered with the mass ratio $r = 0.05$ and the single set of initial conditions $X_1(0) = X_2(0) = 0.1$ and $\dot{X}_1(0) = \dot{X}_2(0) = 0$.

The wealth of results obtained (see Fig. 2.6) has shown, first and foremost, that the above conjectures were perfectly valid. Indeed, each of the dots on Fig. 2.6(a) indicates a stable solution and thus:

1) an increased stabilization capability is possible by varying the natural frequency of the sliding mass alone, and
2) the maximum stabilization possible appears to take place when $\omega_1=\omega_2$, or equivalently $k_1=r=0.05$ here since k is set to unity.

In analyzing these results, it could be argued that the increase in stabilization could simply be a result of an increase in stiffness and a corresponding reduction of the (negative) damping ratios of the system since it is the dashpot value c which is fixed. These comments suggest that a more definite proof of the increased stabilization would require the analysis of the most negative damping ratio for each of the stable systems of Fig. 2.6(a). This effort yielded Fig. 2.6(b), which also displays the trends stated above, thereby demonstrating their validity. Note further that the largest stabilized damping ratio observed was 3.5% which is almost twice what is required for the F-16[6] while the mass ratio of 0.05 is quite reasonable. It is then concluded that the proposed friction based LCO mechanism is indeed possible.

Having established the existence of an increased domain of stable solutions, it is important to assess the phenomenological characteristics of these solutions and to compare them with those obtained with $k_1=0$. In fact, four different types of solutions were observed when $k_1\neq0$ that can be characterized as single frequency stick-slip (SFSS), single frequency continuous slip (SFCS), multiple frequency stick-slip (MFSS), and

multiple frequency continuous slip (MFCS). The term single frequency is used here somewhat freely to describe a solution with a simple period and with minimal harmonics, see Fig. 2.7 for such a solution (continuous slip example). Note in particular that the magnitude of the third harmonic of the response of the mass M_1 is only 1% of its fundamental counterpart. For comparison, "multiple" frequency solutions, see Figs 2.8 and 2.9, exhibit a beating phenomenon (see Figs 2.8(a) and 2.9(a)) that is associated with the presence of two frequencies close to the dominant one, see Fig. 2.8(b). The corresponding phase plane plots (Figs 2.8(b), 2.9(c)) clearly show the complexity of these motions as compared to the single frequency solution, see Fig. 2.7(c). A different perspective into the phase plane features can be obtained by sampling the time histories at specific times. In forced response problems, the sampling is accomplished every cycle of the excitation but in the present self-excited problem, it was found convenient to monitor the displacement and velocity of mass M_1 when the relative motion achieved maximum values. The corresponding sampled phase plane plots are shown in Fig. 2.10. For a periodic motion, only a single dot appears, as seen for the SFCS solution. The MFCS solution on the contrary leads to a close curve while the MFSS solution is characterized by a similar curve and a densely populated domain. It is tentatively concluded from those figures that the corresponding MFCS and MFSS solutions are aperiodic and chaotic, respectively. Note that the difference in behavior between $k_1 = 0.039$ and 0.040 was not easily detectable from the time histories and/or full phase plane plots but is quite clear from the Poincare-type plot of Fig. 2.10.

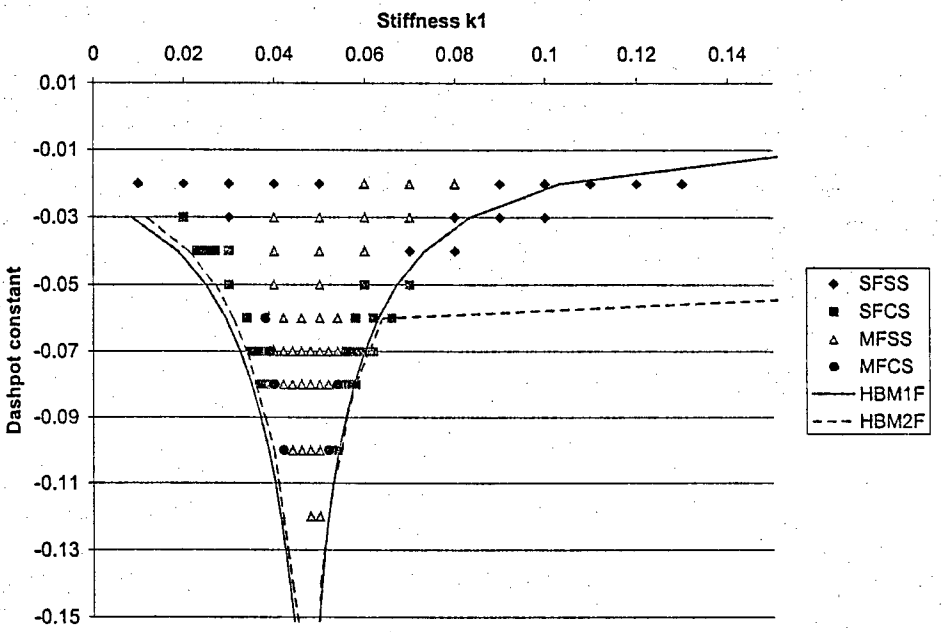

a) Damping vs. stiffness

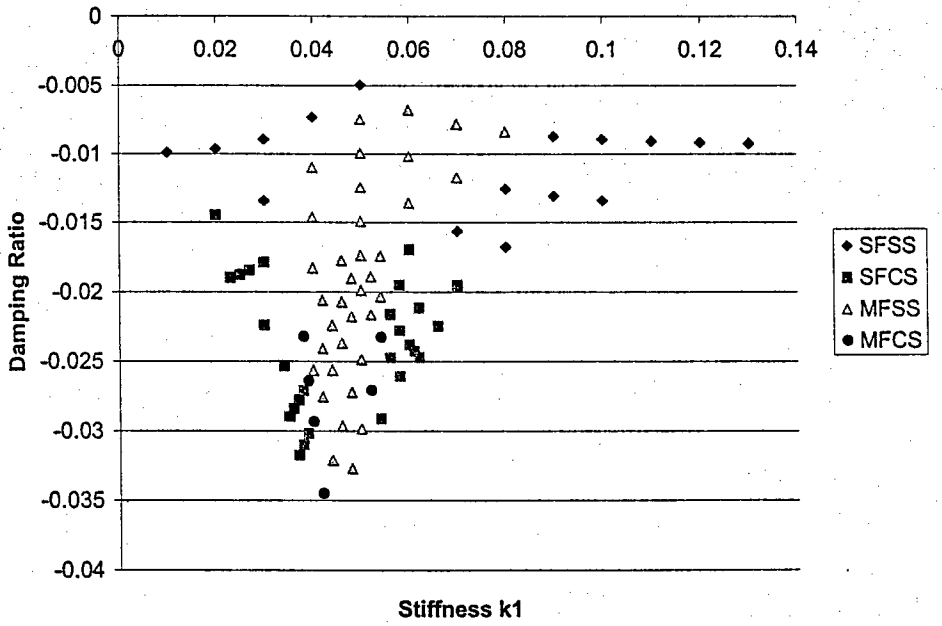

b) Damping ratio vs. stiffness

Fig. 2.6 Domain and type of stable solutions for $M_2 = 0.05$.

It was next desired to analyze the "magnitude" of the response as a function of the stiffness k_1 and the damping constant c. Since an amplitude cannot be properly defined in the multiple frequency situation, it was decided to study the highest level of response obtained in the steady state part of the computed response instead, see Fig. 2.11. Note that the curves are not plotted continuously at the change of solution type, i.e. from single to multiple frequency and vice versa. The general tendency of these curves is that the level of response decreases from the edges of the stable zone toward its center $k_1 \approx r = 0.05$, as expected from the increase in energy transfer. Further, the largest response is substantially increased by the beating phenomenon of Figs 2.8(a) and 2.9(a), i.e. as the solution switches from a single to two dominant frequencies.

2.2.3 Changes in Solution Types – Bifurcations

The arrangement of the 4 solutions types in the $c - k_1$ or $\zeta_2' - k_1$ domain, see Fig. 2.6, is very interesting. Near the edges of the stable zone, it appears that the single frequency solution only is present. Further, it exhibits a stick-slip (SFSS) behavior only for the smallest values of the negative damping and a continuous slip (SFSS) through most of the domain. This observation is physically expected as a continued slip is likely to provide an increased dissipation and in that respect is consistent with the $k_1 = 0$ findings of Fig. 2.4(a). As the stiffness k_1 is varied (increased or decreased) toward the center of the stable domain ($k_1 \approx r$), a change of solution takes place and the single frequency solution switches to a multiple frequency one, first maintaining the continuous slip (for sufficiently large negative damping), then exhibiting stick phases.

The appearance of the multiple frequency solutions, not seen in the simpler, $k_1 = 0$ case, may be associated with the two natural frequencies of the linear system. Indeed, for small mass ratios and for values of $k_1 \approx r$, the two system frequencies are close to each other and could be producing the tightly spaced peaks of Fig. 2.9(b). Further, when k_1 is exactly equal to r, the corresponding (negative here) damping ratios are also equal so that contributions of both linear modes to the response would be certainly be expected in this case. As the stiffness k_1 deviates from the mass ratio r, the two damping ratios rapidly differ from each other so that the response should emphasize more heavily one of the two modes, i.e. the one characterized by the most negative damping ratio. These observations provide a tentative explanation for the presence of three dominant frequencies near the center of the stable domain, i.e. $k_1 \approx r$, but only one frequency near the edges of this region as seen in Fig. 2.6.

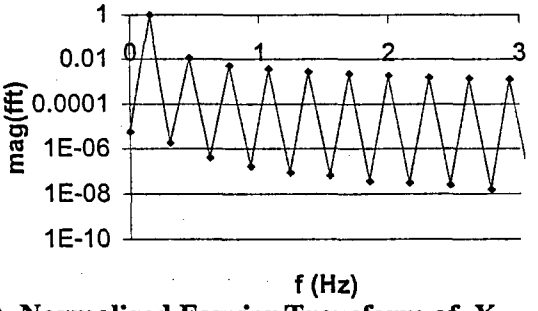

a) Normalized Fourier Transform of X_1

Fig. 2.7 A typical "single" frequency continuous slip solution, $M_2 = 0.05$, $k_1 = 0.06$, $c = -0.07$.

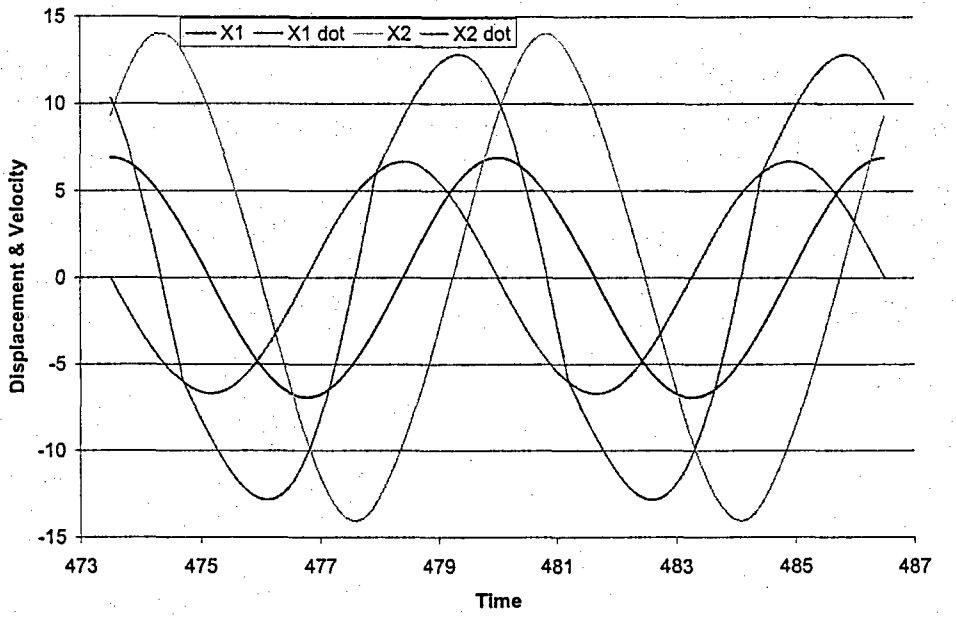

b) Time histories

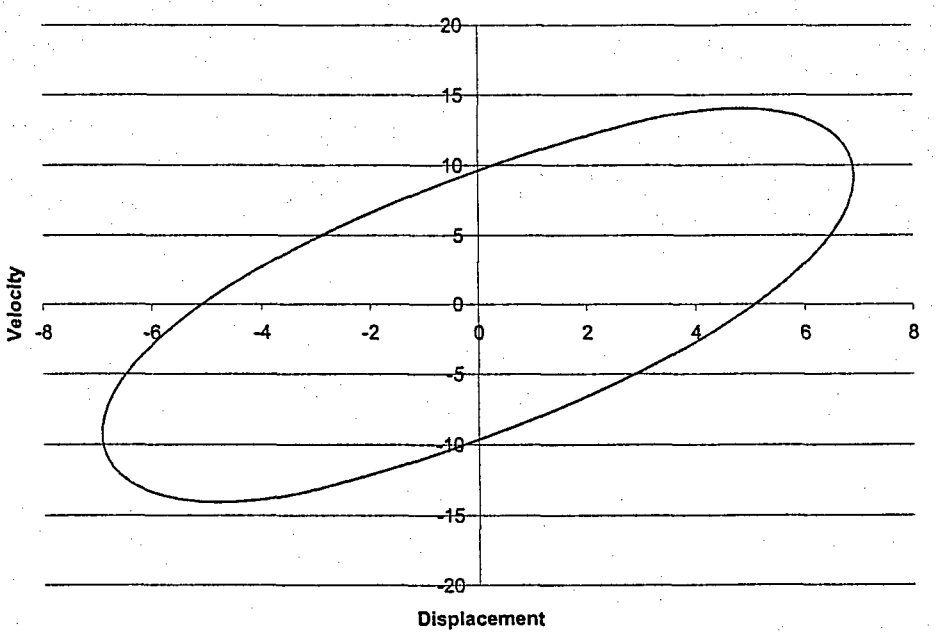

c) Phase plane plot

Fig. 2.7, continued

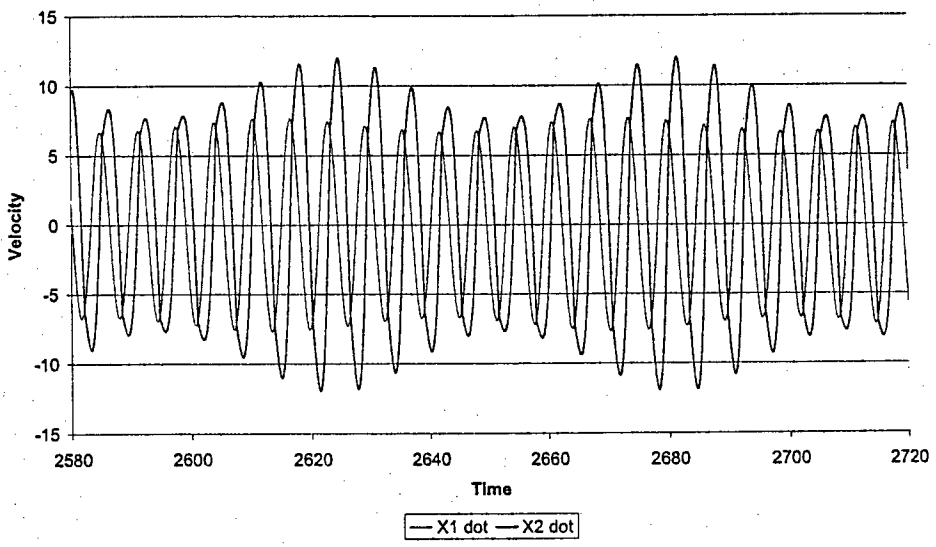

a) Time history of velocities

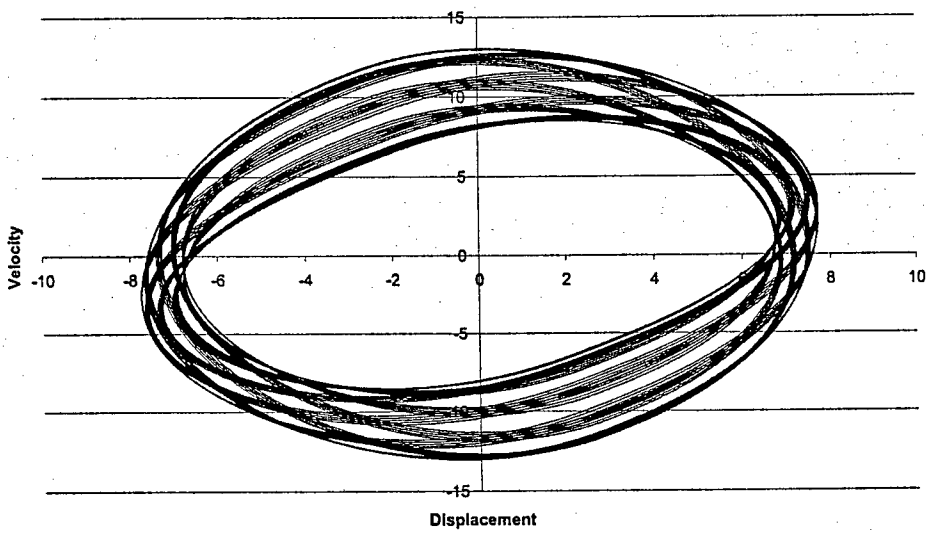

b) Phase plane plot

Fig. 2.8 A typical "multiple" frequency continuous slip solution, $M_2 = 0.05$, $k_1 = 0.039$, $c = -0.07$.

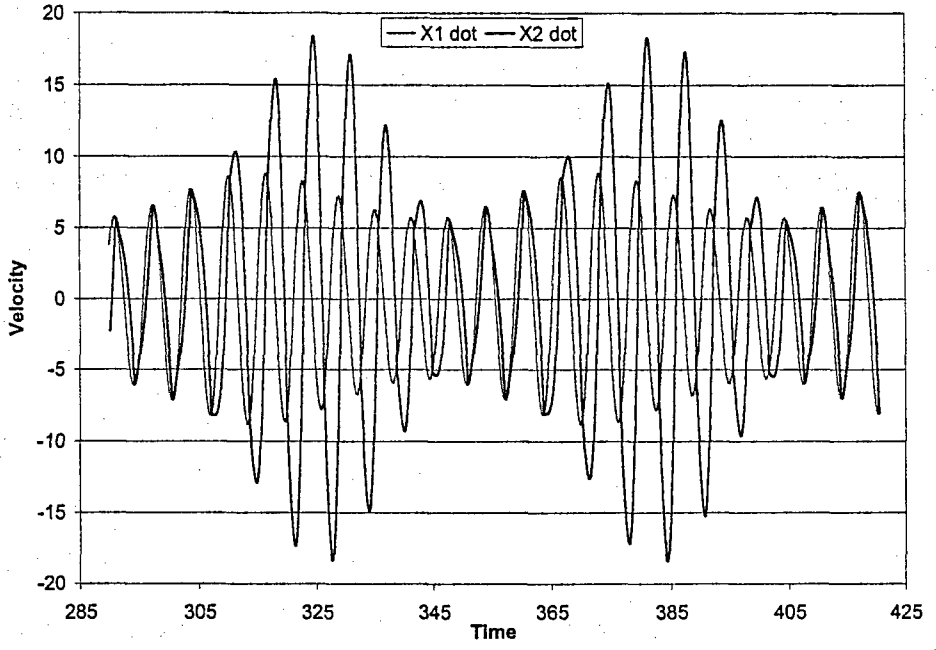

a) Time history of velocities

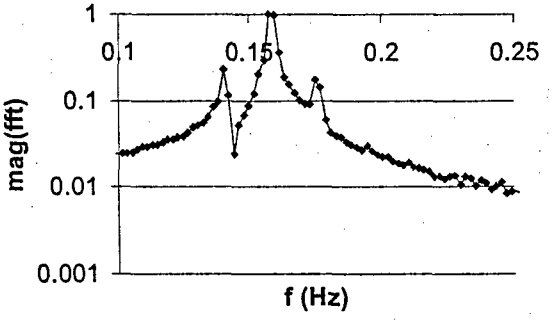

b) Normalized Fourier Transform of X_1

Fig. 2.9 A typical "multiple" frequency stick-slip solution, $M_2 = 0.05$, $k_1 = 0.04$, $c = -0.07$.

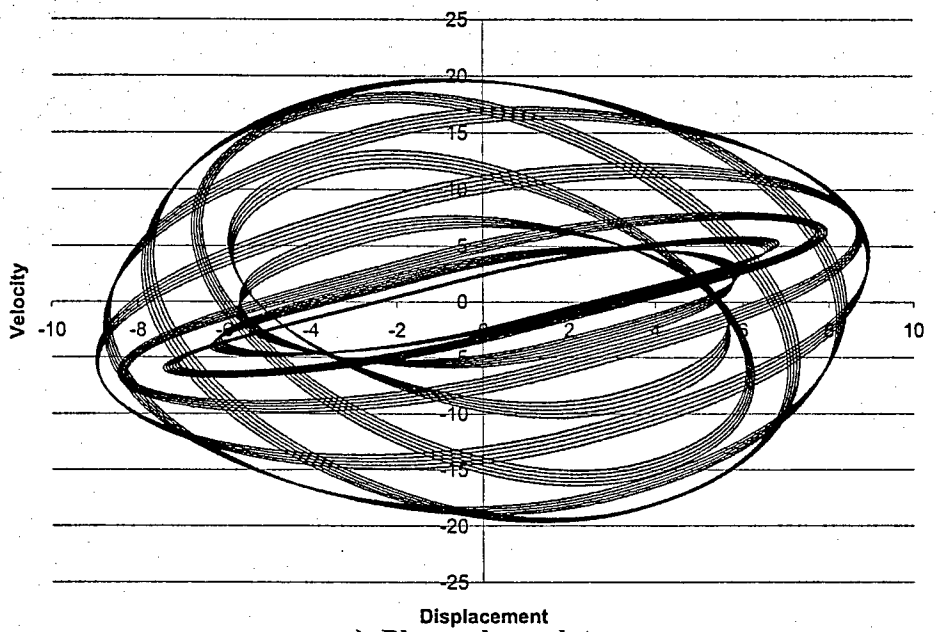

c) Phase plane plot

Fig. 2.9, continued

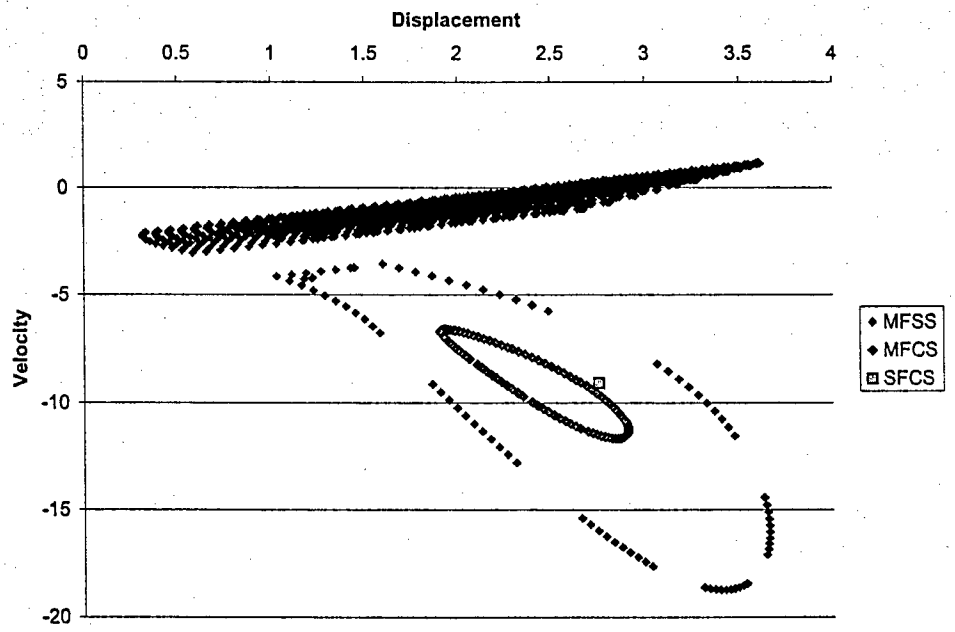

Fig. 2.10 Sampling of the phase plane plots for $M_2 = 0.05$, $c = -0.07$, $k_1 = 0.038$ (SFCS), 0.039 (MFCS), and 0.04 (MFSS).

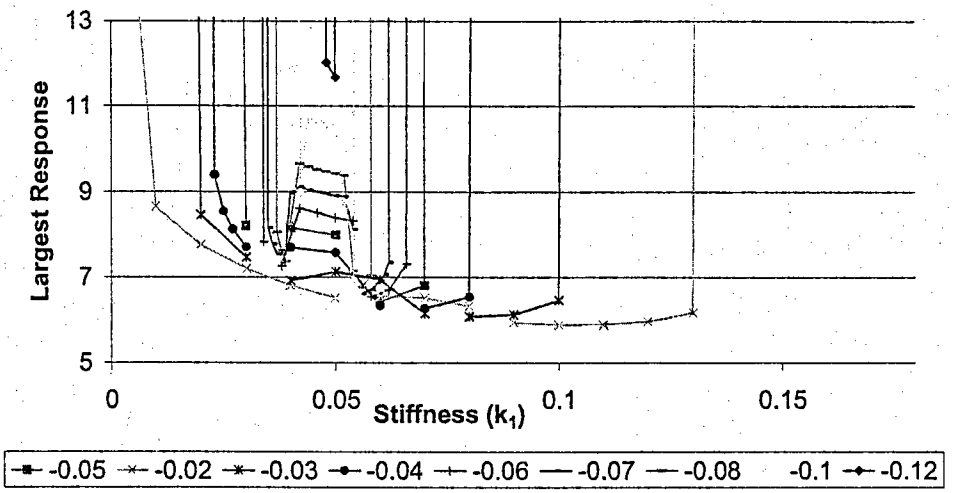

Fig. 2.11 Largest response of mass M_1 as a function of the stiffness k_1 for different values of the damping constant c.

A more formal approach can be undertaken to better clarify the transition, bifurcation in fact, of solutions from single to multiple frequencies. This approach, referred to as Floquet analysis[19], relies on the availability of the periodic, steady state solution at a time t, $\underline{x}(t)$. If the equations of motion can be linearized around this steady state solution, the response after one cycle, $\underline{x}(t)+\delta\underline{x}(t+T)$, corresponding to an imposed perturbations at the beginning of the cycle, i.e. $\delta\underline{x}(t)$, can be expressed as

$$\delta\underline{x}(t+T)=P\,\delta\underline{x}(t). \tag{2-28}$$

In this equation, P is a square transition matrix which can be identified by proceeding in turn with small perturbations of each of the state variables (4 in the present context) and computing the corresponding perturbed solutions after one cycle. Repeating the argument of Eq. (2-28), the perturbation after n cycles is related to the original one, $\delta\underline{x}(t)$, by the matrix P^n. Then, the steady state solution $\underline{x}(t)$ will be stable, i.e. the effects of the

perturbation $\delta\underline{x}(t)$ will disappear as $t \to \infty$, if $P^n \to 0$ when $n \to \infty$ or equivalently if the eigenvalues of P are all less than 1 in magnitude.

This result is valid in forced vibrations cases in which time is defined by the excitation. In self excited problems however, it is possible for the perturbed solution to converge to the unperturbed steady state response but time shifted by δt. In fact, this situation occurs for $\delta\underline{x}(t) = \dot{\underline{x}}(t)\,\delta t$ as $\underline{x}(t) + \delta\underline{x}(t)$ is then simply $\underline{x}(t + \delta t)$. Thus, after one period, the perturbed response is $\underline{x}(t + \delta t + T) = \underline{x}(t + \delta t)$ from the periodicity of the exact steady state solution. From this relation, it is thus concluded that an eigenvalue of +1 should always be present in P in self excited problems.

The estimation of the matrix P was performed for c = -0.07 and a series of values of k_1 for which a single frequency solution is encountered, i.e. $k_1 \in (0.34, 0.3885]$ and the corresponding eigenvalues (complex and imaginary parts) are plotted in Fig. 2.12. The persistent eigenvalue at +1 is clearly seen and so is the convergence of two eigenvalues toward the unit circle as $k_1 \to 0.3885$. From this last observation, it is tentatively suggested that the transition from a single to multiple frequencies is a Hopf bifurcation.

Considering this data for monotonically decreasing values of k_1 provides also a perspective on the loss of stability that occurs for $k_1 \approx 0.34$. Specifically, it is noted that the real eigenvalue of value <1 is slowly progressing toward the unit circle, suggesting that the loss of stability is accomplished through the occurrence of a double eigenvalue at +1.

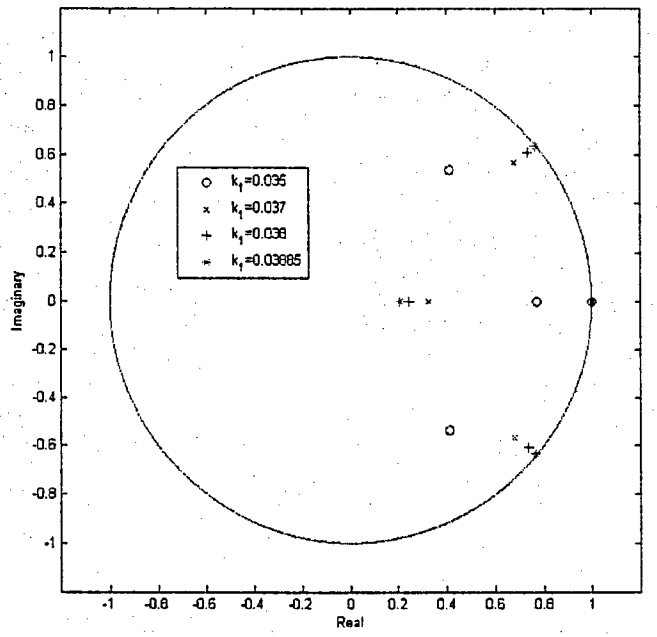

Fig. 2.12 Eigenvalue plot of Floquet analysis, c = -0.07.

2.3 Assessment of Friction on an Aeroelastic System Exhibiting Post Flutter LCO

2.3.1 Primary-Secondary Coupling Through the Friction Element and a Spring

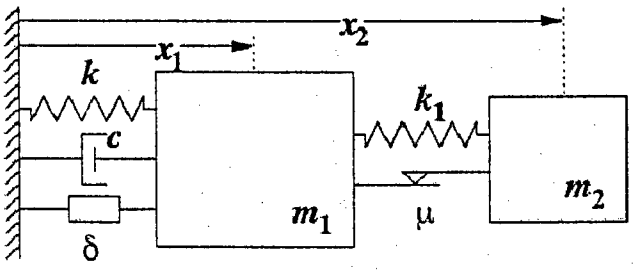

Fig. 2.13 2-degree-of-freedom system with van der Pol force.

The simple system of Fig. 2.5 does not exhibit limit cycle oscillations in the absence of friction, its response exponentially increases as time grows. It was thus necessary to add another stabilizing factor to induce limit cycle oscillations in the absence of friction. One such term often encountered is a van der Pol (vdP) force which is proportional to the product of the square of the displacement and the velocity. This additional force was assumed to act on the primary mass, see Fig. 2.13, yielding the equations of motion

$$M_1\ddot{x}_1 + c\left(1-\delta x_1^2\right)\dot{x}_1 + \left(k+k_1\right)x_1 - k_1 x_2 = F_{31} \tag{2-28}$$

and

$$M_2\ddot{x}_2 - k_1 x_1 + k_1 x_2 = -F_{31} \tag{2-29}$$

where

$$F_{31} = \mu_D N \operatorname{sgn}\left(\dot{x}_2 - \dot{x}_1\right) \text{ during slip} \tag{2-30a}$$

$$\left|F_{31}\right| \le \mu_S N \text{ during stick.} \tag{2-30b}$$

A nondimensionalization of the equations of motion provides significant insight into the behavior of the system. To this end, introduce

$$\omega_1=\sqrt{k/M_1}\ ;\ \omega_2=\sqrt{k_1/M_2}\ ;\ r=M_2/M_1\ ;$$

$$\tau=\omega_1 t\ ;\ y_i=x_i\left(k/\mu_D N\right),\ i=1,2;$$

$$\zeta=c\omega_1/2k\ ;\ \bar{\delta}=\delta k^2/\mu_D^2 N^2\ ;\ \bar{k}_1=k_1/k\ . \tag{2-31}$$

Then, the equations of motion, Eq. (2-28)-(2-30), can be rewritten as

$$y_1'' + 2\zeta\left(1-\bar{\delta}y_1^2\right)y_1' + \left(1+\bar{k}_1\right)y_1 - \bar{k}_1 y_2 = \bar{F}_{31} \tag{2-32}$$

and

$$r y_2'' - \bar{k}_1 y_1 + \bar{k}_1 y_2 = -\bar{F}_{31} \tag{2-33}$$

where $(.)'$ denotes the derivative with respect to τ,

$$\bar{F}_{31} = \operatorname{sgn}(y_2' - y_1') \text{ during slip} \tag{2-34a}$$

and

$$\left|\bar{F}_{31}\right| \le \mu_S / \mu_D \text{ during stick.} \tag{2-34b}$$

Note in particular from Eq. (2-32)-(2-34) that the amplitude of response is proportional to μ_D if $\mu_S = \mu_D$ and $\delta = 0$. Further, this property also holds for nonzero values of δ provided that $\bar{\delta}$ is held constant.

As in the previous section, a numerical approach was adopted to study the response of the system. As before, M_1 and M_2 were selected to be 1 and 0.05, and k was set to 1. Further, the static and dynamic coefficients of friction were selected equal, $\mu_S = \mu_D = \mu$. The other parameters were varied to provide a thorough perspective on the response of the system.

The system of Fig. 2.13 was analyzed with different values of the van der Pol constant δ and the amplitude of response and stability plots for each of these values was generated. Shown in Fig. 2.14-2.17 are the results corresponding to $\delta = 0.025$ (Fig. 2.14 and 2.15) and $\delta = 0.04$ (Fig. 2.16 and 2.17). To clarify the discussion of these figures, note first that the van der Pol system is stable for all cases considered and thus stabilization must occur for $\delta > 0$. Further, the response of the van der Pol system without friction is a single frequency (continuous slip) solution.

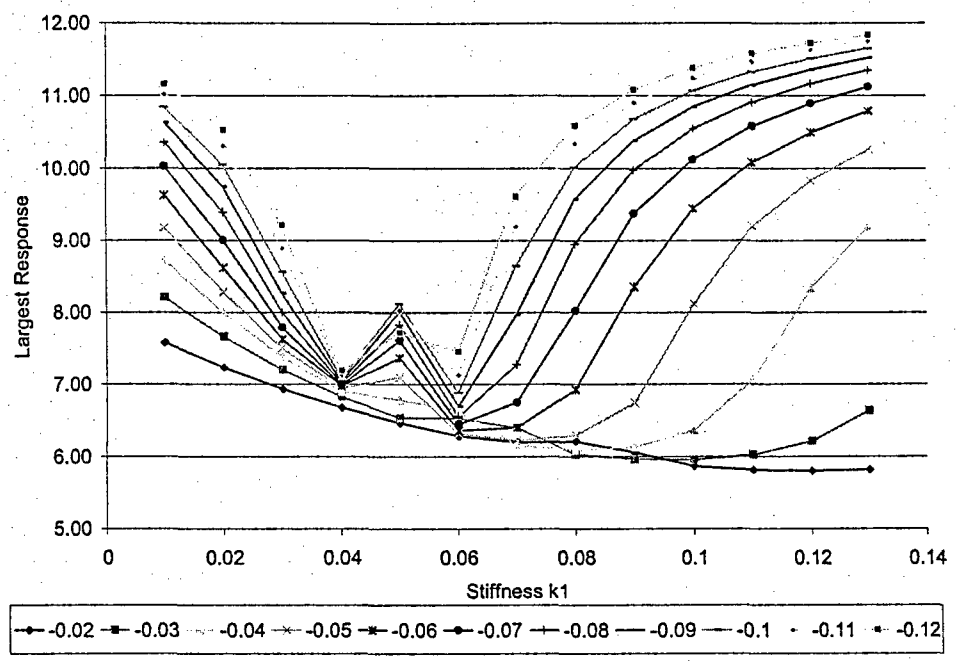

Fig. 2.14 Largest response of mass M_1 as a function of the stiffness k_1 for different values of the damping constant c, $\delta = .025$, and $\mu = 0.25$.

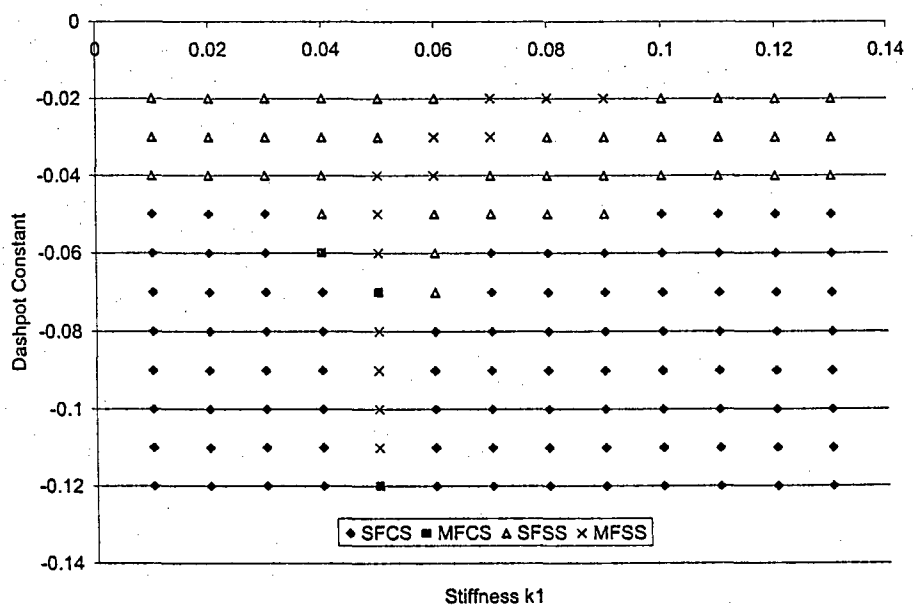

Fig. 2.15 Domain and type of stable solutions $\delta = 0.025$ and $\mu = 0.25$.

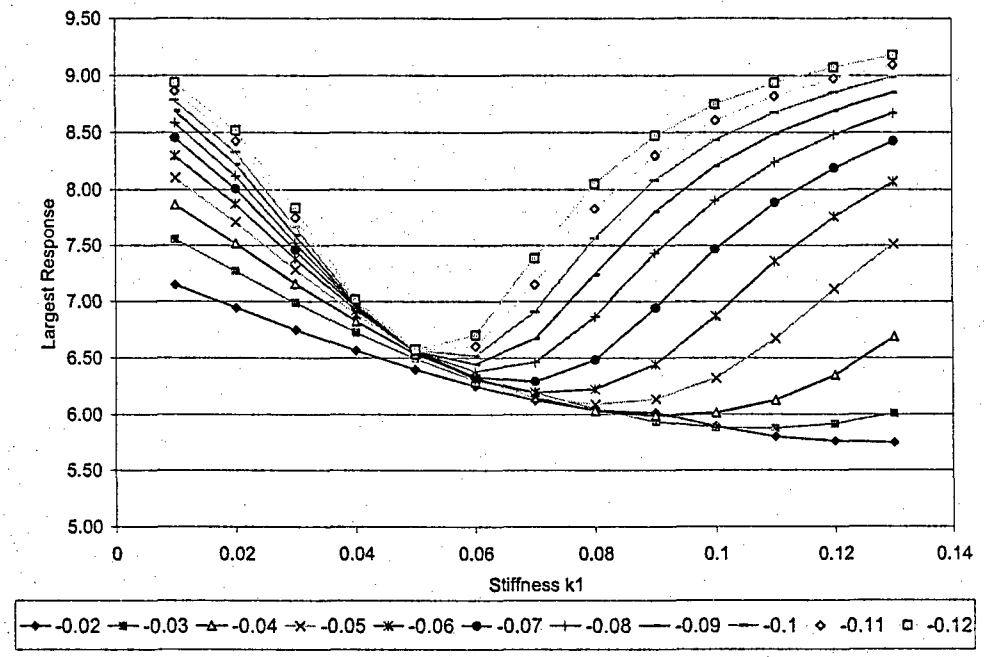

Fig. 2.16 Largest response of mass M_1 as a function of the stiffness k_1 for different values of the damping constant c, $\delta = 0.04$, and $\mu = 0.25$.

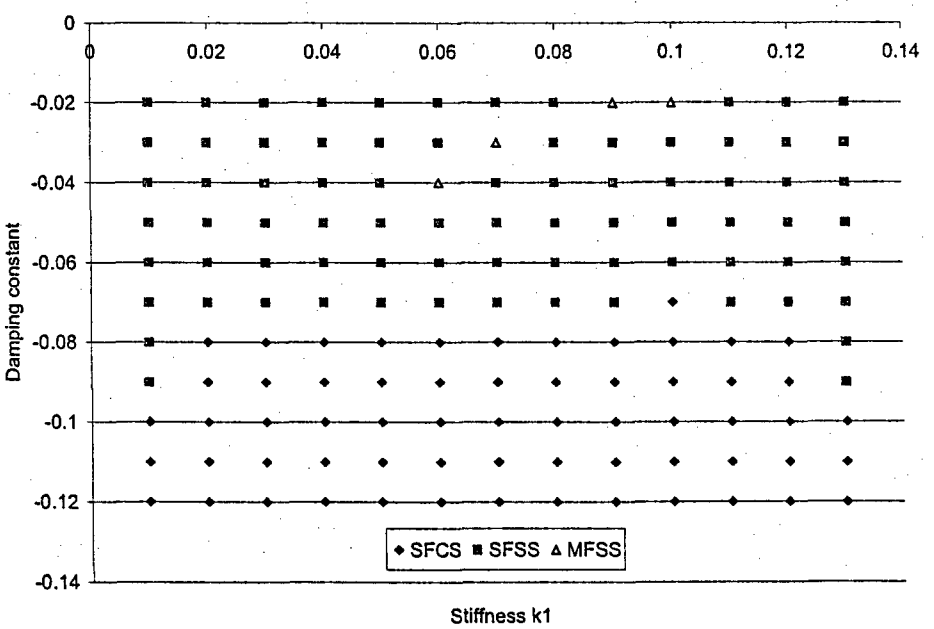

Fig. 2.17 Domain and type of stable solutions for $\delta = 0.04$, and $\mu = 0.25$.

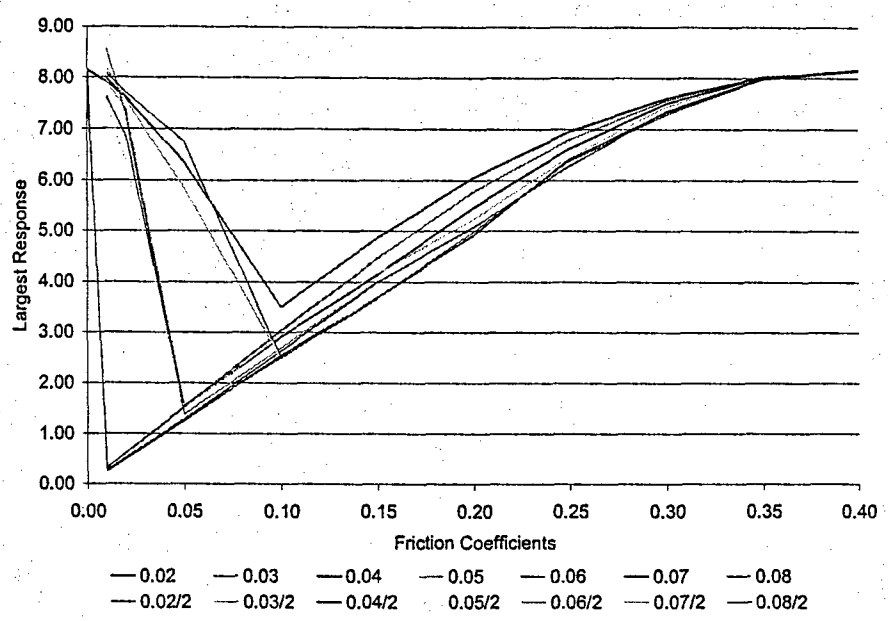

Fig. 2.18 Largest response of mass M_1 as a function of the coefficient of friction m, for different stiffnesses k_1, $c = -0.04$, and $\delta = 0.06$ (The notations /2 refers to a second solution for that k_1).

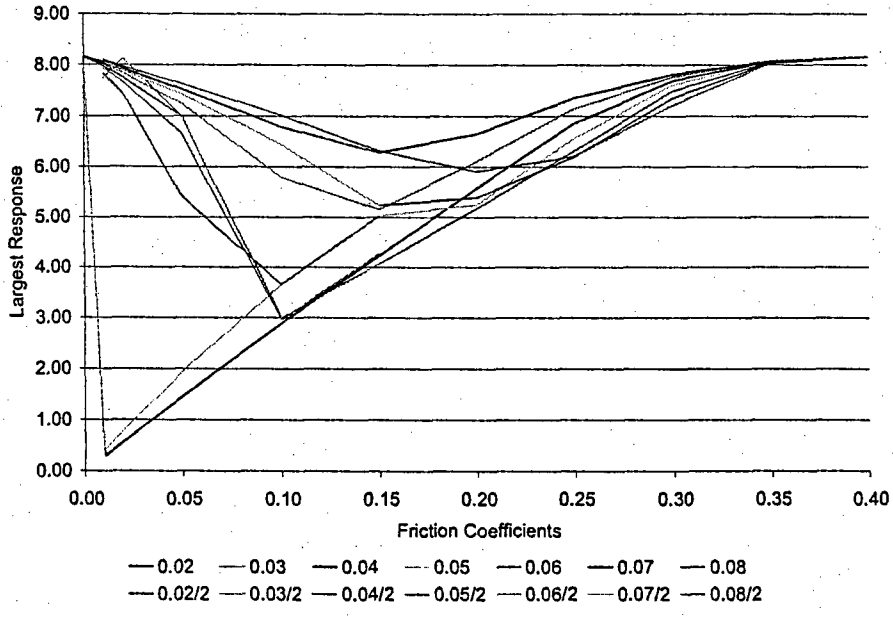

Fig. 2.19 Largest response of mass M_1 as a function of the coefficient of friction m, for different stiffnesses k_1, $c = -0.09$, and $\delta = 0.06$ (The notations /2 refers to a second solution for that k_1).

Comparing Fig. 2.6(a), 2.15, and 2.17, it is first seen that the unstable regions of Fig. 2.6(a) are replaced by stable single frequency continuous slip motions characteristic of a van der Pol dominated response. Note further that the domain of multiple frequency solutions shrinks as δ is increased leaving mostly single frequency motions. This finding may be explained by noting that the multiple frequency solutions typically lead to large amplitudes because of the beating, see Fig. 2.11. For such large amplitudes however, the stabilization of the van der Pol term is significant forcing a decrease, and eventually disappearance, of the beating effect. The decreased presence of the multiple frequency solutions is also visible from the amplitude of response plots, Fig. 2.11, 2.14, and 2.16, where they imply higher amplitudes than the neighboring single frequency solutions. Notice on these same figures that the sharp transitions to instability in Fig. 2.11 are replaced by smooth increases toward the amplitude corresponding to the van der Pol alone.

Another change in the character of the solution concerns the transition from stick-slip to continuous slip. It can be seen from Fig. 2.6(a), 2.15, and 2.17 that stick-slip solutions typically occur at low values of the negative damping ratio and correspond to smaller response level for which the dissipation during the slip phase is sufficient to stabilize the motions. Continuous slip solutions on the contrary appear at higher response levels where the amplitude of response is large enough to force the continuous motion of the sliding block. It is seen from Fig. 2.15 and 2.17 that the value of the negative damping ratio at which the stick-slip to continuous slip transition occurs increases (in magnitude) as the van der Pol parameter δ is increased. This result is in fact expected as

an increase in δ promotes stability and forces lower response levels thereby favoring stick-slip solutions. An increase of the damping constant (larger negative) must then take place to increase the energy introduced in the system and to induce a continuous slip behavior.

The V-shape of the amplitude plot, slightly visible for $\delta = 0$ (Fig. 2.11), quite clear for $\delta = 0.025$ (Fig. 2.14), and obvious for $\delta = 0.04$ (Fig. 2.16), demonstrates that an amplitude of response substantially below the van der Pol alone level can be achieved with friction. Thus, friction can also play an important role in reducing the level of response of existing limit cycle oscillations. Note further that friction is most effective when $k_1 \approx 0.05$, especially for large negative damping ratios, as was already noted in the previous section.

The above discussion has focused on the behavior of the response as a function of δ, c, and k_1 for a fixed value of μ (= 0.25) and it is now desired to assess the role of the friction coefficient. To this end, the value of δ was set to 0.06 and the response of the system of Fig. 2.13 was determined for two damping coefficients, i.e. c = -0.04 and -0.09, as function of k_1 and μ. Surprisingly, it was found for both values of c that two stable solutions exist for low coefficients of friction, see Fig. 2.18 and 2.19. Each of these two solutions essentially involves a single stabilization factor: the very low amplitude solution is associated with the low friction coefficient without any significant effect of the van der Pol term. In such conditions, a stable solution must exhibit a small amplitude as the low level of friction will not provide much dissipation. At the contrary, the large amplitude solution is only marginally affected by the small frictional term and it is

primarily the van der Pol force that dictates the response. As the coefficient of friction increases, its effect on the high amplitude solution increases implying a decrease of the response level. Further, a higher coefficient of friction provides a balance of the unstable aerodynamic forces at higher amplitude levels. Thus, the amplitude of the lower (resp. higher) solution increases (resp. decreases) until they both merge into a single one solution as seen in Fig. 2.18 and 2.19. The value of the coefficient of friction at which the merging of the solutions occurs is a particular good operating point as it yields the smallest value of the maximum stable solution. Note further that the existence of two solutions occurs at high negative aerodynamic damping only when the natural frequencies of the two blocks alone are identical or almost so.

2.3.2 Primary-Secondary Coupling Through the Friction Element, a Spring, and a Dashpot

Dissipation associated with the relative motion of the two masses may include more than just friction, most notably viscous effects, and it is finally desired here to assess how the presence of an additional damping mechanism would affect the conclusions drawn in connection with the system of Fig. 2.13. To this end, a dashpot (viscous element) was added between the two masses, see Fig. 2.1, and a parametric study of the response magnitude and character (i.e. single vs. multiple frequency and continuous slip vs. stick-slip or stuck behavior) was undertaken.

It was demonstrated earlier that the coincidence of the natural frequencies of the primary and secondary systems is a particularly critical condition since it leads to a

maximum transfer of energy from the primary to the secondary where it can be dissipated by friction. The effectiveness of the frictional device is thus maximum in that configuration. Accordingly, the present study of the effects of the damping coefficient c_1 was performed under this matching requirement, i.e. with $k_1 = 0.05$. Finally, the coefficients of friction were selected to take on the representative values $\mu_S = \mu_D = 0.25$ and the van der Pol parameter was chosen as the intermediate value of $\delta = 0.025$. The steady state response of the system of Fig. 2.1 was then computed for a series of values of c_1 and c and the largest response (e.g. the amplitude of the motion in "single" frequency solutions) as well as the character of the solutions (i.e. single vs. multiple frequency, continuous slip vs. stick-slip vs. stuck configuration) was recorded, see Fig. 2.20 and 2.21.

It should first be noted from Fig. 2.20 the existence of a minimum value of the largest response of the primary mass at some intermediate value of the damping coefficient c_1. When c_1 is less than this threshold, it would appear that the friction and the dashpot reinforce each other to provide an increased dissipation and correspondingly a reduced response. A more refined perspective on this effect may be obtained from the classification of the various solutions involved, see Fig. 2.21. Specifically, it is seen that there exists a thin layer of values of c_1 near $c_1 = 0$ in which the character of the solution changes rapidly, from multiple to single frequency. In fact, a comparison of Fig. 2.20 and 2.21 indicates that it is also in this small zone that the largest response decreases.

It is thus concluded that this decrease goes hand in hand with a change of character of the solution, from multiple to single frequency. To complete the analysis, the

time histories of the response of the primary system (mass M_1) were inspected for values of c_1 in this thin layer, i.e. for $c_1 \in [0,0.001]$, see Fig. 2.22. It is clearly seen from these figures that the decrease of the largest response is in fact associated with a decrease of the level of beating, not with a noticeable decrease in the mean of the steady state response. It remains then to explain how this change of character takes place and why it is so sensitive with respect to c_1.

In this context, consider the plots of the largest response and the corresponding classification obtained with $c_1 = 0$, see Fig. 2.14 and 2.15, and note that the multiple frequency solutions only exist in a narrow zone of stiffnesses k_1 around $k_1 = 0.05$. It was argued earlier that the appearance of the beating is associated with a Hopf bifurcation in which an eigenvalue of the perturbed problem reaches the unit circle. Damping naturally provides decay over a given time and thus forces these eigenvalue away from the unit circle, toward the origin. For c_1 large enough, i.e. 0.001 in the case considered, the largest eigenvalue never reaches the unit circle and the single frequency solution is maintained throughout. Two more observations can be made in this regard. First, a minimum of the largest response does not occur, see Fig. 2.14, for the two least negative values of c, c = -0.02 and -0.03, consistently with Fig. 2.15 since the corresponding solutions for $c_1 = 0$ are both single frequency. Finally, note that the amplitude of the single frequency motions for c_1= 0.001 and k_1= 0.05, i.e. 6.7-6.9 (see Fig. 2.20), are very close to the interpolation of the values obtained from Fig. 2.14 for c_1= 0 and k_1= 0.04 and k_1= 0.06 suggesting a continuity of the solution as a function of k_1 in the absence of multiple frequency bifurcation.

The above discussion has clarified the behavior of the solutions for small values of c_1 but has not addressed the increase in response observed in Fig. 2.20 for $c_1 > 0.001$. In fact, it was found that the increase in damping of the relative motions of the two blocks leads primarily to a decrease of the amplitude of these motions and that the decrease is large enough to decrease the energy dissipated per cycle, even with the increase of c_1. Thus, the amplitude of response of the primary mass must increase as noted in Fig. 2.20. The decrease of amplitude of the relative motions also increases the likelihood of a sticking and thus justifies the continuous slip to stick-slip transition that is observed on Fig. 2.21 for all c values as c_1 increases. For very large values of c_1, the two blocks stick together and the motion is governed by the negative dashpot c and the van der Pol restoring force.

It was desired to confirm the above observations in another situation, namely for a different value of the van der Pol coefficient δ. To this end, the computations were repeated with $\delta = 0$ and the results, largest response and classification, are presented in Fig. 2.23 and 2.24. The narrow zone in which both transition from multiple to single frequency and decrease of the largest response occur is again present, albeit broader in Fig. 2.23 and 2.24 as compared to Fig. 2.20 and 2.21. Further, the ensuing increase of the amplitude of response as the damping coefficient c_1 is increased is also shown. All results thus appear consistent with those of Fig. 2.20 and 2.21.

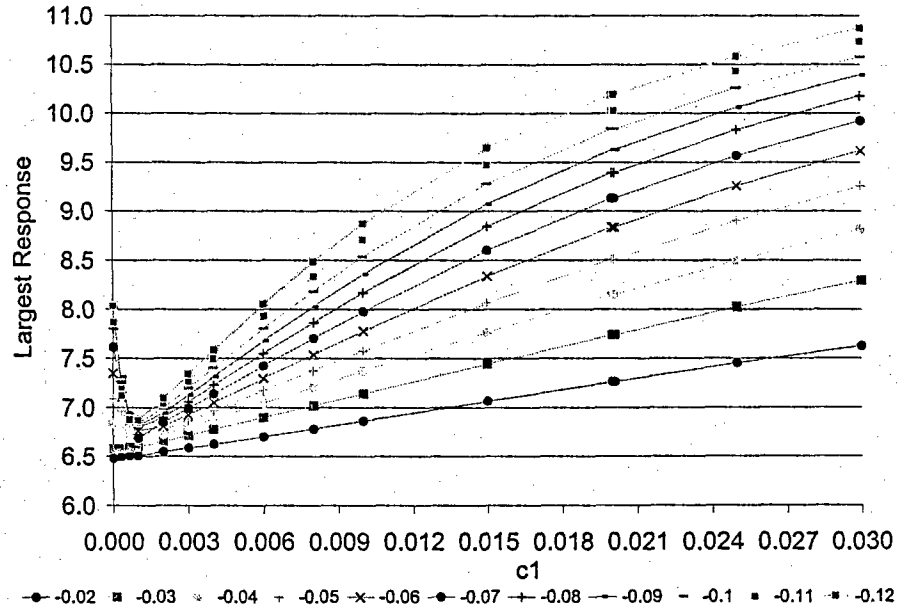

Fig. 2.20 Largest response of mass M_1 as a function of the damping coefficient c_1 for different values of the damping constant c, $k_1 = 0.05$, $\delta = 0.025$, and $\mu = 0.25$.

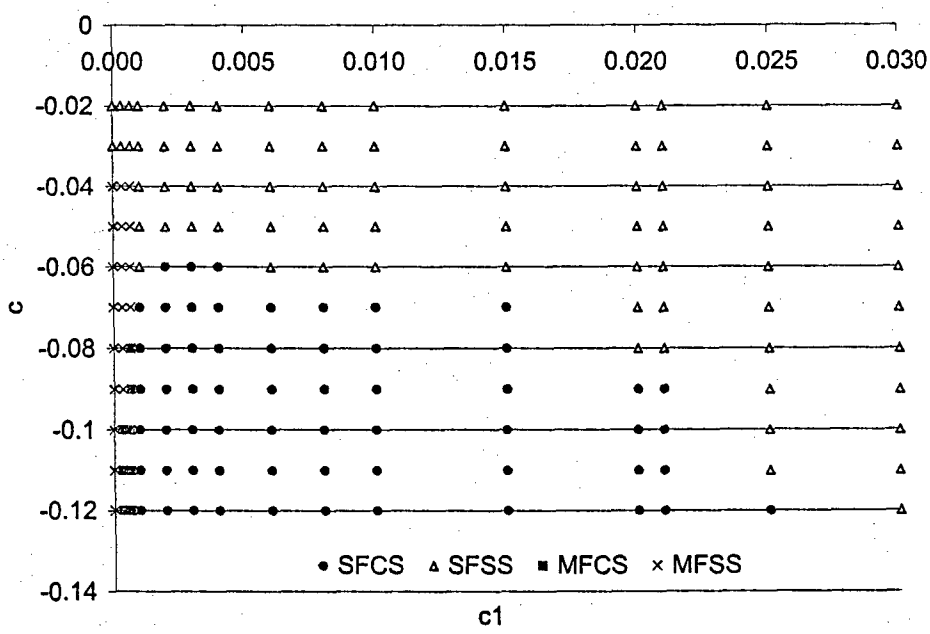

Fig. 2.21 Domain and type of stable solutions, $k_1 = 0.05$, $\delta = 0.025$, $\mu = 0.25$.

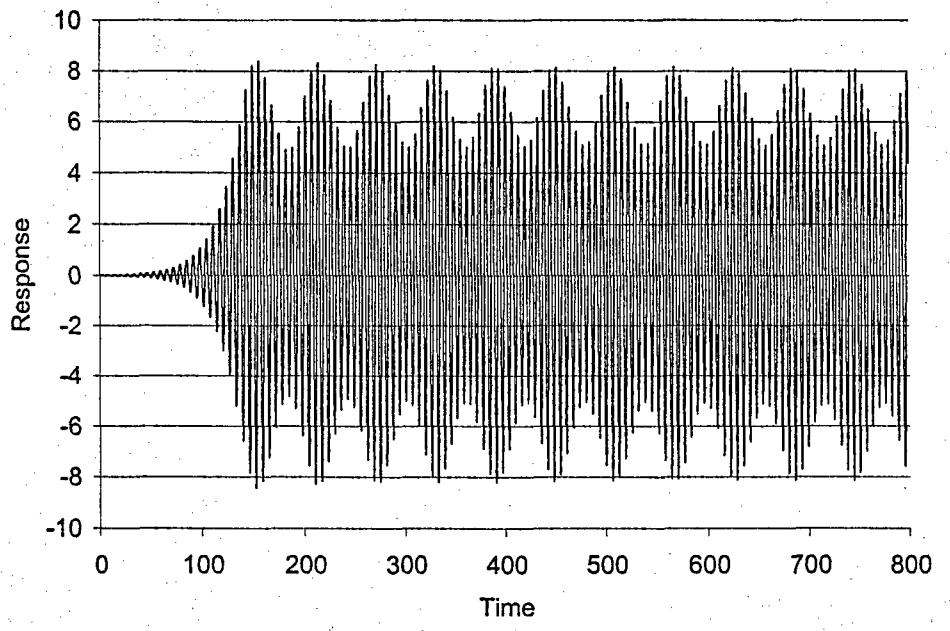

a) $c_1 = 0$

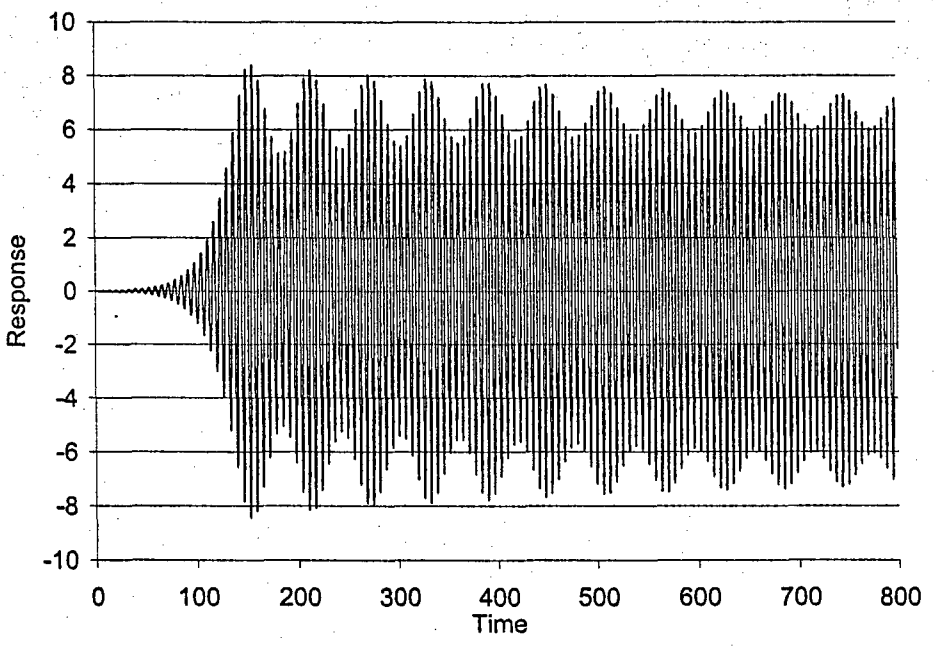

b) $c_1 = 0.000333$

Fig. 2.22 Time history of the response of the mass M_1 for different values of c_1, $c = -0.10$, $\mu = 0.25$.

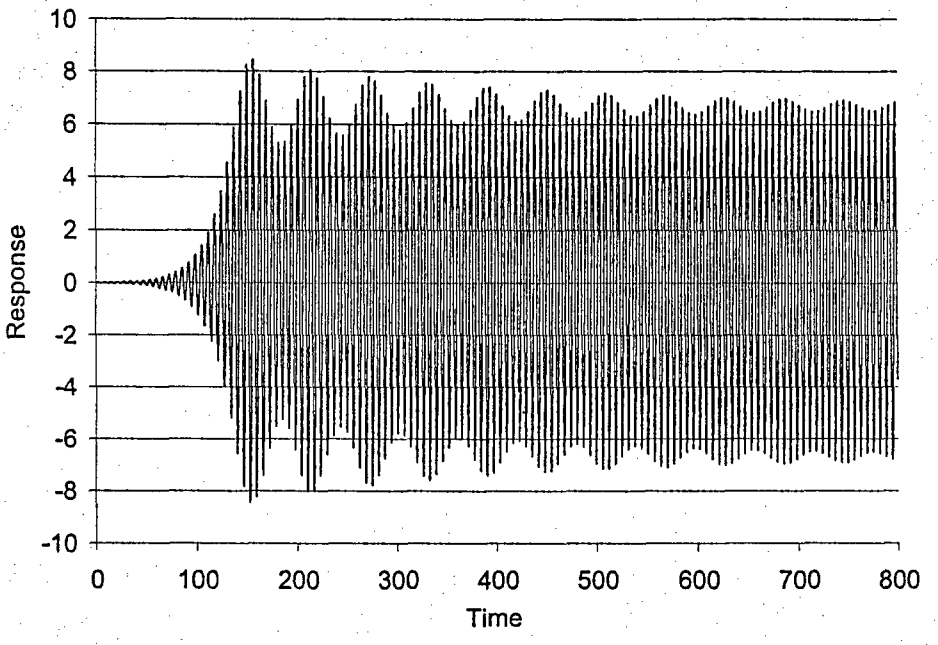

c) $c_1 = 0.00667$

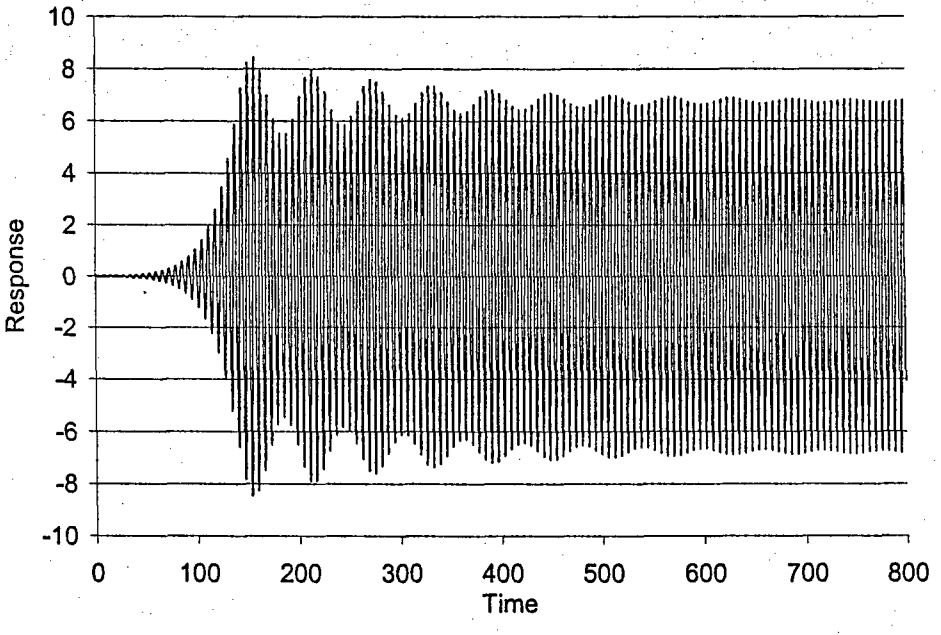

d) $c_1 = 0.001$

Fig. 2.22, continued

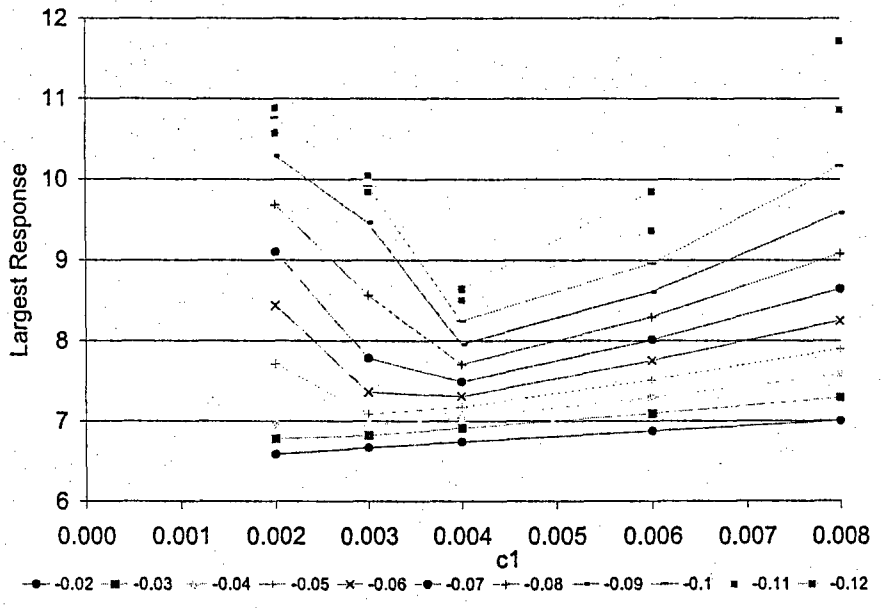

Fig. 2.23 Largest response of mass M_1 as a function of the damping coefficient c_1 for different values of the damping constant c, $k_1 = 0.05$, $\delta = 0$, and $\mu = 0.25$.

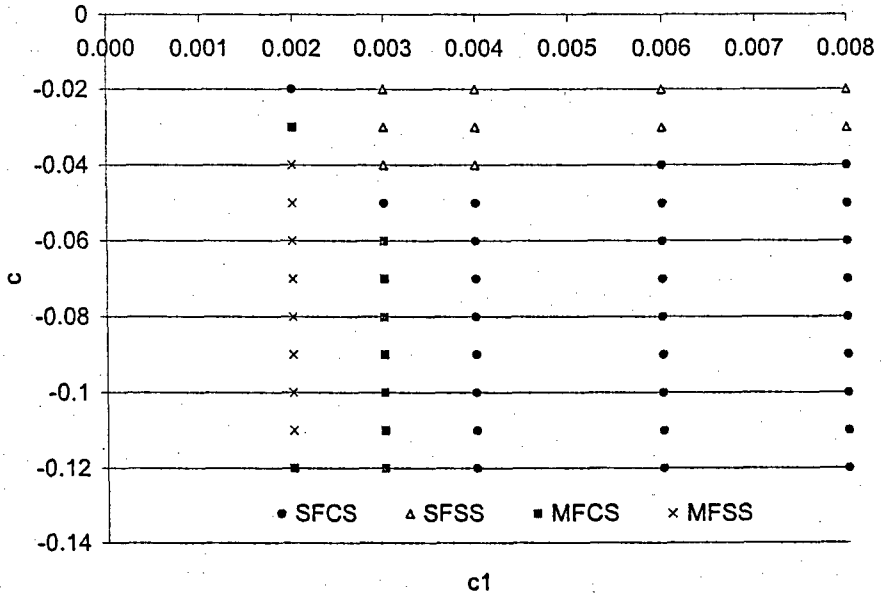

Fig. 2.24 Domain and type of stable solutions, $k_1 = 0.05$, $\delta = 0$, and $\mu = 0.25$.

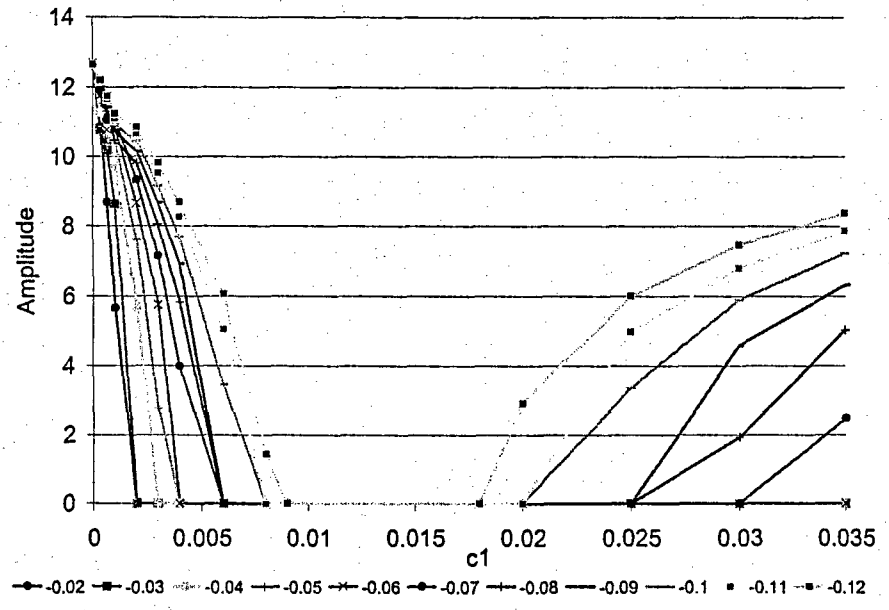

Fig. 2.25 Largest response of mass M_1 as a function of the damping coefficient c_1 for different values of the damping constant c, $k_1 = 0.05$, $\delta = 0.025$, and $\mu = 0$.

The above findings and discussion demonstrate the benefit of a small viscous damping in addition to the friction as a mean of controlling the solution character, more notably the single to multiple frequency bifurcation. A larger viscous damping is however not advisable as it leads to a reduction of the dissipation potential of the secondary system.

Having established the role in friction alone and in concert with a viscous damping element, it is desired next to evaluate the stabilization potential of the viscous element alone. To this end, the computations were reiterated but for $\mu = 0$ with $\delta = 0.025$ and the corresponding amplitudes of the response of the primary mass are shown in Fig. 2.25 as function of c_1. Interestingly, it is found that the steady state amplitude is zero for a finite range of values of c_1, $c_1 \in [0.009, 0.018]$ for all values of c considered,

demonstrating that the equilibrium position is then stable even with the presence of the negative dashpot c. The study of the linearized system (i.e. without the van der Pol term) is appropriate to explain this behavior and accordingly, the complex mode shapes and eigenvalues of the linear, non-classically damped 2-degree-of-freedom system were determined. At low values of c_1, both mode shapes involve large relative motions which further increase as c_1 is increased so that both modal damping ratios increase and eventually become positive (e.g. for $c_1 = 0.009$ when $c = -0.12$). The system is then stable and the steady state amplitude is 0. Further increases in c_1 first lead to small increases of the relative motions of both, then of only one of the mode shape with the other one exhibiting a decrease. Notwithstanding the increase in c_1, this reduction in relative motion of the mode shape is significant enough to force a reduction of the corresponding modal damping which eventually becomes negative (e.g. for $c_1 = 0.018$ when $c = -0.12$). The equilibrium is then no longer stable. Further increases of c_1 lead to further reductions of the relative motions of that mode which eventually converges to [1 1] as c_1 becomes very large. That is, the motions associated with this unstable mode correspond to the stuck configuration and the steady state response of the system is governed by the van der Pol restoring force on the stuck system, exactly as in the case $\mu \neq 0$.

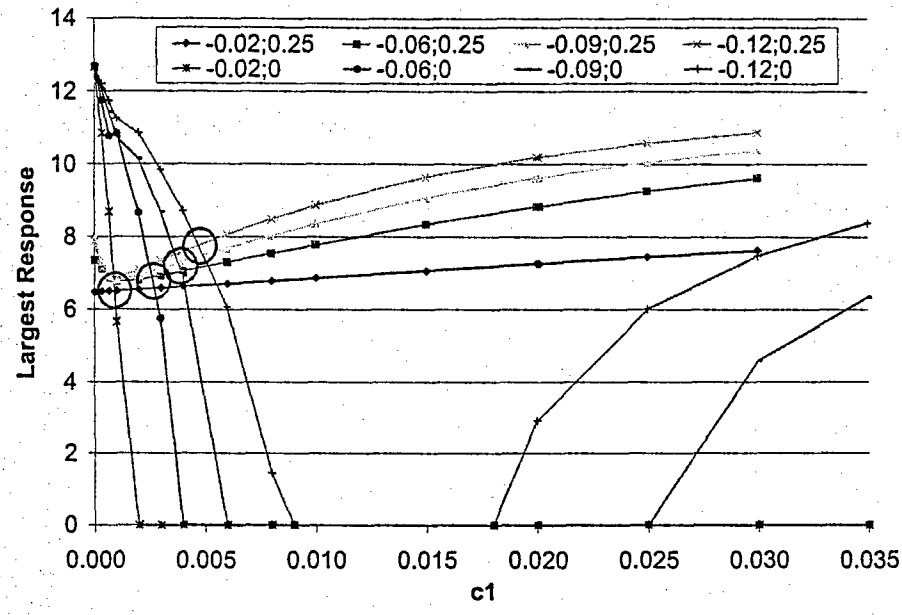

Fig. 2.26 Largest response of mass M_1 as a function of the damping coefficient c_1 for different values of the damping constant c and coefficient of friction μ, noted as $c;\mu$. $k_1 = 0.05$, $\delta = 0.025$. The crossings between the corresponding $\mu = 0$ and $\mu = 0.25$ curves are circled in red.

A comparison of the curves of Fig. 2.20 and 2.25, see Fig. 2.26 for a few values of c, is of particular interest. Most importantly, note that the curves corresponding to $\mu = 0.25$ and $\mu = 0$ cross each other at a relatively low value of the damping coefficient c_1. For values of c_1 smaller than this threshold, the largest response of the steady state motions of the system with friction is less than its frictionless counterpart. On the contrary, for values of c_1 larger than the threshold, the frictionless system is the one exhibiting the smallest response. In fact, in the interval $c_1 \in [0.009, 0.018]$ (for $c \geq -0.12$), the frictionless system returns to equilibrium while the one with friction maintains a fairly large amplitude limit cycle oscillation! In this case, friction may

significantly increase the LCO amplitude, albeit it is a purely dissipating mechanism. The explanation of this surprising observation resides in the sticking potential of friction. Consider for example the response of the system with $c_1 \in [0.009, 0.018]$ and $c \geq -0.12$ to a small perturbation. As explained above, the frictionless system has a stable equilibrium for these parameter values and thus the perturbation decreases with time, returning to zero after an infinite time. The system with friction does not exhibit this behavior. Specifically, at the first occurrence of a zero relative velocity, the system becomes stuck because the forces involved (inertia, dashpot c_1, and spring k_1) are too small to maintain slip. Accordingly, there is no more dissipation and the response of the primary mass increases rapidly under the action of the negative dashpot. Eventually, the response becomes large enough to force slipping and dissipation resumes in both the dashpot c_1 and the friction element and convergence to a limit cycle takes place. If this limit cycle is perturbed, for example through a reduction of the responses of the two masses, sticking will occur at the next occurrence of a zero relative velocity and the motion will then grow back under the sole action of the aerodynamic effects (negative dashpot).

It is thus concluded that friction does not always lead to a decrease of the amplitude of LCO.

2.4 Harmonic Balance

The harmonic balance method is an approximate technique for the estimation of the periodic steady state response of nonlinear systems. In this approach, the response is

assumed in the form of a limited Fourier series the unknown constants of which are evaluated by matching as many $\cos n\omega t$ and $\sin n\omega t$ components as possible in the equations of motion. Note in the present context of self excited vibrations that the fundamental frequency ω is also unknown.

The harmonic balance method will be used here to obtain an approximation of the continuous slip response of the system of Fig. 2.5. At the contrary of the exact formulation, this development is not seriously affected by the value of k_1 and thus was carried out directly in the general case $k_1 \neq 0$ and then particularize to $k_1 = 0$ for comparison with the exact formulation and the numerical simulation results. It might seem at first that the displacements of the two masses should both be expressed as sine and cosine of all frequencies $n\omega t$ but it should be recognized that the system of Fig. 2.5 is time invariant and thus that any specific time can be considered as the temporal origin t=0. It is particularly convenient here to select this point to match a maximum value of the relative displacement of the two masses. Under this condition, a single harmonic approximation of the system response is

$$x_1 = A_z \cos \omega t + B_z \sin \omega t \text{ and } y = x_2 - x_1 = Y \cos \omega t . \qquad (2\text{-}35)$$

Next, it is required to obtain the corresponding representation of the nonlinear forces, i.e. the force of friction here. Given the above form of the relative response, it is directly found that a one term Fourier series is

$$\mu_D N \operatorname{sgn}(\dot{x}) \approx \frac{4\mu_D N}{\pi} \sin \omega t \qquad (2\text{-}36)$$

The estimation of the unknown parameters A_z, B_z, Y, and ω is then achieved by introducing Eq. (2-35) and (2-36) in the equations of motion

$$M_1\ddot{x}_1 + c\dot{x}_1 + (k+k_1)x_1 - k_1x_2 = F_{31} \text{ and } M_2\ddot{x}_2 - k_1x_1 + k_1x_2 = -F_{31} \quad (2\text{-}37)$$

where

$$F_{31} = \mu_D N \operatorname{sgn}(\dot{x}_2 - \dot{x}_1). \quad (2\text{-}38)$$

This process leads to a set of four nonlinear algebraic equations for the unknowns. After some manipulations, it was found that

$$(\sigma - rp^2)\left[(1-p^2)(1-p^2-rp^2) + 4\zeta_2'^2 p^2\right] - \sigma r p^2(1-p^2-rp^2) = 0 \quad (2\text{-}39)$$

$$B_z = -\frac{4}{\pi r p^2}\frac{\mu_D N}{k}; \; A_z = \frac{(r+1)p^2 - 1}{2\zeta_2' r p^3}\frac{4\mu_D N}{\pi k} \quad (2\text{-}40)$$

and

$$Y = \frac{rp^2}{(\sigma - rp^2)} A_z \quad (2\text{-}41)$$

where

$$p = \omega/\omega_2'; \; r = M_2/M_1; \text{ and } \sigma = k_1/k \quad (2\text{-}42)$$

The solution of Eq. (2-39) is achieved first to yield the value of the frequency p. The remaining parameters are then estimated from Eqs (2-40) and (2-41). When the stiffness k_1 vanishes, the cubic characteristic equation (Eq. 2-39) is easily solved to yield

$$p^2 = 1 - \frac{\left(r + 4\zeta_2'^2\right) \pm \sqrt{\left(r + 4\zeta_2'^2\right)^2 - 16\zeta_2'^2(1+r)}}{2(1+r)}. \quad (2\text{-}43)$$

A two-frequency harmonic balance approximation was also obtained by considering both ωt and $3\omega t$ sine and cosine terms in both $x_1(t)$ and $y(t)$. That is,

$$x_1 = A_1 \cos\omega t + B_1 \sin\omega t + A_3 \cos 3\omega t + B_3 \sin 3\omega t \tag{2-44}$$

and

$$y = x_2 - x_1 = C_1 \cos\omega t + D_1 \sin\omega t + C_3 \cos 3\omega t + D_3 \sin 3\omega t\,. \tag{2-45}$$

Since the temporal origin t=0 is selected to correspond to a peak of the relative response, one must have $\dot{y}(0) = 0$ or

$$3\,D_3 + D_1 = 0\,. \tag{2-46}$$

Further, the 2-harmonic Fourier series of the friction force is easily shown to be

$$\mu_D N \,\mathrm{sgn}(\dot{x}) \approx \frac{4\mu_D N}{\pi}\sin\omega t + \frac{4\mu_D N}{3\pi}\sin 3\omega t\ . \tag{2-47}$$

Then, introducing Eqs (2-44), (2-45), and (2-47) in the equations of motion, Eqs (2-37) and (2-38) and comparing terms in $\sin\omega t$, $\cos\omega t$, $\sin 3\omega t$ and $\cos 3\omega t$ leads to the following 8 equations

$$\left(1-p^2\right)A_1 + 2\zeta_2' \,p\,B_1 - \sigma\,C_1 = 0 \tag{2-48}$$

$$-2\zeta_2' \,p\,A_1 + \left(1-p^2\right)B_1 - \sigma\,D_1 = -\frac{4}{\pi} \tag{2-49}$$

$$\left(1-9p^2\right)A_3 + 6\zeta_2' \,p\,B_3 - \sigma\,C_3 = 0 \tag{2-50}$$

$$-6\zeta_2' \,p\,A_3 + \left(1-9p^2\right)B_3 - \sigma\,D_3 = -\frac{4}{3\pi} \tag{2-51}$$

$$-r\,p^2\,A_1 + \left(\sigma - r\,p^2\right)C_1 = 0 \tag{2-52}$$

$$-r\,p^2\,B_1 + \left(\sigma - r\,p^2\right)D_1 = \frac{4}{\pi} \tag{2-53}$$

$$-9\,r\,p^2\,A_3+\left(\sigma-9\,r\,p^2\right)C_3=0 \tag{2-54}$$

$$-9\,r\,p^2\,B_3+\left(\sigma-9\,r\,p^2\right)D_3=\frac{4}{3\pi} \tag{2-55}$$

Equations (2-46) and (2-48)-(2-55) represent a set of 9 equations for the unknown parameters of the response and the frequency p. The solution strategy proceeds as follows. First, Eqs (2-49), (2-51), (2-53), and (2.55) are combined to produce 3 homogenous equations and 1 non-homogenous one. The former equations form with Eqs (2-46), (2-48), (2-50), (2-52) and (2-54) a set of 8 homogenous equations which are linear in the 8 coefficients A_1, ..., D_3 for a given value of p. To obtain a non-trivial solution, it is thus required that p be chosen so that the determinant of the matrix of coefficients of these equations vanish. The nonlinear equation resulting from this condition is a polynomial of order 16 in p. For each of its roots, the coefficients A_1, ..., D_3 can then be evaluated by solving the system of linear equations formed by 7 of the 8 homogenous equations and the non-homogenous one.

The above procedures were followed to obtain 1- and 2-harmonic approximation of the continuous slip response of the system of Fig. 2.5 and their accuracy was assessed by comparison with the numerical simulation and/or the exact formulation. The special case $k_1 = 0$ was considered first and the results are presented in Fig. 2.4. Clearly, there are two frequencies satisfying Eq. (2-43) (one for the + sign, the other for the - sign) and thus the harmonic balance solution yields two estimates of the continuous slip solution, one of which (R) approximates the true response while the other is a fictitious solution (F). It is seen from Fig. 2.4 that the accuracy of the harmonic balance (solution R) is not

very good in the small domain of existence of these continuous slip solutions. Further, the inclusion of a second harmonic does not seem to improve substantially the accuracy of the estimates of the amplitude and frequency of response, see Fig. 2.4 in which (HBM)-CS and (HBM2)-CS are the 1- and 2-harmonic approximations of the continuous slip solutions.

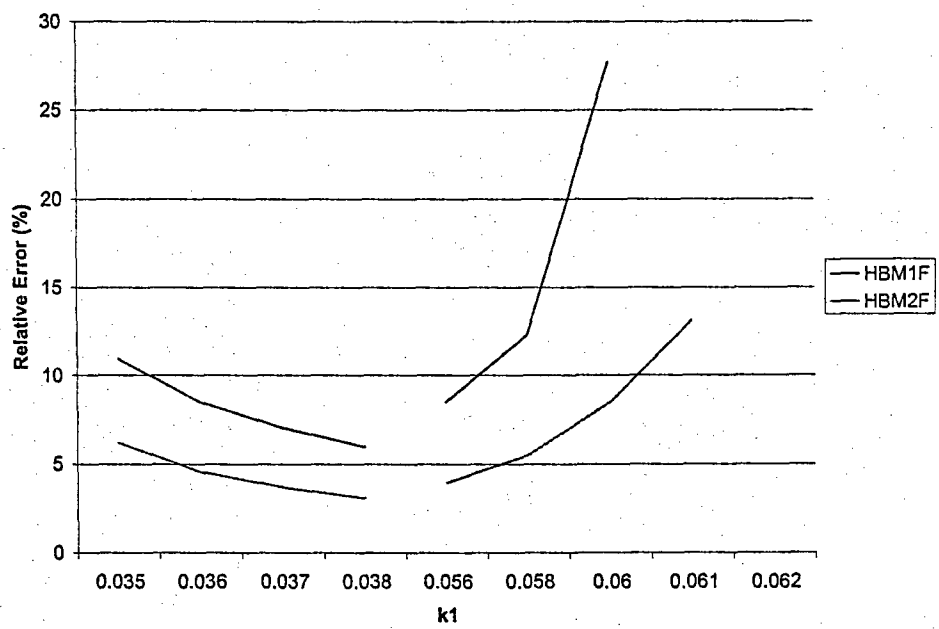

Fig. 2.27 Relative errors (in %) in the maximum response of mass M_1 as predicted by the harmonic balance method with 1 and 2 harmonics as functions of k_1, $M_2 = 0.05$, $c = -0.07$ (Note the split horizontal axis).

The accuracy of the harmonic balance method was also assessed for a broad range of $k_1 \neq 0$ situations. Shown in Fig. 2.27 are typical relative errors on the maximum response obtained in the SFCS domain by using the 1- and 2-harmonic approximations and corresponding to a frequency close to the one obtained by numerical simulation.

Given these good qualitative results, the harmonic balance method was also used to estimate the boundary of the stabilization domain, see the curves HBM1F and HBM2F on Fig. 2.6. It appears from all these results that the harmonic balance estimates were qualitatively correct in predicting the amplitude of the response and that the addition of a second harmonic provided an improved quantitative matching with the simulation results.

The difference in accuracy of the harmonic balance method for $k_1 = 0$ and $k_1 \neq 0$ may result from the naturally harmonic character of the response of the sliding mass in the latter case as opposed to the parabolic time histories obtained in the former case.

CHAPTER 3

DESIGN AND TESTING OF A FRICTION DEVICE

The second part of this thesis focuses on the design, fabrication, and testing of a friction device similar to the disk-torsional spring system of Fig. 1.2 which was later tested in the Deutsches Zentrum für Luft und Raumfahrt (DLR) transonic wind tunnel. The results of Chapter 2 serve here as stepping stone for the parameter selection of the device components.

3.1 Design and Fabrication

The initial plan for the friction device was an installation inside the airfoil, consistently with Fig. 1.2, but this option led to some daunting challenges, e.g. fabricating a novel airfoil (cost constraint), fabricating a novel airfoil with enough space internally for the device, having access to the device once the airfoil was finished, etc. In this light, it was proposed by DLR to mount the device rigidly to the airfoil but outside of the wind tunnel, i.e. on the balance rigs located on either side of the wind tunnel and airfoil. The first bending natural frequency of the airfoil is known to exceed 100Hz while the vibrations of the device were expected to take place near the flutter frequency, i.e. around 30Hz. It was thus argued that the airfoil would appear rigid and thus that the 2-dimensional character of the problem would not be compromised by the friction mechanism being lumped at the ends of the airfoil as opposed to being distributed along the span.

Even then, the design of the friction device was very substantially constrained in regards to weight, size, and to a smaller extent cost. From the standpoint of validation of the present findings, it was desired to achieve an inertia ratio of at least 5% for the effects of friction to be most noticeable but to maintain the occurrence of the flutter/LCO in the transonic range, it was necessary to limit this ratio to about 3%. The size limitations originated from the need to maintain the balance rig in its present configuration.

The lack of access to the balance rig, and thus to the friction devices, during the wind tunnel testing was the next important issue to be resolved. Indeed, to minimize the forces on the wind tunnel walls and to permit the use of porous walls, the central section of the wind tunnel, including the balance rigs, is confined to a plenum which is depressurized, and thus not accessible, during the operation of the wind tunnel. Further, repressurization is possible when the wind tunnel is down but the repressurization/ depressurization process requires about 1 hour, i.e. a significant portion of the total testing time available. For validation of the theoretical results, it was however desired to proceed with a parametric study of the effects of the disk properties (inertia I_D and/ or stiffness k_D) and friction force (μN) on the response of the airfoil-device system. This situation motivated the search for ways to vary the inertia/stiffness of the disk and the friction force remotely. While no simple means for changing the inertia/ stiffness remotely was devised, it was decided to vary the friction force by regulating the normal force through the compression of linear springs by a linear actuator.

While the use of linear actuators provided the remote variation capability desired, it also incurred a large increase in dead weight incompatible with the tight limits of mass

and inertia to maintain the LCO in the transonic range. The only solution found to this problem was the mounting of the actuator system on the *laboratory fixed* frame of the balance rig. The solution of the weight issue then triggered a new problem: the transmission of the normal force and normal force only (no tangential force nor moment) from the laboratory fixed actuator system to the disk moving in the plane perpendicular to the force to be applied. This last significant difficulty was resolved primarily through the use of the cage of a thrust ball bearing inserted between the disk and the actuator system. The well lubricated balls of the bearing allowed the relative motion, transferred the normal force, and generated only a minimal side (tangential) force with good lubrication. Finally, the offset of the normal forces on the actuator and the disk induced by the motion of the latter would normally generate a moment on the actuator system (severely limited by the manufacturer) and potentially (through any deformation) a non-uniformity of the pressure applied on the disk. Both of the potential issues were resolved by inserting a spherical ball contact along the path of the force transmission in the actuator system. That is, the actuator system pushed on the ball which then in turn pushed on the thrust bearing cage. The point contacts between the ball and the contacting shaft insured the transmission of a normal force only.

The detailed design of the friction device and actuator system was then undertaken, with regular interaction with DLR, within the software SolidWorks using an accurate CAD/CAM model of the balance rig provided by DLR. The final detailed model, shown in Fig. 3.1-3.3, can be summarized as follows. The torsional frictional device is composed of a disk connected to the airfoil (outside of the wind tunnel section)

through a torsional spring machined to a specific stiffness. The disk is sandwiched between two steel rings providing the friction. The normal force is provided by the actuator system shown on the right in Fig. 3.3, i.e. generated by a linear actuator based on a step motor. The motor pushes on three parallels springs to generate a controllable force the magnitude of which is monitored through a load cell mounted in series and a LVDT recording the translation of the motor. The force is then transmitted from the load cell to a small spherical ball, thereby preventing the transmission of anything else than a normal force, and then to a "thrust washer". This subsystem is composed of a disk and the cage of a thrust bearing, the latter of which is squeezed between the thrust washer disk and the external friction ring of the device. The bearing cage permits the transmission of the normal force even with relative motion of the two disks (thrust washer and friction disks). Note that the bearing cage was loosely held in place (preventing it from falling) by three springs connected to long arms themselves attached to the support of the actuator system. The actuator permits the variation of the normal force while a change of the natural frequency of the frictional device is allowed by the addition/removal of masses at the periphery of the disk and through the switch of torsional springs (2 different stiffnesses were available).

The fabrication of the various parts was performed by the two ASU machine shops as well as an outside machine shop.

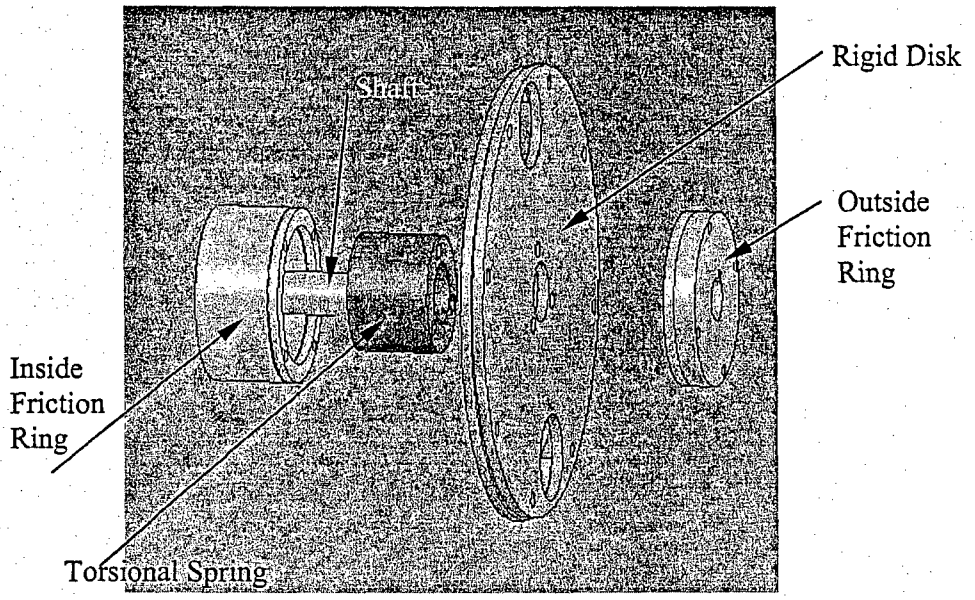

Fig. 3.1 Exploded view of the disk, spring, and friction ring system.

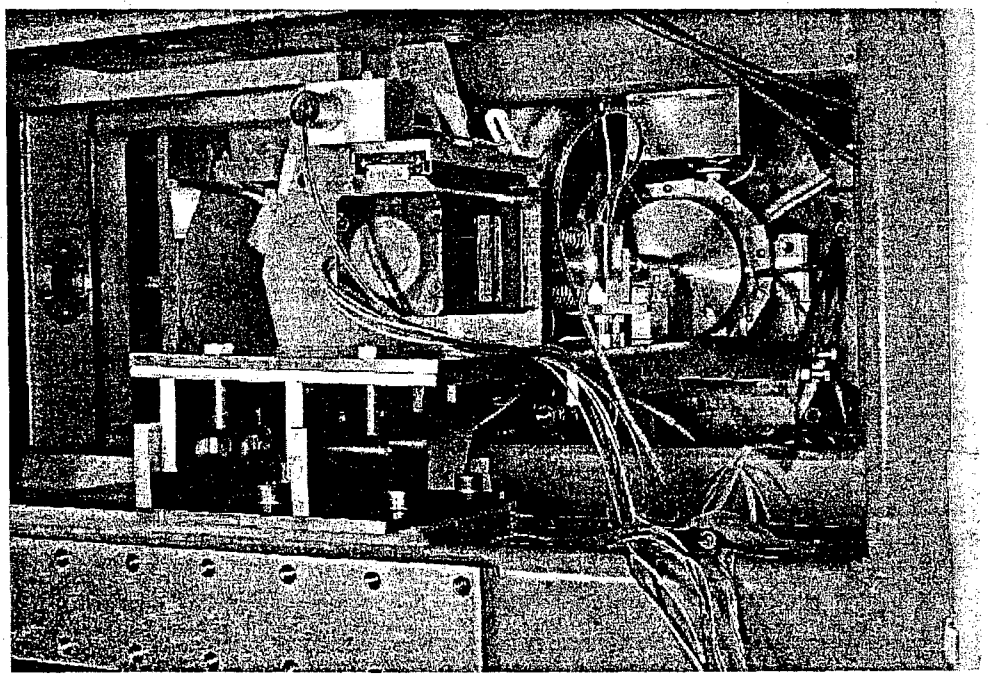

Fig. 3.2 Complete view of the airfoil, friction device, and actuator system in the balance rig in the DLR wind tunnel.

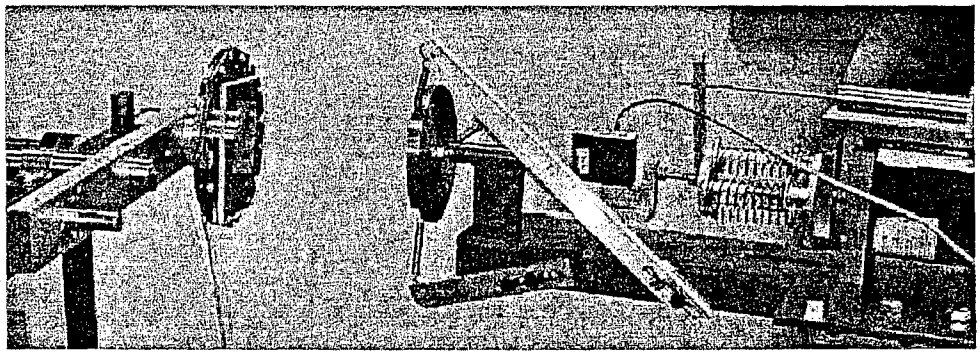

Fig. 3.3 Complete view of the friction device and actuator system in ASU vibrations laboratory.

3.2 Instrumentation

The instrumentation of the DLR wind tunnel permits the measurement of the pressure at a series of locations on the wind tunnel walls, of the lift and moment on the airfoil, of the plunging displacement and pitching angle, and of the displacements at selected locations on the airfoil. Of primary importance for the present validation were the plunging displacement and pitching angle but also the relative angle of torsion θ. This measurement was obtained through the reading of the strain in the coils of the torsional spring (from a strain gauge mounted directly on the thin coils). The calibration factor between angle and strain was obtained experimentally for each spring. The procedure for exciting and controlling the airfoil and other details on the experimental capabilities were the same as those used in prior investigation of transonic LCO at DLR.

3.3 Testing in ASU Vibrations Laboratory

The primary purpose of the testing that took place in the ASU Vibrations Laboratory was to validate the design and fabrication, i.e. to demonstrate that relative

motions of the disk with respect to its support could take place and that these motions could be controlled by the force actuator. In particular, it was desired to assess the capability of the device to exhibit stick, stick-slip, and continuous slip motions. To this end, the device was mounted on a bar of a design similar to the device support in the wind tunnel. This bar was then attached to a frame, itself mounted on the Ling shaker of the ASU Vibrations Laboratory as to impart plunging and mostly pitching of the bar. The shaker was used to provide a harmonic excitation at or near 30Hz, i.e. similar to what could be expected in the wind tunnel. The normal force applied was varied to assess the capability of the device to exhibit the required motions.

The exact classification of the observed motions was not always very easy because of the noise present in the measurement, about 10 microstrains. Nevertheless, it is believed that all three types of motions were indeed noted. Stuck motions were observed for low excitation levels from the shaker and large normal forces as expected and are not discussed further here. Continuous slip responses were initially noted at zero normal force, see Fig. 3.4, but also for nonzero forces, see Figs 3.5 and 3.6. Stick-slip motions were observed first, see Figs 3.7 and 3.8, with sticking taking place at the peak displacements but an intermediate, asymmetrical sticking phase has also been encountered, see Figs 3.9 and 3.10. It is unclear what created the asymmetry in the response, two possible sources are the torsional-axial coupling of the spring and/or the variations of the normal force (see the load cell time history on Figs 3.9 and 3.10) which could have resulted from vibrations of the shaker. In regards to the former issue, note that the spring wants to displace axially as it is twisted in a direction (compression or

extension) that is dependent on the direction of torsion (clockwise or counterclockwise). If the force applied by the friction rings is not the same on the two sides, this axial-torsion coupling would induce a variation of the normal force that is related to the torsion angle which might produce the asymmetrical behavior observed.

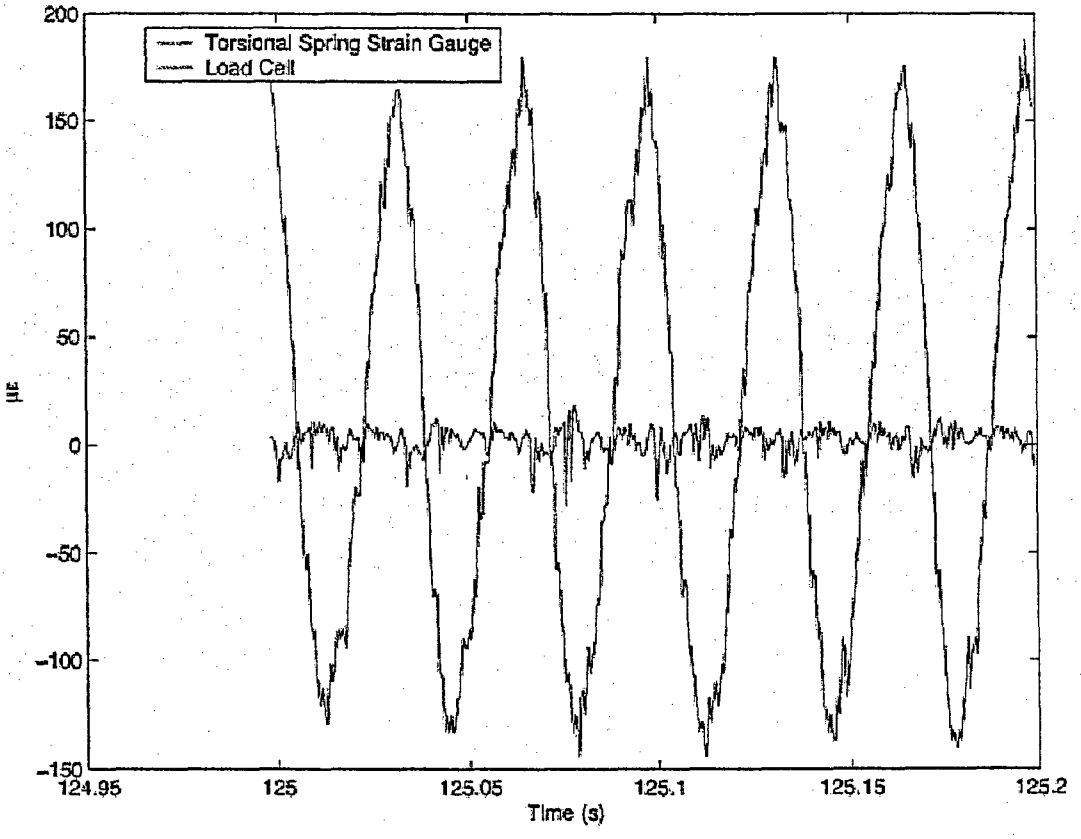

Fig. 3.4 Continuous slip response with zero normal force at 30Hz excitation.

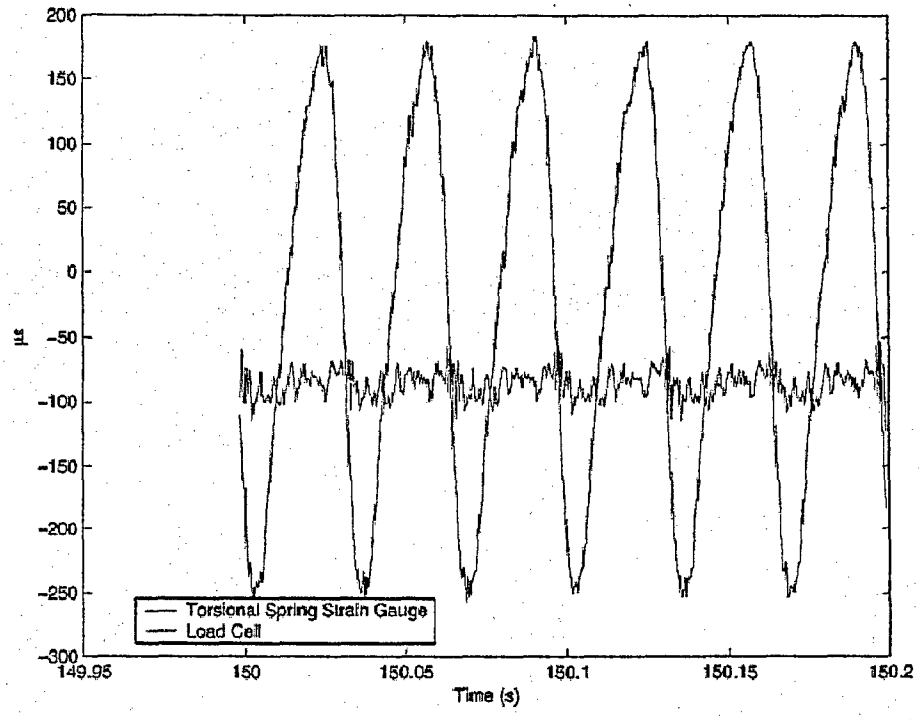

Fig. 3.5 Continuous slip response with nonzero normal force at 30Hz excitation.

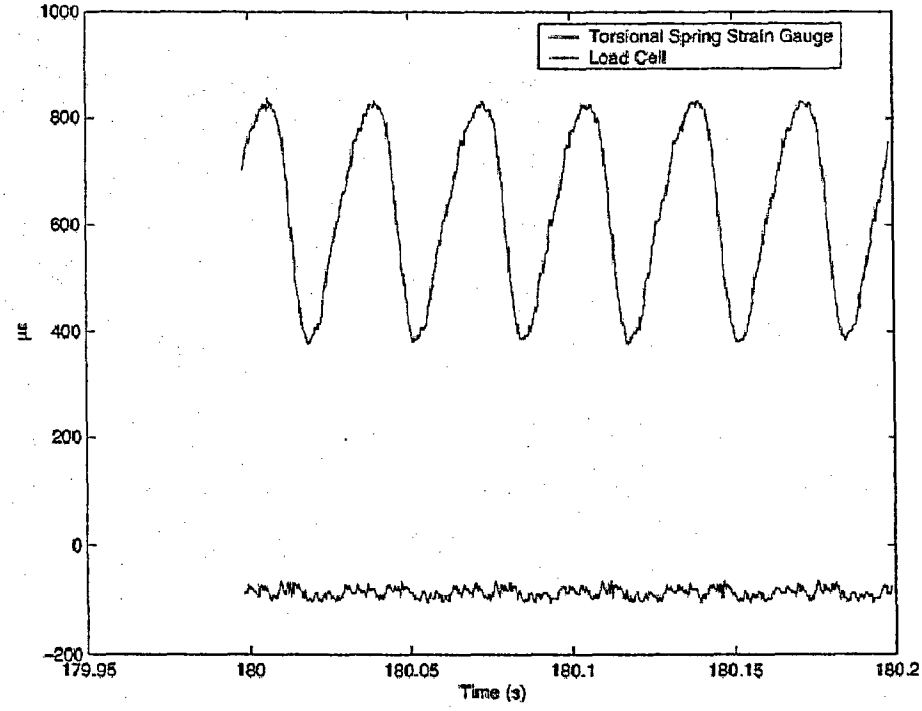

Fig. 3.6 Continuous slip response with nonzero normal force at 30Hz excitation.

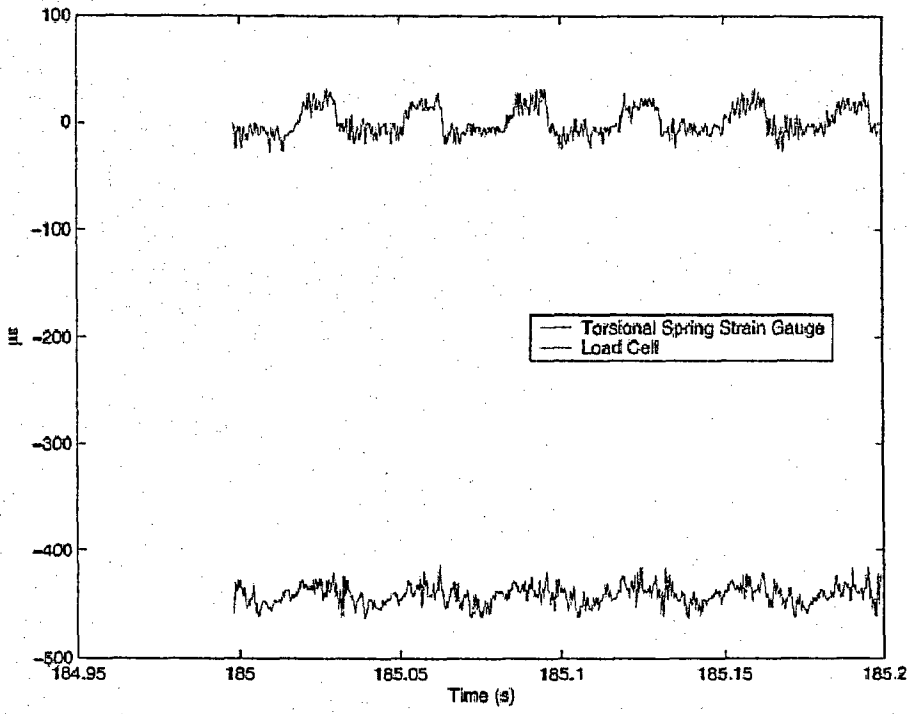

Fig. 3.7 Stick-slip response with nonzero normal force at 30Hz excitation.

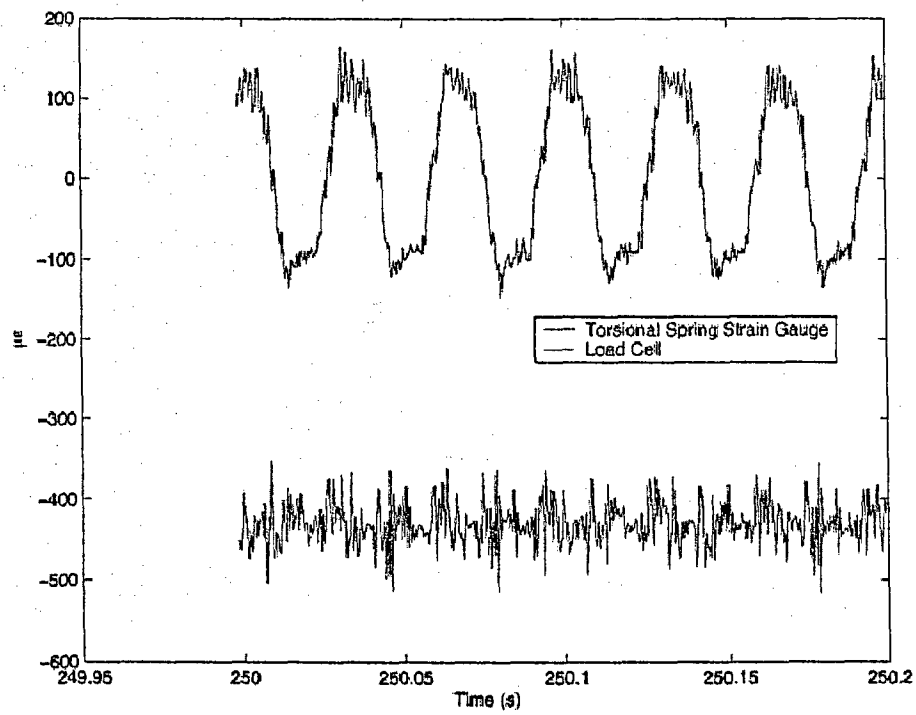

Fig. 3.8 Stick-slip response with nonzero normal force at 30Hz excitation.

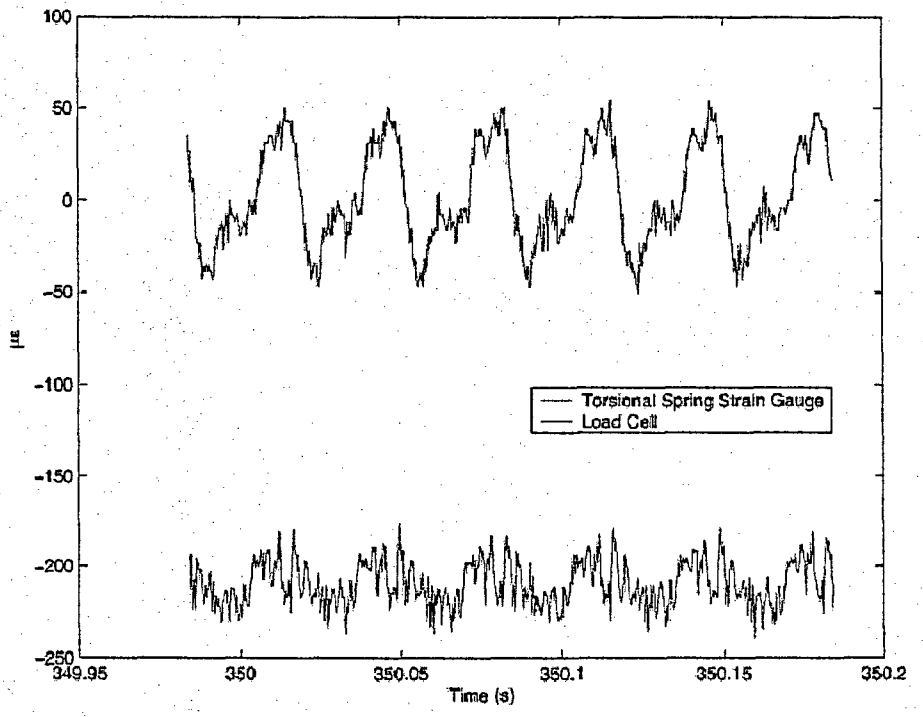

Fig. 3.9 Stick-slip response with nonzero normal force at 30Hz excitation.

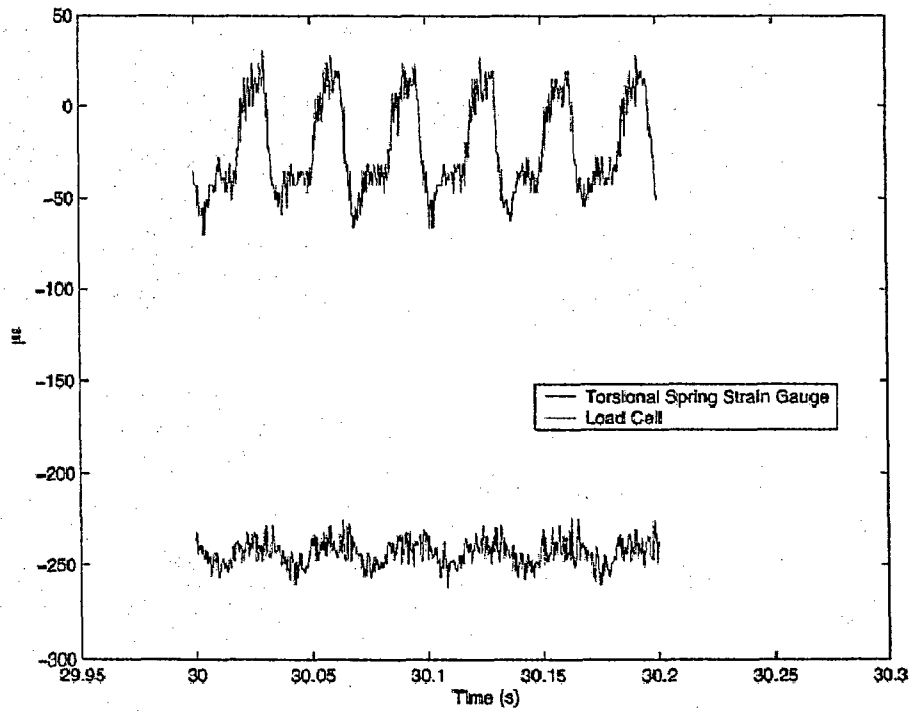

Fig. 3.10 Stick-slip response with nonzero normal force at 30Hz excitation.

3.4 Testing in the DLR Transonic Wind Tunnel

Albeit complex, the friction device/actuator system combination worked perfectly as designed and led, for the first time, to the generation and recording in the DLR wind tunnel of transonic limit cycles with active internal friction at Mach numbers close to 0.6.

The first important observation to be drawn is that such experimental analyses are possible and that internal relative motions can indeed be excited in LCO scenarios.

Some of the recorded LCO are shown in Fig. 3.11 and 3.12. Although only a limited set of LCO records were obtained, some observations can nevertheless be made. Consider for example the evolution of the time histories of the response (plunging, pitching, and torsion) as a function of the Mach number. While the plunging and pitching time histories show a clean single frequency behavior seemingly independent of the Mach number, the relative torsion angle displays a much richer behavior. Indeed, for $M_\infty = 0.598$ and neglecting the high frequency noise, the time history of θ appears at first to be almost purely a single frequency solution. A closer inspection however suggests that the rise of θ is steeper than its fall, especially near the peak. As the Mach number is increased, this effect becomes more pronounced and a flattened peak is obtained for $M_\infty \geq 0.606$, suggesting the possibility of a sticking phase. The lack of symmetry of this flattening implies a full Fourier series, including even harmonics at the contrary of the solutions obtained computationally so far.

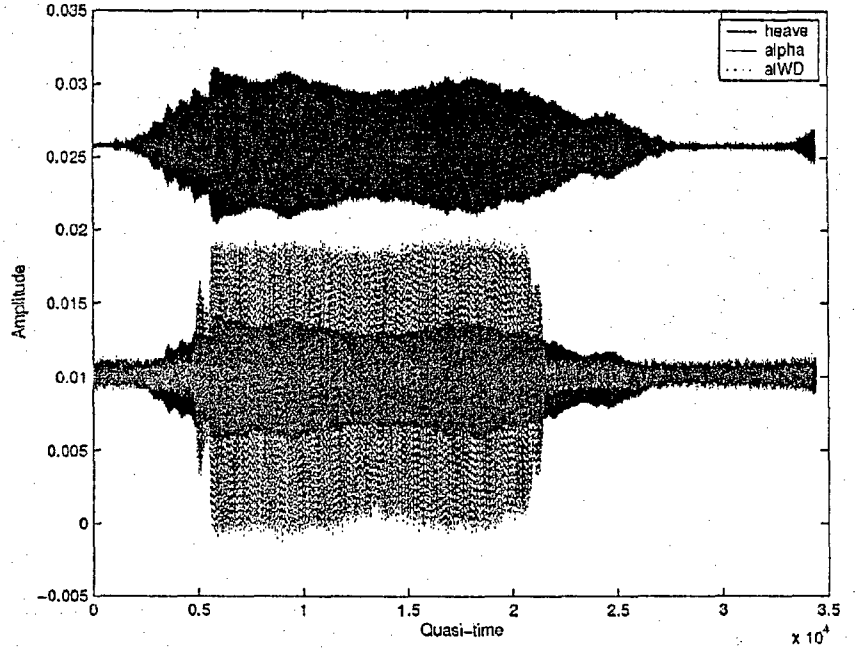

a) $M_\infty = 0.598$

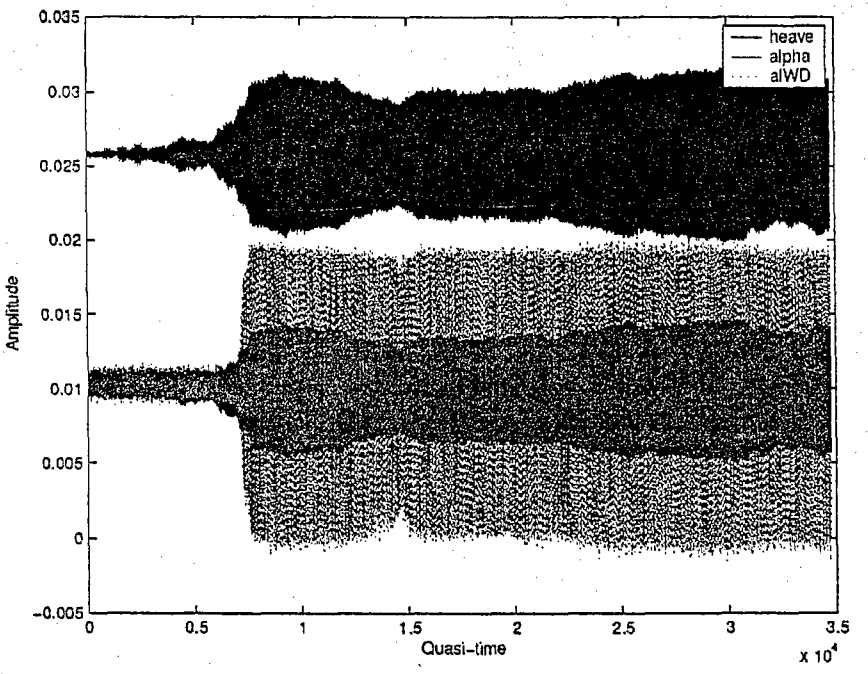

b) $M_\infty = 0.600$

Fig. 3.11 Time histories of the plunging displacement ("heave"), the pitching angle ("alpha"), and the relative torsional angle ("alWD") recorded in the DLR wind tunnel for a normal force of 21 N.

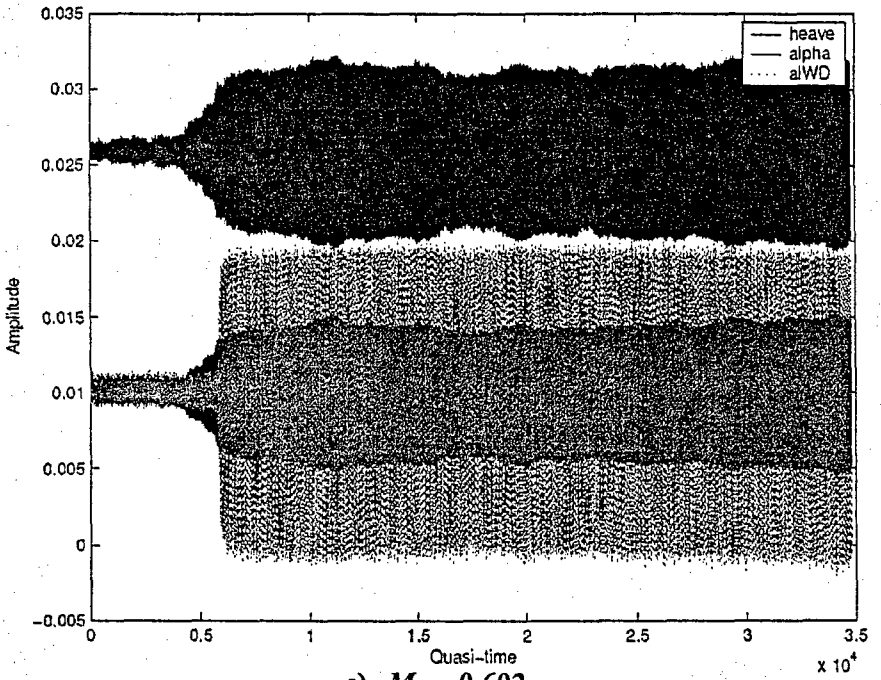

c) $M_\infty = 0.602$

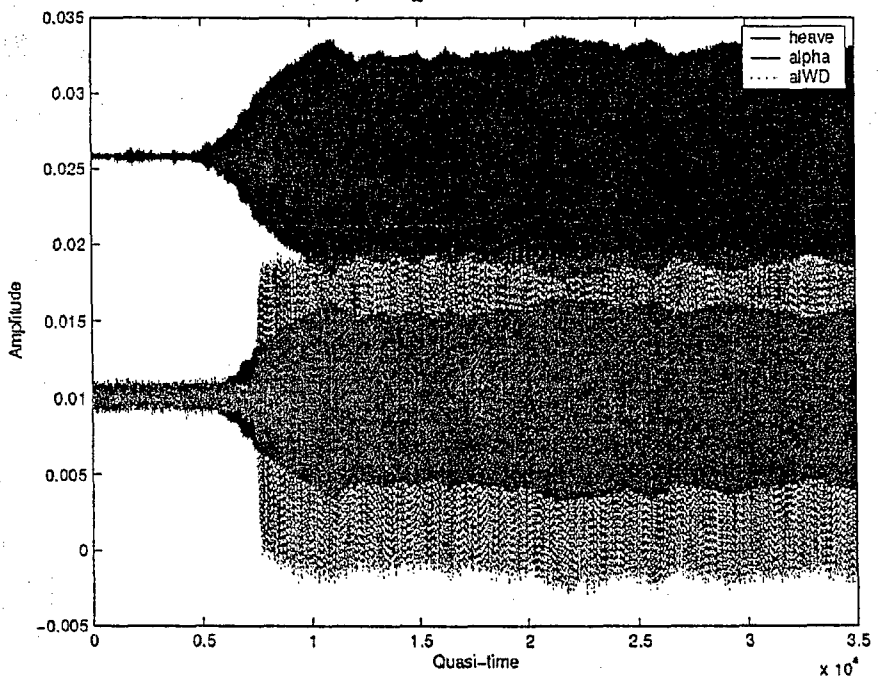

d) $M_\infty = 0.604$

Fig. 3.11, continued

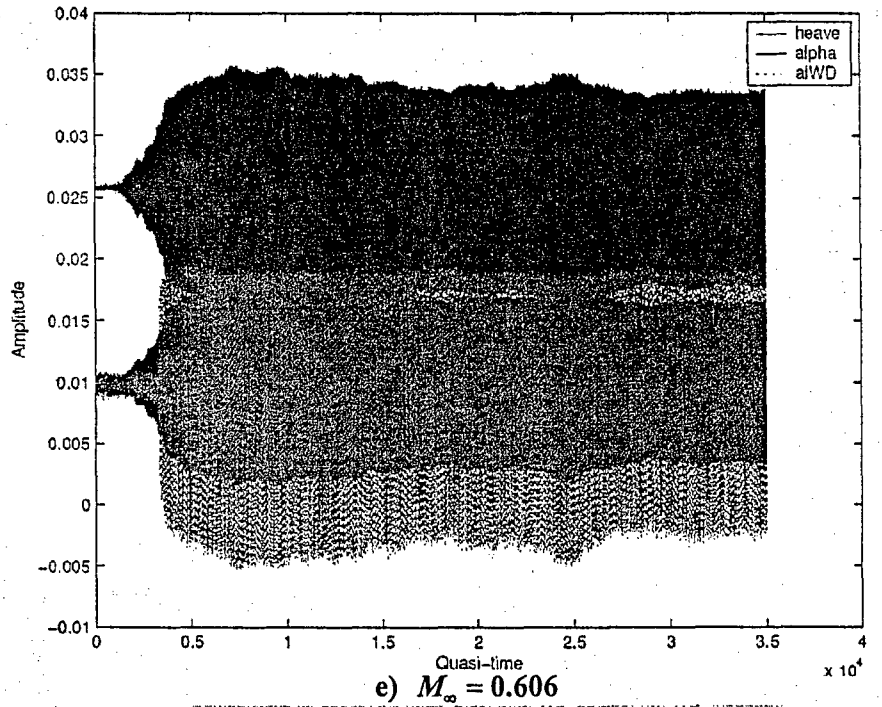

e) $M_\infty = 0.606$

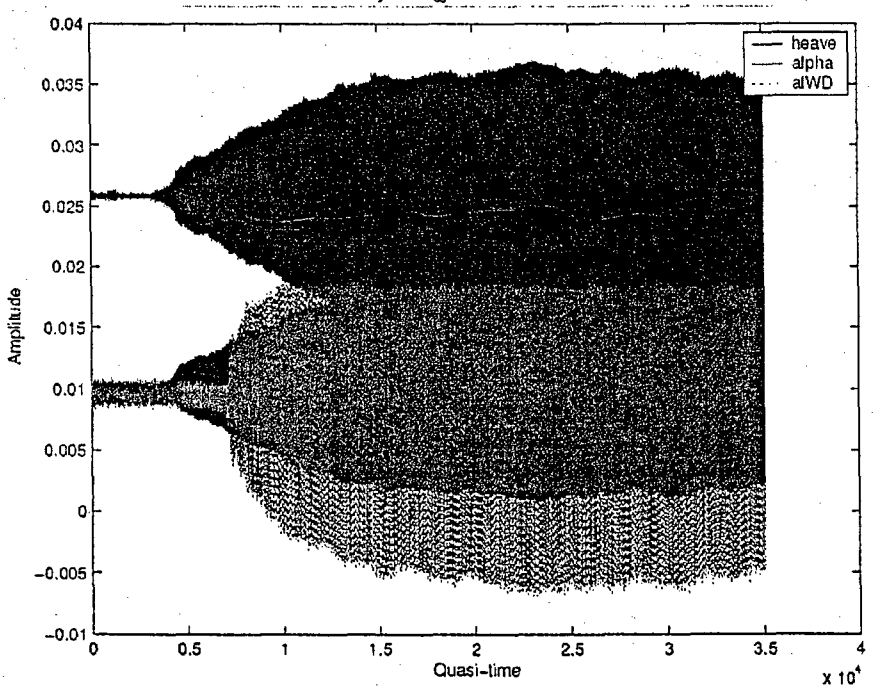

f) $M_\infty = 0.608$

Fig. 3.11, continued

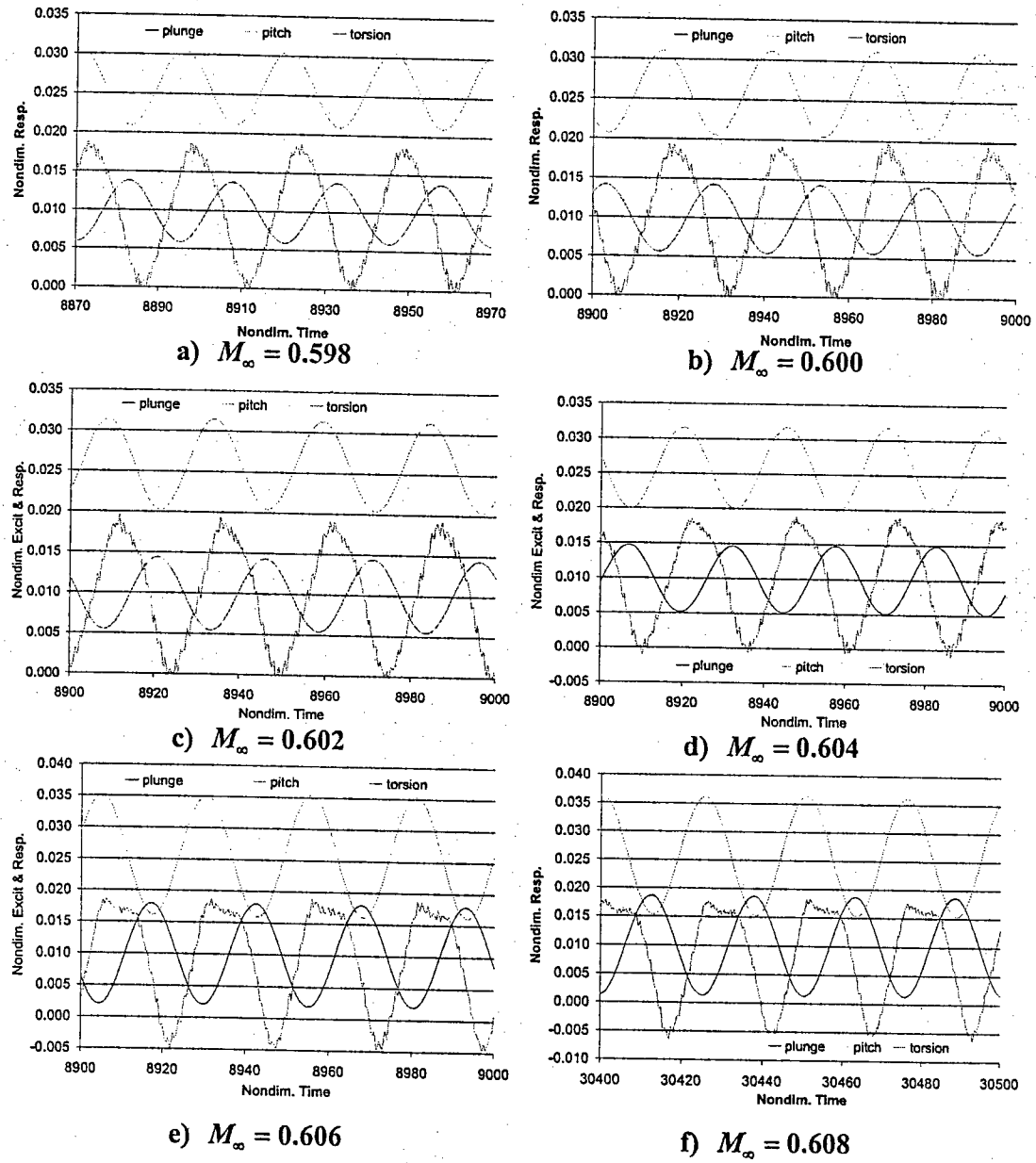

Fig. 3.12 Zoomed time histories of the plunging displacement ("heave"), the pitching angle ("alpha"), and the relative torsional angle ("alWD") recorded in the DLR wind tunnel for a normal force of 21 N.

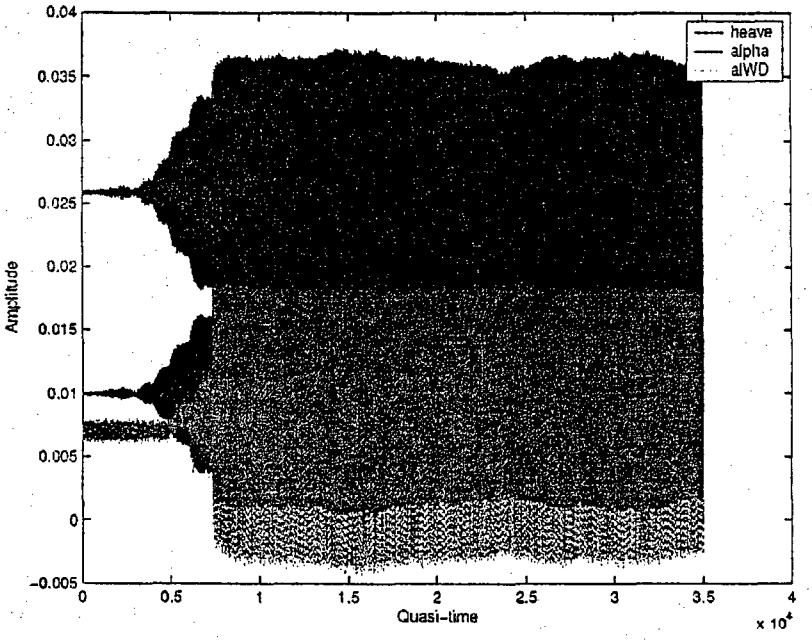

a) Overall time histories at a normal force of 50 N

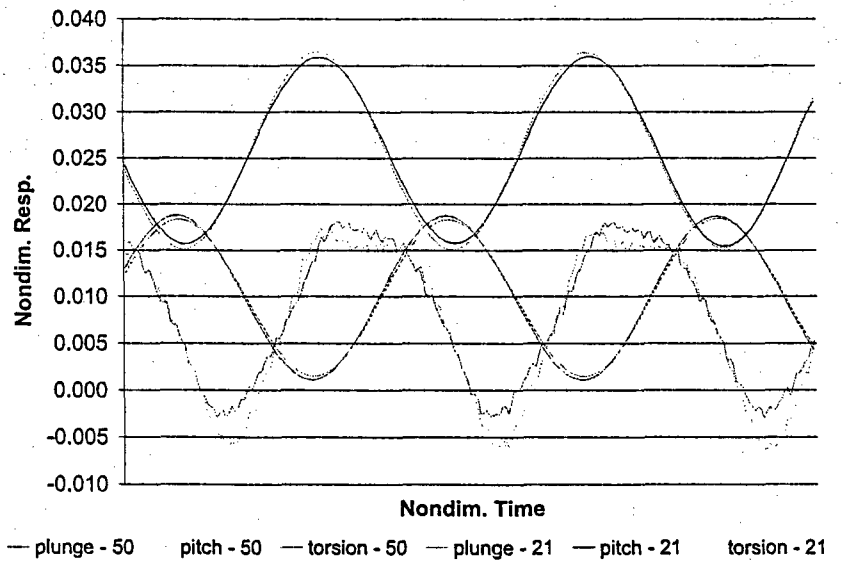

b) Zoomed time histories at a normal force of 50 N

Fig. 3.13 Time histories of the plunging displacement ("heave"), the pitching angle ("alpha"), and the relative torsional angle ("alWD") recorded in the DLR wind tunnel for $M_\infty = 0.608$.

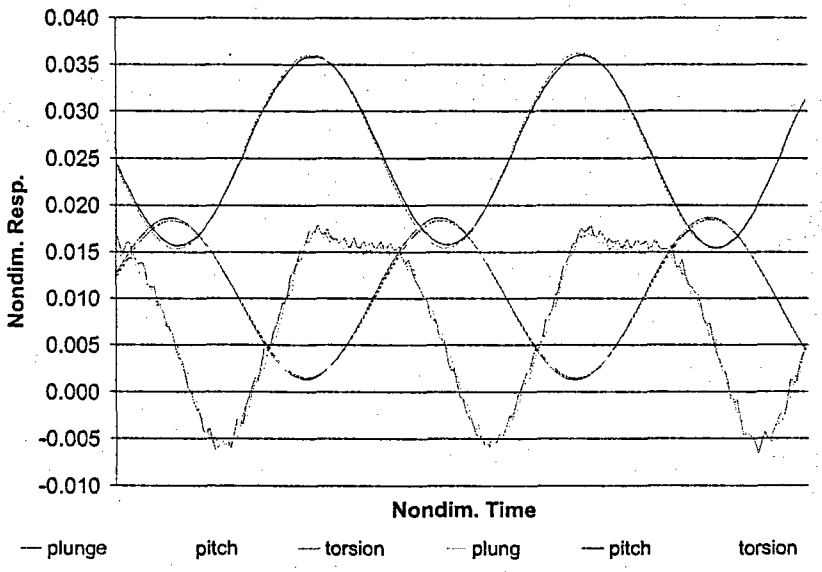

c) Repeatability check at 50 N

Fig. 3.13, continued

What about the effects of the normal force? Shown in Fig. 3.13(a) and (b) are the time histories of the three variables for a Mach number of 0.608 and a normal force of 50N, as opposed to the 21N used in Fig. 3.11(f) and 3.12(f). A comparison of the time histories of the 21N and 50N is given in Fig. 3.13(b) from which it is concluded that the increase in normal force has led to a decrease of the torsional response and, correspondingly, to a small increase in the plunging and pitching amplitudes. The small changes that are involved in Fig. 3.13(b) ought to be confirmed as genuine and not the result of noise or variability. To this end, several cases were repeated to provide a baseline for the assessment of the noise and variability. In fact, a repeat measurement of the LCO for $M_\infty = 0.608$ and a 50N normal force is available and the two sets of time histories are plotted in Fig. 3.13(c). It is clear from this figure that the repeatability is

high so that small differences, such as those noted in Fig. 3.13(b) can indeed be interpreted as genuine changes in the response.

In closing this chapter, it should be noted that the flutter speed of the system in stuck mode was found to be higher than $M_\infty = 0.608$ in an earlier set of tests. In fact, it was necessary to excite the airfoil by a shaker during the tests to obtain the LCO measurements of Figs 3.11-3.13. It is thus concluded from these two observations that the results presented are of a subcritical nature.

CHAPTER 4

CONCLUSIONS

The focus of this thesis has been on the assessment of the effects of internal friction on the response of aeroelastic systems exhibiting either explosive flutter or limit cycle oscillations. In the first part of this work, a two-degree-of-freedom system has been extensively studied that models a wing with an internal, sliding component. The largest mass of the system represents the wing while the smallest one is associated with the sliding component. A dashpot of negative constant was introduced to model the unstable linear aerodynamic effects, while an additional van der Pol restoring force was included to characterize possible stable nonlinear aerodynamic effects. Both of these components were assumed to act only on the largest mass (wing). The sliding mass was finally assumed to be connected to the wing through a friction slider, a spring ($k_1 \geq 0$), and possibly a dashpot (positive viscous damping, $c_1 \geq 0$).

The system was analyzed first without a van der Pol term. Further, in the absence of elastic deformation during sliding, i.e. for $k_1 = 0$, it was shown that an exact procedure can be followed to transform the nonlinear equations of motion into a set of nonlinear algebraic equations and that a stabilization of the unstable aerodynamic forces was possible. The most negative damping that could be stabilized in this configuration was in fact shown to be $2r/\pi^2$ (for $r << 1$) where r denotes the ratio of the two masses of the system. The system was found to exhibit periodic motions with possible stick phases. The introduction of a nonzero spring constant was shown to lead to an increased stabilization potential that is maximum in a "tuned damper" configuration, i.e. when the natural frequency of the primary component (the wing alone) closely matches the natural

frequency of the secondary alone (sliding mass on spring k_1). In addition to this benefit, a broader set of motions was also observed. Besides periodic (referred to as single frequency here) solutions, multiple frequency motions were also found to exist, especially near the tuned damper configuration while the single frequency solutions were typically obtained near the stability border. Both continuous slip and stick slip multiple frequency motions were noted which were shown to be either aperiodic or chaotic. Further, the transition from single to multiple frequency was shown to be a Hopf bifurcation. It was finally observed that the maximum steady state response of the wing is typically minimum for the single frequency motions occurring just next to the bifurcation. A sharp increase in response level is obtained after bifurcation that results from the beating induced by the presence of multiple frequencies.

The inclusion of a van der Pol term did not significantly change the above findings with the noted exception that the system is always stable even in the absence of friction in which case it experiences a continuous slip single frequency motion. In fact, it was observed that the van der Pol term leads to a significant reduction of the large amplitude beating excursions obtained otherwise in connection with multiple frequency solutions and appears to postpone the Hopf bifurcation. In regards to stick slip vs. continuous slip, the decrease in response implied by the presence of the van der Pol term was found to increase the likelihood of stick slip motions which typically occur at lower response levels than continuous slip solutions do. The effects of the coefficients of friction (the static and dynamic coefficients were assumed equal here) was studied next. It was first noted that the amplitude of continuous slip motions (single or multiple

frequency) is linearly scaled by the coefficient of friction and this parameter plays no further role in these cases. When stick phases occur, a more complex dependency on the coefficient of friction is obtained. Next, it was found that 2 stable solutions can be obtained for low coefficients of friction. One such solution has a low amplitude and is dominated by friction effects alone with little influence of the van der Pol term. The reverse statement holds for the other solution, the amplitude is large with the stabilization dictated by the van der Pol force with little effect of friction. As the coefficient of friction increases, these two solutions become closer together and eventually merge. The amplitude of response then appears to increase monotonically with further increases of the coefficient of friction. The effects of a second, viscous damper in parallel to the friction element was finally considered. It was found that the two damping mechanisms do not necessarily reinforce each other and that the friction hinders the viscous dissipation when stick occurs. In fact, nonzero amplitude limit cycle oscillations were noted with friction in situations where the equilibrium (zero response) would in fact be stable without friction.

The second part of the thesis focused on the design, fabrication, and testing of an actual friction device on an airfoil. The basic design of the system is a rotating disk connected to the airfoil by a torsional spring of natural frequency closely matching that of the airfoil to achieve the tuned damper arrangement discussed above. The spring was instrumented with strain gauges to measure the angle of torsion of the system. Finally, a complex system was designed to produce the required normal force to induce friction on the moving airfoil without transmitting any shear or moment. The preliminary testing of

the system was accomplished in shaker tests conducted in the ASU Vibrations Laboratory. The system was shown to exhibit the basic motions expected, i.e. continuous slip and stick slip responses. The friction device was then installed on a NLR 7301 airfoil in the DLR transonic wind tunnel operating at a Mach number near 0.6. Subcritical limit cycle oscillations were observed in which the friction played a significant role. The limited data obtained demonstrates a slight decrease in response by increasing the normal force applied, i.e. by increasing the level of friction.

REFERENCES

[1]Cunningham Jr., A.M. and Meijer, J.J., "Semi-Empirical Unsteady Aerodynamics for Modeling Aircraft Limit Cycle Oscillations and Other Nonlinear Aeroelastic Problems," International Forum on Aeroelasticity and Structural Dynamics, Manchester, U.K., Jun. 1995.

[2]Edwards, J.W., "Transonic Shock Oscillations and Wing Flutter Calculated with an Interactive Boundary Layer Coupling Method," Euromech-Colloquium 349 Simulation of Fluid-Structure Interaction in Aeronautics, Göttingen, Germany, Sep. 1996.

[3]Dowell, E.H., "Panel Flutter: A Review of the Aeroelastic Stability of Plates and Shells," *AIAA Journal*, Vol. 8, No. 3, 1970, pp. 385-399.

[4]Conner, M.D., Tang, D.M., Dowell, E.H. and Virgin, L.N., "Nonlinear Behavior of a Typical Airfoil Section with Control Surface Freeplay: A Numerical and Experimental Study," *Journal of Fluids and Structures*, Vol. 11, 1997, pp. 89-109.

[5]Tang, D.M., Dowell, E.H. and Virgin, L.N., "Limit Cycle Behavior of an Airfoil with a Control Surface," *Journal of Fluids and Structures*, Vol. 12, 1998, pp. 839-858.

[6]Chen, P.C., Sarhaddi, D. and Liu, D.D., "Limit Cycle Oscillation Studies of a Fighter with External Stores," AIAA-98-1727.

[7]Mignolet, M.P., Liu, D.D., and Chen, P.C., "On the Nonlinear Structural Damping Mechanism of the Wing/Store Limit Cycle Oscillation," *Proceedings of the 40th Structures, Structural Dynamics, and Materials Conference*, St. Louis, Missouri, Vol. 3, Apr. 12-15, 1999, pp. 2148-2161.

[8]Sinha, A., and Griffin, J.H., "Friction Damping of Flutter in Gas Turbine Engine Airfoils," *Journal of Aircraft*, Vol. 20, 1983, pp. 372-376.

[9]Sinha, A., and Griffin, J.H., "Effects of Friction Dampers on Aerodynamically Unstable Rotor Stages," *AIAA Journal*, Vol. 23, 1985, pp. 262-270.

[10]Tang, D., Gavin, H.P., Dowell, E.H., "Theoretical/Experimental Study of Gust Alleviation Using An Electro-Magnetic Dry Friction Damper," *44th Structures, Structural Dynamics, and Materials Conference*, Apr. 7-10, 2003, Norfolk, Virginia. Paper AIAA 2003-1520.

[11]Choi, G.G., *Effects of Internal Friction on Aeroelastic Systems*, M.S. Thesis, Arizona State University, May 2005.

[12]Dietz, G., Personal Communication, Sept. 2003.

[13]Tondl, A., "Quenching of Self-Excited Vibrations: Equilibrium Aspects," *Journal of Sound and Vibration*, Vol. 42, No. 2, 1975, pp. 251-260.

[14]Tondl, A., "Quenching of Self-Excited Vibrations: One- and Two-Frequency Vibrations," *Journal of Sound and Vibration*, Vol. 42, No. 2, 1975, pp. 261-271.

[15]Tondl, A., "Quenching of Self-Excited Vibrations: Effects of Dry Friction," *Journal of Sound and Vibration*, Vol. 45, No. 2, 1976, pp. 261-271.

[16]Den Hartog, J.P., "Forced Vibrations With Combined Coulomb and Viscous Friction," Trans. of the ASME, APM-53-9, 1931, pp. 107-115.

[17]Pesheck, E., and Pierre, C., "Phase Space Interpretation And Stability Analysis Of A Self Excited, Friction Damped Turbine Airfoil," Proceedings of the ASME Design Engineering Technical Conferences, DETC97/VIB-3913, 1997.

[18]Agelastos, A.M., *A Preliminary Assessment of the Role of Friction in "Hump" Mode Flutter*, Honors Thesis/BSE, Arizona State University, August 2002.

[19]Wiggins, S. *Introduction to Applied Nonlinear Dynamical Systems*, Springer, New York, 1990.

ATTACHMENT B:

THESIS OF GOANG GAE CHOI

EFFECTS OF COULOMB FRICTION ON AEROELASTIC SYSTEM

by

Goang Gae Choi

A Thesis Presented in Partial Fulfillment
of the Requirements for the Degree
Master of Science

ARIZONA STATE UNIVERSITY

August 2005

EFFECTS OF COULOMB FRICTION ON AEROELASTIC SYSTEM

by

Goang Gae Choi

has been approved

July 2005

APPROVED:

_____, Chair

_____

_____

Supervisory Committee

ACCEPTED:

_____

Department Chair

_____

Dean, Division of Graduate Studies

ABSTRACT

The appearance of limit cycle oscillations in aeroelastic systems has usually been associated with nonlinearity in the aerodynamics and/or in the structural restoring forces. It has, however, been recently suggested that nonlinearity in the damping mechanism, more notably friction between a small moving part (or many such parts such as stores and missiles) and the wing, may indeed be a source of post-flutter limit cycle oscillations. The present work provides a numerical validation of this expectation by studying the response at and above flutter of a flat plate and a NACA0012 airfoil both exhibiting an internal friction mechanism and placed in a inviscid and incompressible flow.

The aerodynamic of the flat plate, dictated by the Theodorsen function, is linear and thus the frictionless system is either stable or flutters. Time marching computations were carried out with a rational approximation of the Theodorsen function on the system with an internal friction component. These results demonstrate the existence of a rich collection of limit cycle oscillations in a range of flow speeds extending above the flutter speed of the flat plate with its frictional device stuck by about 3% for a device whose inertia is 5% of the inertia of the flat plate. This significant increase in stability zone demonstrates the good potential stabilization of friction.

The second airfoil, a NACA0012 section also placed in an inviscid, incompressible flow, had been found in earlier studies to exhibit limit cycle oscillations at and slightly above its flutter speed. The inclusion of a friction device is once again seen to be beneficial as significant reductions of the amplitude of the limit cycles (e.g. by a factor of 3) can be obtained by appropriately "tuning" the friction device.

The nature, i.e. periodic, aperiodic, chaotic and continuous vs. stick slip, and magnitude of all limit cycle oscillations encountered are discussed in details.

ACKNOWLEDGEMENT

I would like to express my sincere appreciation to my committee chairman and advisor, Dr. Marc P. Mignolet for his support and encouragement throughout my program of study. It has been a rewarding and gratifying experience to have had the opportunity to engage in this level of education with Dr. Mignolet.

My thanks and appreciation are also extended to Dr. Danny D. Liu for his help and constructive advice throughout the progress of my work. I thank Dr. Liu for his generosity for me to use the facilities of ZONA TECHONOLOGY. It was great opportunity to discuss with brilliant and enthusiastic peoples in ZONA TECHONOLOGY.

I wish to also thank Dr. Kyle D. Squires for his consenting to be one of the committee members on a short notice.

I also thank Dr. L. Tang for his technical and theoretical helping in CFL3D issues.

I would like to thank my family. I thank my parents, Jongsoon Kim and Joonsik Choi for their continued support and confidence in me throughout the period in abroad. Special gratitude is extended to my wife, Sun Hee Byun, without whose assistance, love and encouragement for this work would not have been possible. I thank you all.

Finally, the support of this research by the Air Force Office of Scientific Research under grant F49620-02-1-0066 is gratefully acknowledged.

TABLE OF CONTENTS

CHAPTER Page

Figure Page

Figure Page

CHAPTER 1

INTRODUCTION

Limit Cycle Oscillations (LCO) have been a prevalent aeroelastic problem on several current fighter aircraft. This phenomenon usually occurs for aircraft with external stores throughout, but not limited to, the transonic flight regime[1,2], although a business jet wing LCO was also reported recently[3]. Complicated by the problem geometry, e.g. the aircraft-store system, the LCO mechanisms still remain to be fully understood. In fact, there exist few analytical techniques available for LCO prediction and an insufficient understanding of its physics.

With aerodynamic feedback, LCO are sustained periodic oscillations which neither increase nor decrease in amplitude over time for a given flight condition. A series of researchers, notably Cunningham and Meijer[4], believe that the wing/store LCO is a purely aerodynamics phenomenon, largely due to transonic shock oscillation and shock induced flow separation. This LCO scenario, which is referred to as the Transonic Shock/Separation (TSS) model, has been suggested by Edwards to be, with viscous effects, one of the major factors contributing to transonic LCO for wings[3].

In 1998, Chen, Sarhaddi and Liu[2] offered a radically different LCO model based on the observation that wing/store LCO can be a post-flutter phenomenon whenever the flutter mode contains low unstable damping. This type of flutter mode is called a "hump

mode". Since the aircraft structure usually exhibits some structural nonlinearity, such as friction, free-play, etc., the moderate growth of amplitudes corresponding to the low negative aerodynamic damping may be suppressed. The result is then a steady state oscillation. The consideration of friction in wing/wing-store LCO studies is rather recent[5]. Here it is referred to as the nonlinear structural damping (NSD) model of the wing/store LCO.

It should be noted that the consideration of friction in flutter analyses is not new, as it is recognized in the turbomachinery community that the friction at the blade root and in shrouds plays a definite stabilizing role. In fact, this observation has led to the use of specially designed friction-based damping systems, referred to as "underplatform" dampers, to damp blade vibrations and increase the flutter speed (e.g. see Ref. 6 and 7). Notwithstanding these similarities, there are substantial differences in the aerodynamic/structure interactions in wing/wing-store LCO and in the turbomachinery blade flutter that render each problem specific.

In light of the above discussion the focus of the present investigation and of a companion one, Ref. 8, is on providing a validation of the potential of friction to stabilize an unstable aerodynamics and/or affect the magnitude of existing limit cycle oscillation.

The purely structural dynamic set up of Fig. 1.1 was a adopted in Ref. 8 as a simple model of an aeroelastic system near/above flutter; the damping coefficient c was taken negative to simulate small amplitude unstable aerodynamic effects and a van der Pol restoring force could be included to represent a potential stabilization of aerodynamic

origin. In this fashion, the effects of friction could be assessed on purely fluttering systems (without the van der Pol term) and those exhibiting aero-driven limit cycles (with van der Pol term). In fact, a comprehensive quantitative analysis of this system was achieved, most notably the stabilization potential of friction was substantiated, and the effects of the various parameters clearly described.

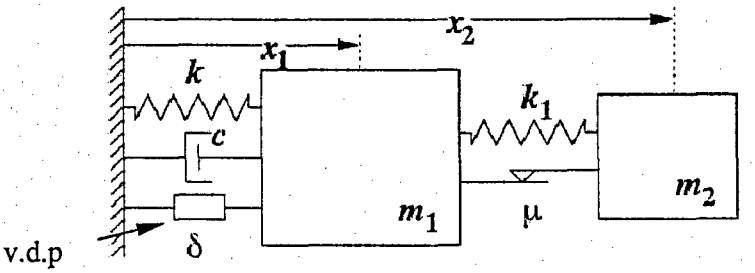

Fig. 1.1 2-degree-of-freedom system with van der Pol (v.d.p) force

The second part of Ref. 8 described the design of an actual friction device and reported the results of wind tunnel tests conducted in the DLR transonic wind tunnel. Some of the finding of this experimental effort confirmed the analysis conducted on the system of Fig. 1.1 while others were unexpected.

In this light, the specific goal of the present investigation is to parallel the analysis of Ref. 8, but on actual aeroelastic systems as opposed to the structural dynamic model of Fig 1.1, and thus to bridge the two components of this earlier study.

In selecting an appropriate structural model for a full aeroelastic analysis, it is first necessary to describe in details how friction will be introduced. The representation of the friction effects is particularly challenging as it is expected that many joints (e.g. between

wing and pylons, between riveted panels, between bolted pieces of spars, ribs, etc.) would likely participate in the damping effects. However, the modeling of these different contacts would not only be a tremendous task but its complexity would render it extremely difficult to determine the role of friction in LCO. To obtain such results, it is suggested to proceed with the following structural simplifications and the aerodynamic modeling that follows.

(i) The friction effects will be assumed to originate from a single, rigid component moving relatively with respect to the wing and to be characterized by a preload N or applied moment M_0 and coefficients of friction μ_S and μ_D.

(ii) The changes of structural geometry that occur due to the relative sliding at the joints will be neglected. This assumption appears justified as all aircraft components are subjected to a large preload so that a large amount of energy can be dissipated with only small relative motions at the joints. Accordingly, there will be no effect of the sliding on the aerodynamics.

Combining the above two assumptions suggests that the friction mechanism should appear internal to the wing, e.g. modeled through a block sliding inside the structure in a rough track (Fig. 1.2) or through a rigid component experiencing rubbing while rotating, e.g. as a rotating disk squeezed between two stationary rings (Fig. 1.3 and Fig. 1.4).

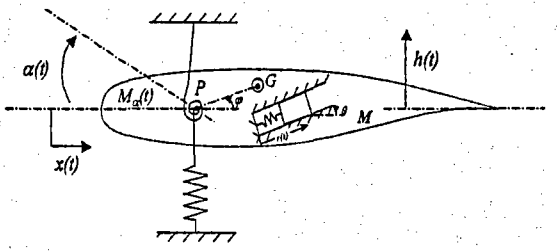

Fig. 1.2 Aeroelastic system with sliding block

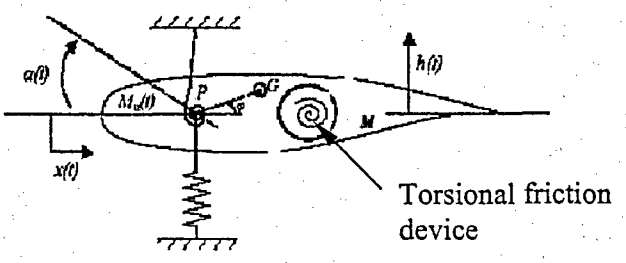

Fig. 1.3 Aeroelastic system with rotating disk

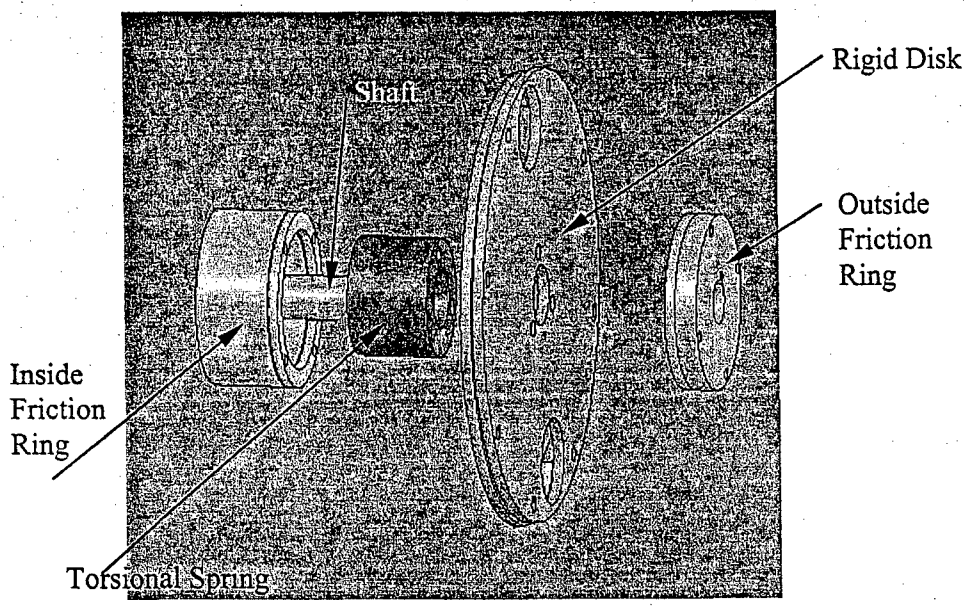

Fig. 1.4 Exploded view of the torsional friction device[8]

Both of these models will be used in the ensuing chapters to assess the role of friction on aeroelastic systems exhibiting either a pure fluttering behavior (chapter 2) or post flutter limit cycle oscillations (chapter 3). In both cases, an inviscid incompressible aerodynamics is assumed and fully coupled aerodynamic/structural dynamic computations are performed.

It should be noted that these models are meant to be *generic*, i.e. that their equations of motion may be considered representative, albeit possibly simplified, of the equations of motion of a physical wing/wing-store system expressed in modal coordinates as opposed to the physical coordinates used here. A one to one correspondence between the properties (mass or inertia, stiffness, ...) of the friction device and of a physical component (store or missile for example) is not suggested here.

CHAPTER 2

FLAT PLATE WITH INTERNAL FRICTION

As a first step forward understanding the effect of friction on aeroelastic system, the simplest airfoil, i.e. a flat plate, will be considered that supports a torsional friction device, see Fig. 1.3 and 1.4. The system is thus characterized by the three degrees of freedom: plunging, h, (positive downward measured at the elastic axis), pitching about the elastic axis, α, (positive nose-up) and torsion θ (positive clock-wise).

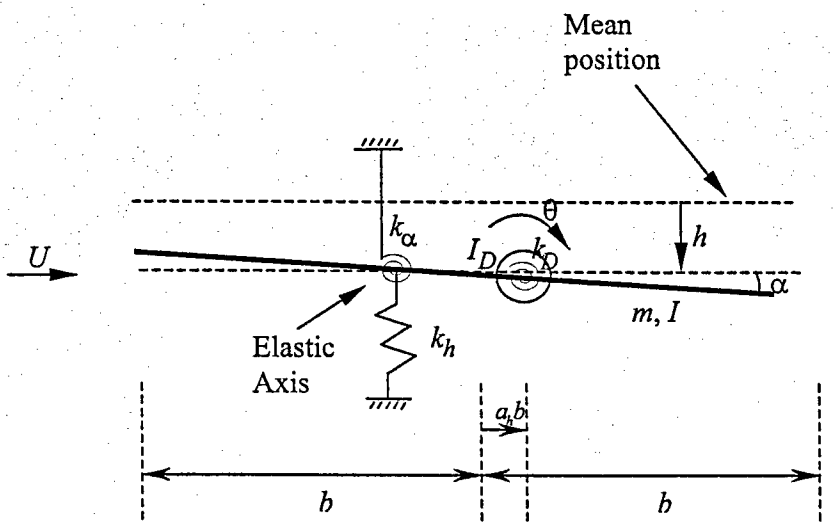

Fig. 2.1 Flat Plate airfoil having three degrees of freedom

The equations of motion for the above system are

$$M\ddot{h} + S_\alpha \ddot{\alpha} + k_h h = -L(t) \tag{2-1}$$

$$S_\alpha \ddot{h} + I_\alpha \ddot{\alpha} + k_\alpha \alpha + k_d(\alpha - \theta) = M_\alpha(t) + M_f \tag{2-2}$$

$$I_d \ddot{\theta} + k_d(\theta - \alpha) = -M_f \tag{2-3}$$

where M is the total mass of the system, S_α is the static moment of the flat plate about elastic axis, I_α is the moment of inertia of the flat-plate about elastic axis and I_d is the moment of inertia of the torsional disk. The symbols k_h, k_α and k_d denote the spring constants of the plunging, pitching, and torsional motions, respectively. Further, U is the free stream velocity and b is the half chord. In regards to forces, L and M_α denote the lift (positive downward) and moment (positive nose-up) respectively, and M_f is the friction moment resulting from the squeezing of the rotating disk by the two rings, see Fig 1.4. This moment can be expressed as

$$M_f = \mu_D \, M_0 \, \mathrm{sgn}\left(\dot{\theta} - \dot{\alpha}\right) \text{ during slip } (\dot{\theta} \neq \dot{\alpha}) \tag{2-4a}$$

$$\text{and } \left|M_f\right| \leq \mu_S \, M_0 \text{ during stick } (\dot{\theta} = \dot{\alpha}) \tag{2-4b}$$

where $\mu_D M_0$ is the moment created by the friction induced shear stresses. If one assumes a uniform stress distribution at the disk ring contact, then it is found that $M_0 = N \frac{2}{3} \frac{\left[R_e^3 - R_i^3\right]}{\left[R_e^2 - R_i^2\right]}$ where N is the normal force between the disk and the ring and R_i and R_e are the internal and external radii of the rings. Finally, μ_D and μ_S are the dynamic and static coefficients of friction, respectively.

Introducing the dimensionless time $\tau = Ut/b$ in Eq. (2-1), (2-2) and (2-3) yields

$$M\frac{U^2}{b^2}h'' + S_\alpha \frac{U^2}{b^2}\alpha'' + k_h h = -L(\tau) \tag{2-5}$$

$$S_\alpha \frac{U^2}{b^2}h'' + I_\alpha \frac{U^2}{b^2}\alpha'' + k_\alpha \alpha + k_d(\alpha - \theta) = M_\alpha(\tau) + M_f \tag{2-6}$$

$$I_d \frac{U^2}{b^2}\theta'' + k_d(\theta - \alpha) = -M_f \tag{2-7}$$

where $(\cdot)'$ denotes the differentiation with respect to τ.

It will be assumed here that the aerodynamics can be assumed as inviscid and incompressible. The resulting aeroelastic system is then linear in the absence of friction and its corresponding response can be sought by standard Fourier transfer function concepts. Specifically, expressing the airfoil motions as

$$h(\tau) = h_0 e^{ik\tau} \tag{2-8a}$$

and

$$\alpha(\tau) = \alpha_0 e^{ik\tau} \tag{2-8b}$$

where the reduced frequency k is defined as

$$k = \frac{\omega b}{U} \tag{2-9}$$

then, it can be shown that the lift and moment may be expressed as [9]:

$$\frac{L(\tau)e^{-ik\tau}}{\rho\pi b U^2} = -k^2\left(\frac{h_0}{b} - a_h\alpha_0\right) + ik\alpha_0 + 2C(k)\left[\alpha_0 + \frac{i}{b}kh_0 + \left(\frac{1}{2} - a_h\right)ik\alpha_0\right] \tag{2-10}$$

$$\frac{M(\tau)e^{-ik\tau}}{\rho\pi b^2U^2} = (\frac{1}{2}+a_h)2C(k)\left[\alpha_0+\frac{i}{b}kh_0+(\frac{1}{2}-a_h)ik\alpha_0\right]$$

$$-k^2a_h(\frac{h_0}{b}-a_h\alpha_0)-(\frac{1}{2}-a_h)ik\alpha_0+\frac{k^2}{8}\alpha_0 \qquad (2\text{-}11)$$

In the above equations, $C(k)$ denotes the Theodorsen function[9,10] simulating the unsteadiness of the wake and expressed as

$$C(k)=\frac{H_1^{(2)}(k)}{H_1^{(2)}(k)+iH_0^{(2)}(k)}=\frac{K_1(ik)}{K_0(ik)+K_1(ik)} \qquad (2\text{-}12)$$

where $H_j^{(2)}(\cdot)$ and $K_j(\cdot)$ denote the Hankel function of the second kind and modified Bessel function both of order j, respectively.

Adopting a rational approximation of this function permits the reformulation of Eq. (2-10) and (2-11) in terms of ordinary differential equations which can be marched in time with Eq. (2-5), (2-6) and (2-7) to obtain the response of the coupled aeroelastic system both without (linear analysis) or with (nonlinear analysis) friction. Specifically, the following approximation of $C(k)$ is used in the ensuing analysis[9,10]

$$C(k)=1-\frac{\xi_1\, ik}{ik+s_1}-\frac{\xi_2\, ik}{ik+s_2} \qquad (2\text{-}13)$$

where $\xi_1=0.165$, $s_1=0.0455$, $\xi_2=0.335$, and $s_2=0.3$.

A comparison of the real and imaginary parts of the Theodorsen function, Eq. (2-12), and its rational approximation, Eq. (2-13), is shown in Fig 2.2. Clearly, the matching is very good so that Eq. (2-13) is appropriate for the present investigation.

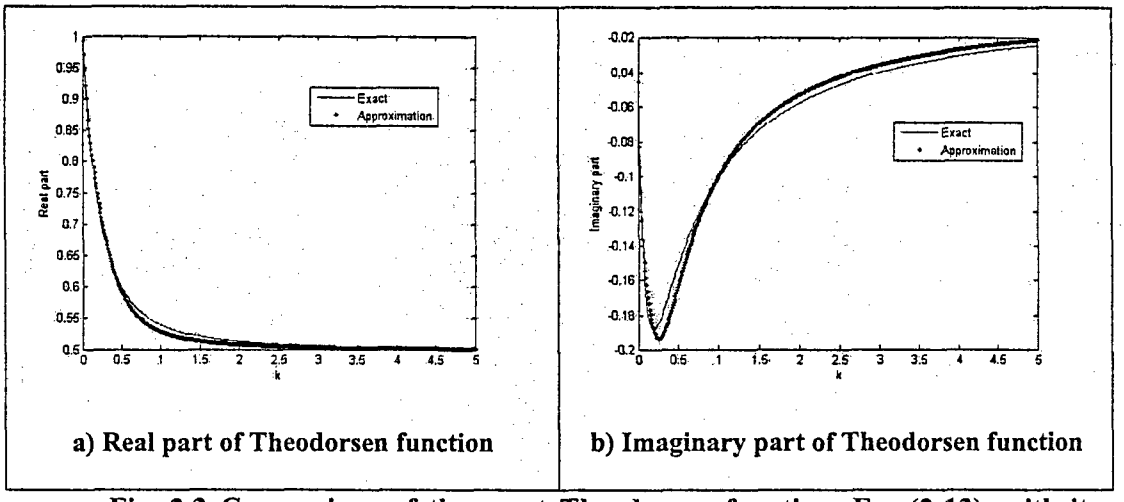

a) Real part of Theodorsen function **b) Imaginary part of Theodorsen function**

Fig. 2.2 Comparison of the exact Theodorsen function, Eq. (2-12), with its rational approximation, Eq. (2-13)

2.1 Time Marching Computation

The approximation of the Theodorsen function by a rational expression is only the first step in rewriting Eq. (2-10) and (2-11) in terms of $h(\tau)$, $\alpha(\tau)$ and their derivatives. Indeed, note that $C(k)$ does not appear alone in Eq. (2-10) and (2-11) but rather through the products $C(k)X_0$ where X_0 denotes either h_0 or α_0 and that there variables are, from Eq. (2-5), the Fourier transform of $h(\tau)$ and $\alpha(\tau)$, i.e.

$$h_0 = h_0(k) = F\{h(\tau)\}\ ;\ \ \alpha_0 = \alpha_0(k) = F\{\alpha(\tau)\} \tag{2-14}$$

Since there are three terms on the right-hand-side of Eq. (2-13), one can write

$$C(k)X_0 = F\{T_i(\tau) + T_{i+1}(\tau) + T_{i+2}(\tau)\} \tag{2-15}$$

where $T_i(\tau)$ arise from the one in Eq. (2-13) while $T_{i+1}(\tau)$ and $T_{i+2}(\tau)$ are associated with the two rational terms in this equation. The application of standard rules of Fourier transformations demonstrates that

$$T_i = X(\tau) \tag{2-16a}$$

$$T_{i+1} \quad : \quad T_{i+1}' + s_1 T_{i+1} = -\xi_1 X' \tag{2-16b}$$

$$T_{i+2} \quad : \quad T_{i+2}' + s_2 T_{i+2} = -\xi_2 X' \tag{2-16c}$$

There are thus four auxiliary functions of time, $T_1(\tau)$ and $T_2(\tau)$ obtained for i=0 and $X(\tau) = h(\tau)$ and $T_3(\tau)$ and $T_4(\tau)$ corresponding to i=2 and $X(\tau) = \alpha(\tau)$.

Other noteworthy Fourier transform properties are

$$ikC(k)X_0 = F\{T_i' + T_{i+1}' + T_{i+2}'\} \tag{2-17a}$$

$$ikX_0 = F\{X'\} \tag{2-17b}$$

and

$$k^2 X_0 = F\{-X''\} \tag{2-17c}$$

Combining Eq. (2-5), (2-6), (2-7), and (2-15) finally yields the equations of motion in the form

$$\left(\frac{M}{\rho\pi b^3} + \frac{1}{b}\right)h'' + \left(\frac{S_\alpha}{\rho\pi b^3} - a_h\right)\alpha'' = -\alpha' - 2(\alpha + T_3 + T_4) - \frac{2}{b}(h' + T_1' + T_2')$$

$$-(1-2a_h)(\alpha' + T_3' + T_4') - \frac{k_h}{\rho\pi b U^2}h \tag{2-18}$$

$$\left(\frac{S_\alpha}{\rho\pi b^3}-a_h\right)h''+(\frac{I_\alpha}{\rho\pi b^3}+ba_h^2+\frac{b}{8})\alpha''=b(1+2a_h)(\alpha+T_3+T_4)+(1+2a_h)(h'+T_1'+T_2')$$

$$+b(\frac{1}{2}-2a_h^2)(\alpha'+T_3'+T_4')-b(\frac{1}{2}-a_h)\alpha'-\frac{k_\alpha}{\rho\pi bU^2}\alpha-\frac{k_d}{\rho\pi bU^2}(\alpha-\theta)+\frac{M_f}{\rho\pi bU^2} \tag{2-19}$$

and

$$I_d\frac{U^2}{b^2}\theta''+k_d(\theta-\alpha)=-M_f \tag{2-20}$$

which must be solved together with Eq. (2-16). Note during stick phases that θ and α are not independent variables since $\dot{\theta}=\dot{\alpha}$. Equation (2-20) then permits the evaluation of M_f.

The ensuing numerical study was conducted at various speeds U and for different spring stiffnesses k_d. The other system parameter values are shown in Table 2.1.

parameter	Explanation	Value
M	Total mass of the airfoil system	20.0 kg/m
S_α	Static moment of airfoil about the elastic axis	2 kg
I	Moment of inertia of airfoil about the elastic axis	1.1875 kgm
I_d	Moment of inertia of torsional disk	0.0625 kgm
k_h	Spring constant of plunging direction	$1.8N/m^2$
k_α	Spring constant of pitching direction	1.25N
b	Semichord	0.5m
a_h	Nondimensional distance from the midchord to the elastic axis	-0.1
μ_S (μ)	Static coefficient of friction	0.001
μ_D (μ)	Dynamic coefficient of friction	0.001
ρ	Density of air	$1.27324kg/m^3$
M_0	Moment term in Eq. (2.4)	1

Table 2.1 System parameter values for the flat plate

2.2 Linear solutions : continuous sticking and frictionless slipping behaviors

Equation (2-16) and (2-18) through (2-20) represent three first order (two during sticking since θ and α are then related variables) and four first order equation. These equations can be rewritten as a set of 10 first order equation in slipping motions and 8 such equations in sticking phases. These equations are in general nonlinear but there are two linear limiting cases. If the motions are such that sticking occurs continuously (for example in the limits $\mu \to \infty$ or $k_d \to \infty$), the friction nonlinearity is not triggered and the equations of motion are linear. This sticking solution will serve as the baseline in the ensuing analysis as it corresponds to the system without moving parts.

The second linear solution corresponds to the continuous slipping motions occurring with $\mu = \mu_D = \mu_S = 0$. In this case indeed, the nonlinear moment M_f always vanishes.

The complexity of the solutions with active friction warrants the detailed analysis of all simple cases first. In this regard, note that the equations of motion for both of the above linear problems (continuous sticking and frictionless slipping) can be rewritten as

$$\dot{\underline{y}} + A\underline{y} = \underline{0} \tag{2-21}$$

where the vector $\underline{y}$ has the 10 components h, $\dot{h}$, α, $\dot{\alpha}$, θ, $\dot{\theta}$, T_1, T_2, T_3 and T_4 for the frictionless slipping problem and only the 8 components h, $\dot{h}$, α, $\dot{\alpha}$, T_1, T_2, T_3 and T_4 for the continuous sticking solution. Since Eq. (2-21) is linear, no LCO is possible : the response $\underline{y}(t)$ either converges to $\underline{0}$ or diverges independently of the initial conditions.

The convergence (stability) or divergence (instability) of $\underline{y}(t)$ is determined by the eigenvalues λ_j of the matrix A. Specifically,

the system is stable, i.e. $\underline{y}(t)$ converges to $\underline{0}$ iff the real parts of all eigenvalues λ_j are >0.

the system is unstable, i.e. $\underline{y}(t)$ diverges iff the real parts of any eigenvalue λ_j is <0.

It is convenient to analyze the response of the two linear cases in terms of natural frequencies and damping ratios. This is achieved by associating to each eigenvalue λ_j a natural frequency ω_j and a damping ratio ζ_j through the linear single-degree-of-freedom relation

$$-\lambda_j = -\omega_j \zeta_j \pm i\omega_j \sqrt{1-\zeta_j^2} \tag{2-22}$$

or

$$\omega_j = \|\lambda_j\| \tag{2-23}$$

and

$$\zeta_j = \frac{\mathrm{Re}(\lambda_j)}{\|\lambda_j\|} \tag{2-24}$$

Stability then occurs when all ζ_j are positive and instability when any of them is negative.

This stability analysis revealed some interesting information, most notably that the system in frictionless slipping mode with the parameter values in Table 2.1 is less stable than its continuous sticking counterpart in that it exhibits its first negative damping ratio at a lower flow speed. For example, the first negative damping ratio arises at approximately U=0.74 m/s (continuous slip) and U=0.995 m/s (continuous stick) for k_d = 0.0165 Nm/rad but they occur at U=0.99208 m/s (continuous slip) and U=0.99232m/s (continuous stick) for k_d = 0.985 Nm/rad. It must, however, be recognized that there are several significant differences in the evolution of the dimensionless natural frequencies (made dimensionless by the time $\frac{b}{U}$) and damping ratios corresponding to these two values of k_d. For the larger one, see Fig. 2.3, classical flutter situations are encountered, two modes of each aeroelastic system (stuck and slipping) appear to cross as the smallest damping ratio becomes negative. Further, note that the natural frequencies and damping ratios of the sticking and slipping systems are very close to each other over the entire range of flow speeds.

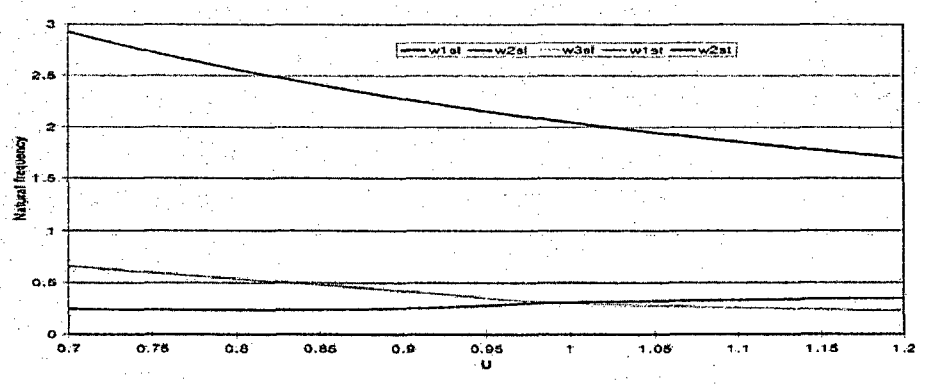

a)

Natural frequencies

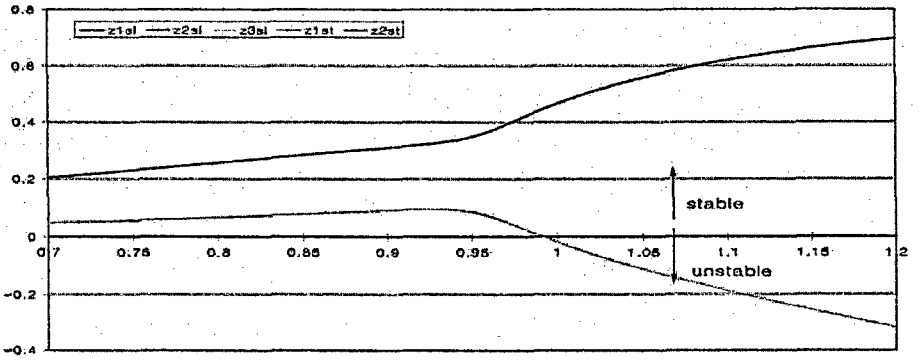

b) Damping ratios

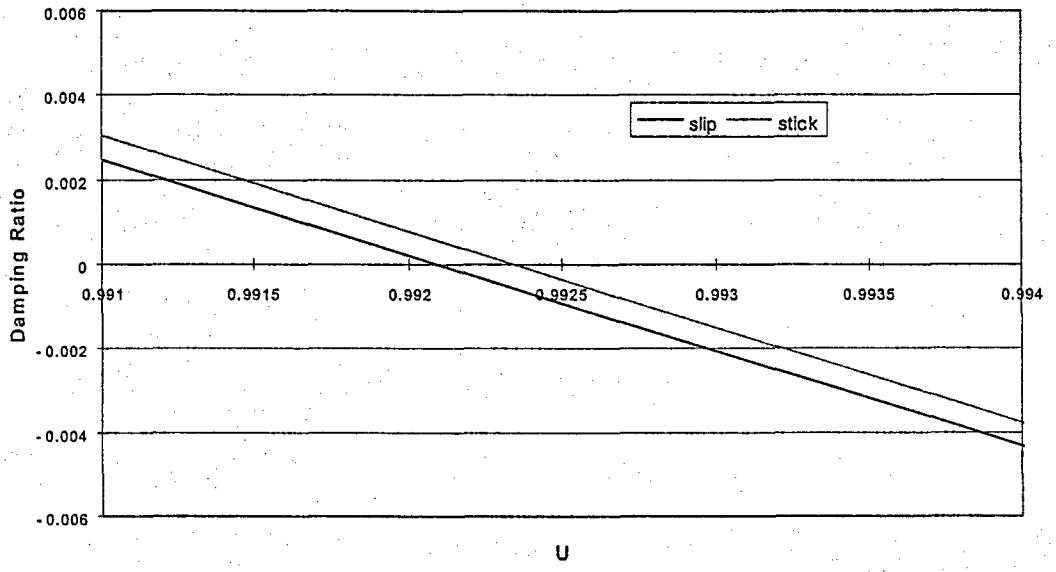

c)

Zoomed damping ratios

Fig. 2.3 Dimensionless natural frequencies and damping ratios of the frictionless slipping ("sl") and continuous sticking ("st") systems as functions of the flow speed, k_d =0.985Nm/rad.

For the smaller value of k_d, the natural frequency of the torsional device alone is the middle frequency (as opposed to the largest one in Fig. 2.3) and its presence affects much more significantly the response of the frictionless slipping system. This system becomes first unstable at a flow speed of approximately 0.74m/s but this does not occur with a mode veering/crossing, see Fig. 2.4. In fact, such a situation does not take place until the speed reaches 0.995m/s. Classical flutter instabilities do take place for both the

continuous sticking and frictionless slipping systems around $U = 1$m/s, see Fig. 2.5, with the sticking system instability speed lower than its slipping counterpart.

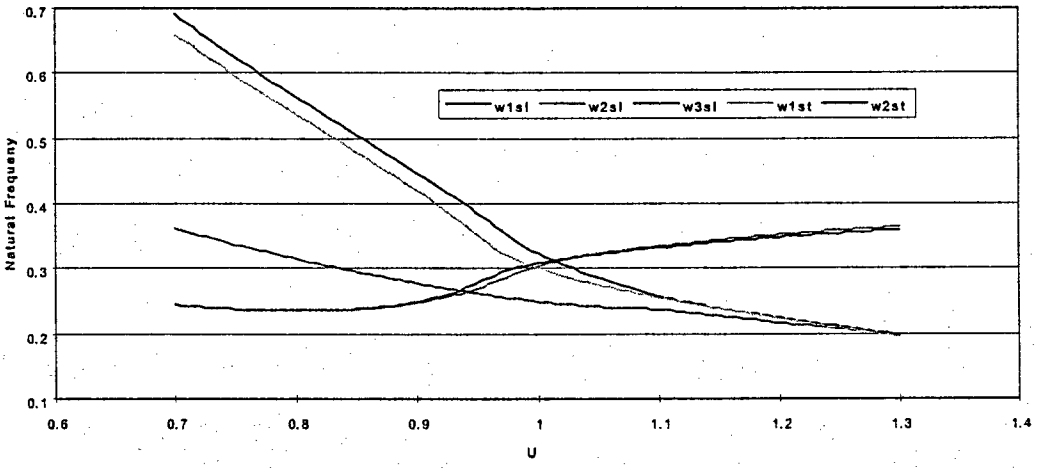

a)

Natural frequencies

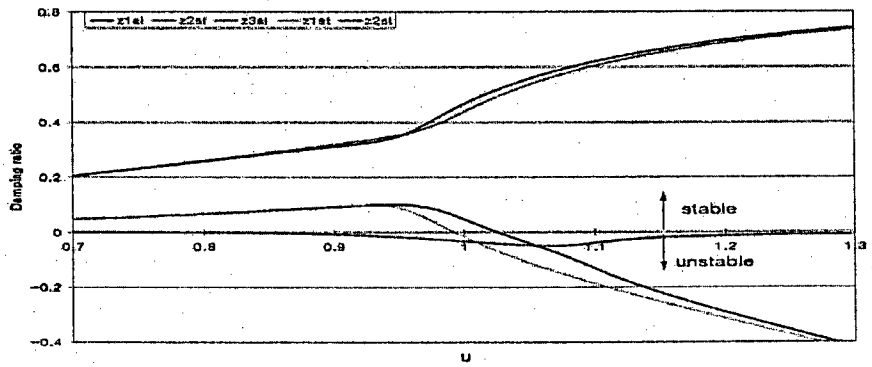

b) Damping ratios

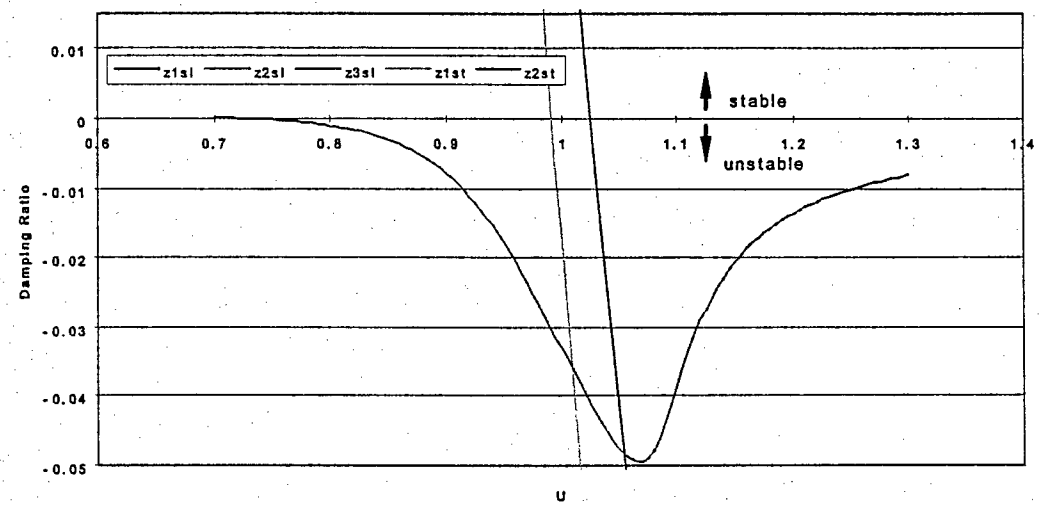

c)

Zoomed damping ratios

Fig. 2.4 Dimensionless natural frequencies and damping ratios as functions of the flow speed, k_d =0.0165 Nm/rad.

The above comments demonstrate that there is, for both torsional spring stiffnesses, a range of flow speeds for which the continuously sticking system is stable while the one in frictionless slip mode is unstable. Thus, if a disturbance is applied that does not induce a relative motion of the disk with respect to the plate, the response of the system will decay. On the contrary, a disturbance that includes such a relative motion may increase unless the system gets stuck again. These observations imply that the system of Fig. 2.1 might exhibit subcritical, as well as supercritical, limit cycle oscillations.

A tentative explanation of the lower flow speed at which instability takes place for the frictionless slipping system as compared to its continuously sticking counterpart is as follows. Note first that the stuck configuration (two degree of freedom) can be viewed as the limit of the slipping one (three degree of freedom) in which the connecting stiffness of the device $k_d \to \infty$. Accordingly, the two natural frequencies of the stuck configuration will be higher than the two lowest natural frequencies of the slipping system. Since the slipping is directly coupled to the pitching dominated motions not to their plunging counterparts, it is expected that the above effect would be more significant on the pitching frequency than on the plunging one and the former would thus be decreased by allowing relative motion of the disk.

How does this change in natural frequency affect the flutter speed? If one relies on the veering of the natural frequencies at flutter, it is predicted that the highest natural frequency of the coupled aerodynamic-structural system decreases while the lowest one increases as the flow speed is increased toward the flutter point. For the system analyzed, the pitching frequency is the highest at zero flow speed and thus a decrease of it, through allowing slipping, may result in a lowering of the flutter speed. This explanation is particularly consistent with the behavior observed for $k_d = 0.985$ Nm/rad.

The above discussion is the characterization of the system behavior in linear frictionless slipping and continuous sticking phases and provides the background for the analysis of the effects of the nonlinear friction force to be accomplished next.

2.3 Nonlinear Responses

An important aspect of the numerical integration of the governing equation is the accurate capturing of the times at which a zero relative speed, $\dot{\theta} - \dot{\alpha} = 0$, is achieved. It is indeed at those moments that the force of friction abruptly changes sign (in the case of continuously slipping motions) but also that slip to stick transition could occur. The appropriate determination of the stick to slip transitions is also important.

An interpolation by cubic and linear polynomials which was adopted in the ensuing computations is presented next.

2.3.1 Transition Handling

If a transition was found to take place during a time step (i.e. a change of sign of the relative velocity or the friction force exceeding the sticking threshold), the time $t_0 \in [t_i, t_{i+1}]$ at which it occurred was estimated by interpolation of the relative velocity (using a cubic polynomial) or the friction moment (linear interpolation).

When a transition (slip to slip, slip to stick, stick to slip) occurs during the time step $t \in [t_i, t_{i+1}]$, the estimate of the response cannot be obtained directly from a shooting of the solution at $t = t_i$ because the friction force definition and the equations of motion would only be valid before the transition takes place. The neglect of the change of character during the time step would produce an error $O(\Delta t)$ and thus would force the selection of a very small time step Δt. To avoid this situation, it is proposed here to first march the solution through the entire time step as if no transition took place, then to

estimate the transition point (time t_0) within the time step, and finally to recompute the response at the end of the time step assuming the correct state in the interval $[t_0, t_{i+1}]$.

Consider first slip to slip or slip to stick transitions. The transition condition, i.e. the vanishing of the relative velocity, is based on the response variables which are continuously differentiable. Thus, the relative displacement, *x(t)*, can be approximated by a cubic polynomial of time in the interval $[t_i, t_{i+1}]$, i.e.,

$$x(t) = x_0 + a\bar{t} + b\bar{t}^2 + c\bar{t}^3 \tag{2-25}$$

and

$$\dot{x}(t) = a + 2b\bar{t} + 3c\bar{t}^2 \tag{2-26}$$

where $\bar{t} = t - t_i$ and $x_0 = x(t_i)$.

The constants *a*, *b*, and *c* are evaluated from the values of the relative displacements and velocities at the beginning and end of the time step assuming that no transition takes place. Specifically, when t=0 and t=Δt

$$x(t_{i+1}) = x_1 = x_0 + a\Delta t + b\Delta t^2 + c\Delta t^3 \tag{2-27a}$$

$$\dot{x}(t_i) = v_0 = a \tag{2-27b}$$

$$\dot{x}(t_{i+1}) = v_1 = a + 2b\Delta t + 3c\Delta t^2 \tag{2-27c}$$

Equation (2-27b) yields the value of *a*, while Eq. (2-27a) and (2-27c) lead to the values of the remaining coefficients as

$$b = \frac{3\gamma - \beta}{\Delta t} \tag{2-28a}$$

$$c = \frac{\beta - 2\gamma}{\Delta t^2} \tag{2-28b}$$

where $\beta = v_1 - v_0$ and

$$\frac{x_1 - x_0}{\Delta t} - a = \gamma \tag{2-28c}$$

On the basis of the cubic interpolation, it is possible to estimate the transition time. Specifically, from

$$\dot{x}(t_0) = v_0 + 2b\bar{t}_0 + 3c\bar{t}_0^2 = 0 \tag{2-29a}$$

it is found that

$$\bar{t}_0 = \frac{-b \pm \sqrt{b^2 - 3v_0 c}}{3c} \tag{2-29b}$$

Stick to slip transitions are governed by the value of the force of friction of which only the value is known (no derivative). It will thus be assumed that the force of friction is linear during the interval or

$$F = F_1 + \frac{(F_2 - F_1)}{\Delta t}\bar{t} \tag{2.30}$$

where F_1 and F_2 are the values of the force of friction at the beginning and end of the time step assuming that no transition took place. The transition occurs when F reaches its threshold value of $\pm\mu_S N$ so that

$$\bar{t}_0 = \frac{\left|\pm\mu_S \cdot N - F_1\right|}{\left|F_2 - F_1\right|} \cdot \Delta t \tag{2.31}$$

Once the transition time has been estimated from Eq. (2-29) or (2-31), cubic interpolations of $h(t)$, $\alpha(t)$ and $\theta(t)$ are carried out and evaluated at the appropriate t_0 to yield approximate values of the response at the transition.

The structural computations are then repeated in the interval $t \in [t_0, t_{i+1}]$ with the correct state (stick or slip).

2.3.2 Time Marching Numerical Result

Based on the analysis of Agelastos[8], it was of particular interest to determine the type of response (single vs. multiple frequency, continuous slip vs. stick slip vs. continuous stick) and the largest steady state responses, both as functions of the two fundamental parameters: the flow speed U which dictates the level of instability in the system and the spring stiffness k_d which controls the transfer of energy from the plate to the friction device. The behavior above both continuous sticking and frictionless slipping flutter speeds was investigated first, and Fig. 2.5 through 2.8 show some typical examples of observed responses.

The simplest motions are characterized by a single frequency (SF) and continuous slip (CS), or SFCS for short. The term single frequency (see Ref. 8) refers here to a solution that exhibits a single fundamental harmonic, these motions are thus periodic as can be seen from the phase plane plot of Fig 2.5(d) and its sampled version of Fig. 2.5(e). Single dots in this latter figure indicate that the crossing of the zero relative velocity always occurs in the same conditions. Stick slip periodic solutions are also possible and

are denoted as SFSS (single frequency stick slip), see Fig. 2.6. The presence of the stick phases is best seen in the plots of the pitching and torsion velocities, see Fig. 2.6(c); they correspond to the intervals during which these two velocities are equal.

Multiple frequency solutions are those that involve at least two frequencies which are not rational with respect to each other. The resulting motions are thus non-periodic and exhibit a beating as seen in Fig 2.7 (continuous slip) and 2.8 (stick slip). As might be expected, the phase plane plots of these multiple frequency (non-periodic) motions are much more complex than those of the periodic solutions. In fact, the MFSS solution of Fig 2.8 appears from Fig. 2.8(e) to be aperiodic which its MFCS counterpart would seem to be chaotic, see Fig. 2.7(e).

A global overview of the response of the system can be obtained by analyzing the two most essential features of the motions, i.e. the type of solution (MFSS, MFCS, SFCS, SFSS) and the *magnitude* of the response, as functions of the two critical parameters U and k_d. The concept of magnitude is not clearly defined for multiple frequency solutions, the largest noted response in the computed steady state domain will be used instead. This value is referred to as the largest response and reduces to the amplitude of response for periodic motions. The characteristics of the response and its largest value are shown vs. U and k_d in Fig. 2.9(a) and 2.9(b).

There figures exhibit many of the features presented in Ref. 8 Indeed, it is seen that the largest speed at which a stable solution exists is obtained for an intermediate value of the spring stiffness k_d (around 0.0165 Nm/rad), that a transition from single to

multiple frequency solutions occurs at a fixed speed as the spring stiffness k_d is increased, and that both continuous slip and stick slip solutions are encountered.

Considering next the largest pitching response, it is seen in particular that the response level decreases first monotonically as a function of the spring stiffness until the transition from single to multiple frequency is encountered. For larger values of k_d, the response exhibits beating which implies the very sharp increase of the largest response seen in Fig. 2.9(b) near $k_d = 0.0157$ Nm/rad.

There are a few differences as well between Fig. 2.9 and their counterparts of Ref. 8. In particular, Fig. 2.9(a) and 2.9(b) do not exhibit the symmetry with respect to the peak stabilization point ($k_d \approx 0.0165$ Nm/rad) that is observed in Ref. 8.

It was also questioned whether the "tuned damper" explanation developed in Ref. 8 in connection with the system of Fig. 1.1 could also be used to justify the maximum stabilization that occurs near $k_d \approx 0.0165$ Nm/rad. An analysis of the natural frequencies of the system in slip mode revealed that they were indeed close to each other but with 20% difference between the third natural frequency and the two that are veering/crossing. This difference is too large for the tuned damper arguments to be the sole justification for the optimality of $k_d = 0.0165$ Nm/rad but it is small enough for these arguments to be considered as the basis for this property.

It was next desired to investigate the behavior of the response in situations where the stuck system is stable while its slipping counterpart is unstable. The analysis of the

corresponding response types and largest responses was achieved first around $k_d \approx 0.985$ Nm/rad. It was found that limit cycle oscillations do occur in the small range of flow speeds $U \in [0.922, 0.923]$ m/s, i.e. from the flutter speed in slip mode to slightly above the flutter speed in stick mode. All finite amplitude limit cycle oscillations found were multiple frequency stick-slip solutions with largest pitching response of the order of 0.2, i.e. approximately twice as large as those seen in Fig. 2.9. The limited zone of flow speeds at which limit cycle oscillations could be achieved for $k_d \approx 0.985$ Nm/rad and the larger response they are associated with, both as compared to $k_d = 0.0165$ Nm/rad, appear to reinforce the, approximate, validity of the tuned damper assumption as the third natural frequency in slip for $k_d \approx 0.985$ Nm/rad is far from the other two, approximately 7 times larger.

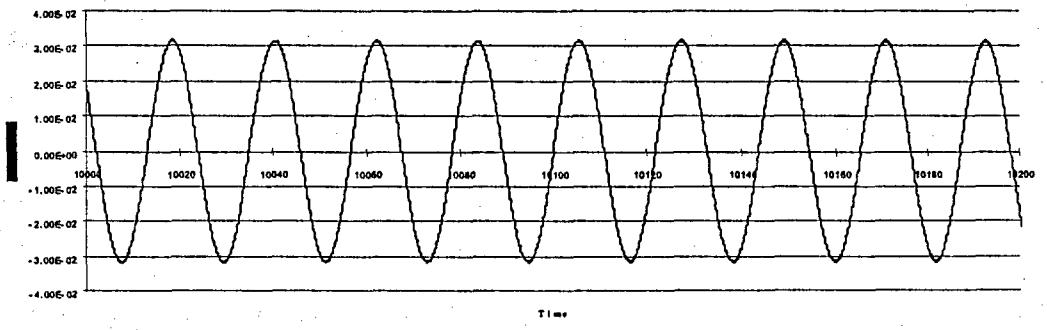

a)

Time history of plunging

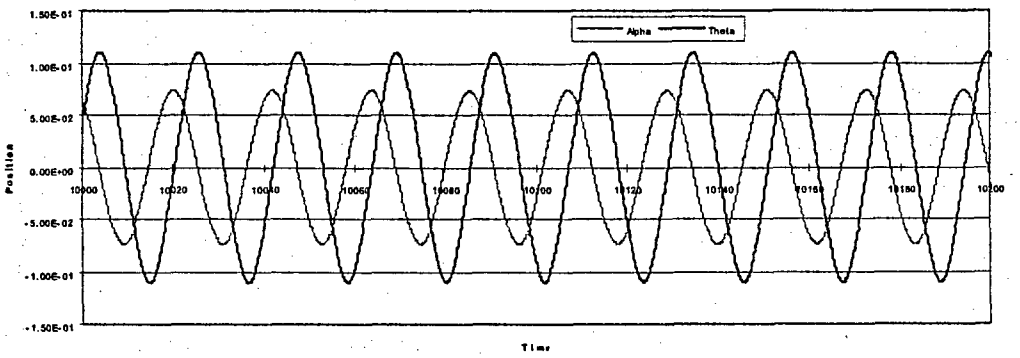

b)

Time history of pitching and torsion

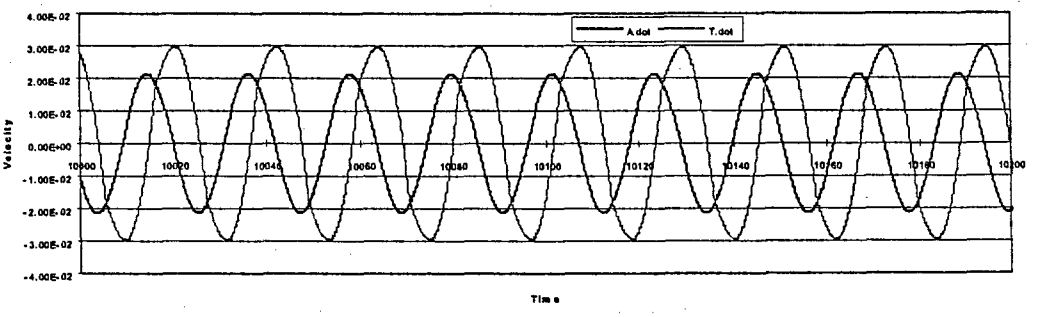

c)

Time history of velocity in pitching and torsion

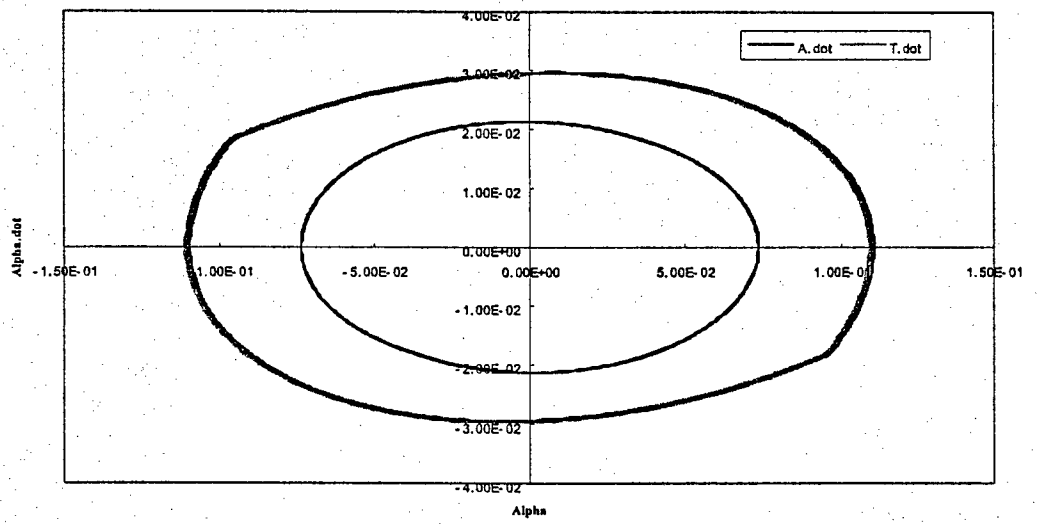

d) Phase plane plot for pitching and torsion

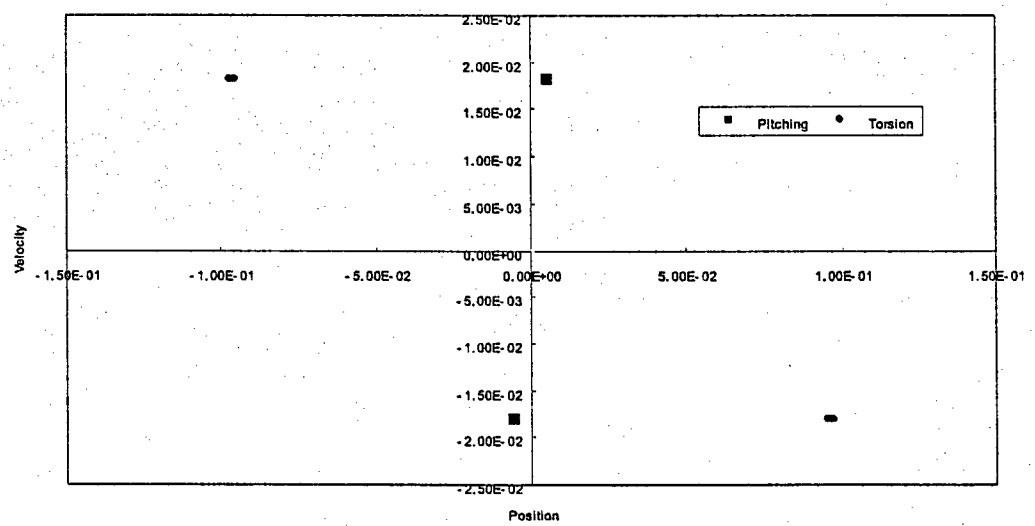

e) Sampled phase plane plot at the moment when the relative velocity becomes zero

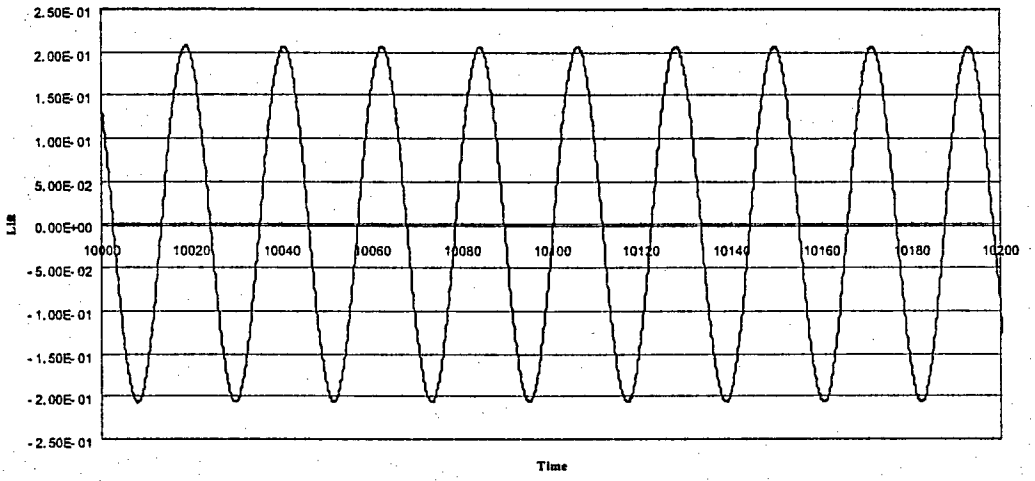

f) Time history of lift

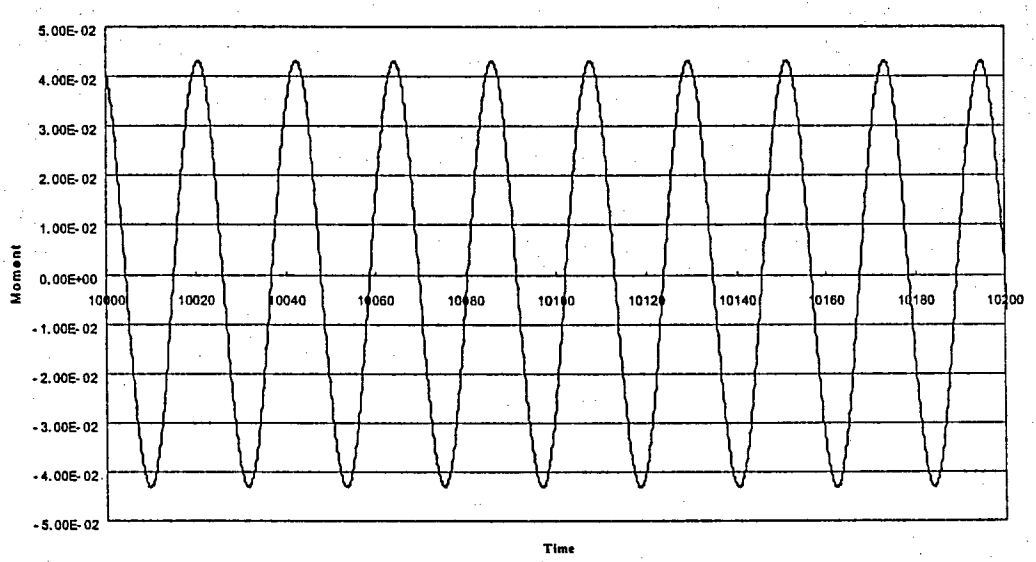

g) Time history of moment

Fig. 2.5 $\mu = 0.001$, k_d=0.0155Nm/rad, U=1.0130m/s (SFCS)

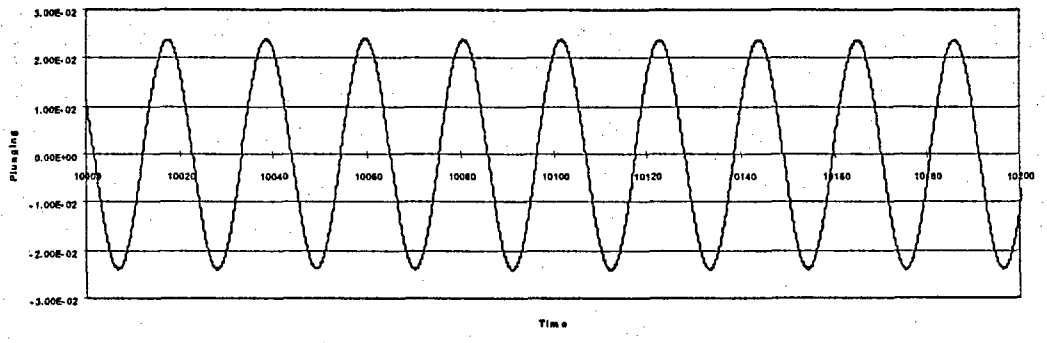

a)

Time history of plunging

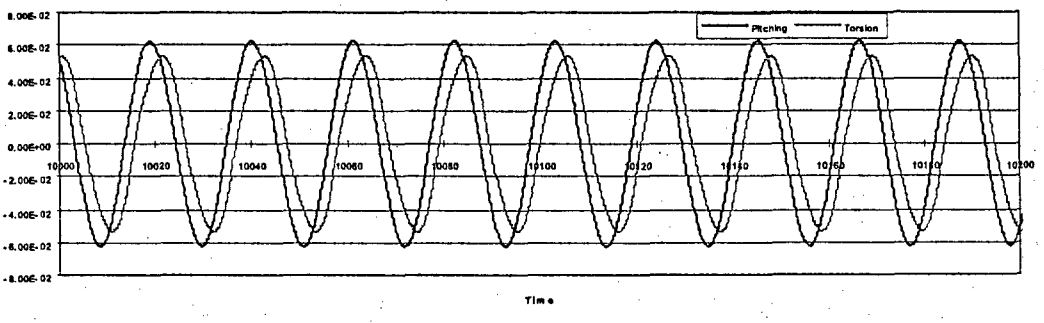

b)

Time history of pitching and torsion

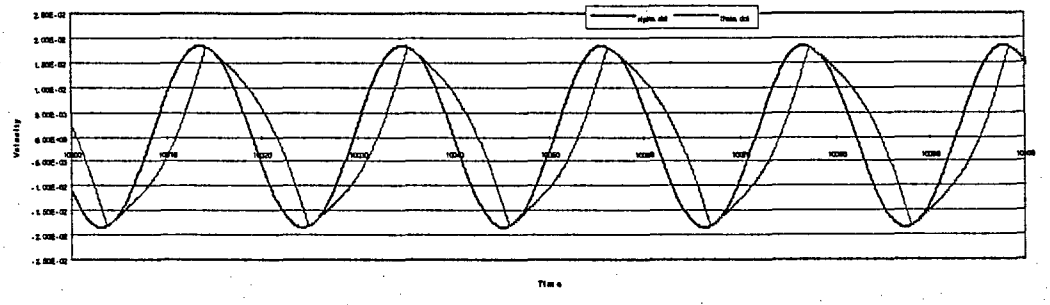

c)

Time history of velocity in pitching and torsion

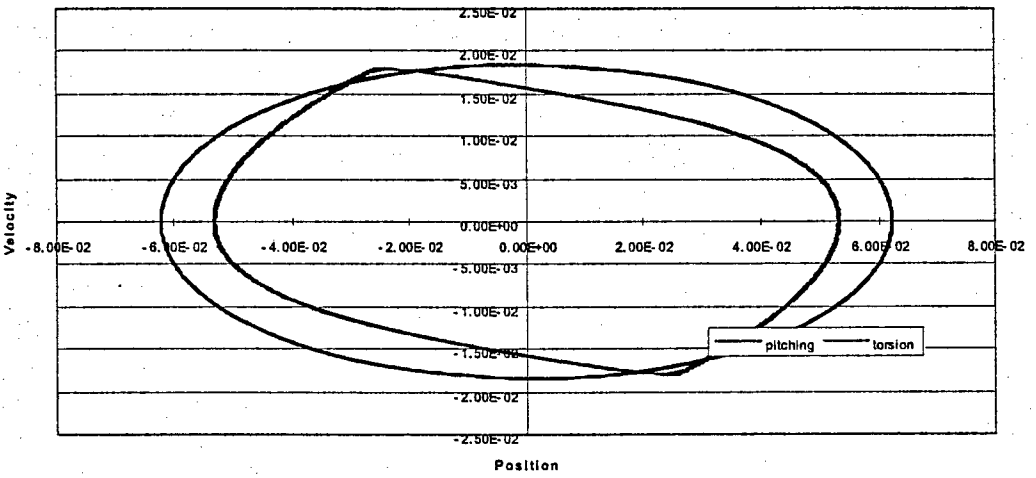

d)

Phase plane plot for pitching and torsion

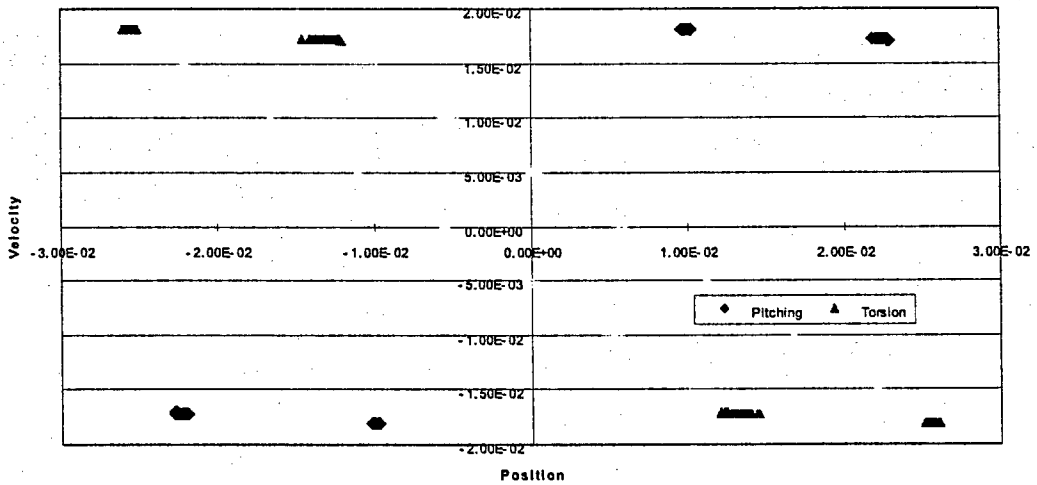

e)

Sampled phase plane plot at the moment when the relative velocity becomes zero

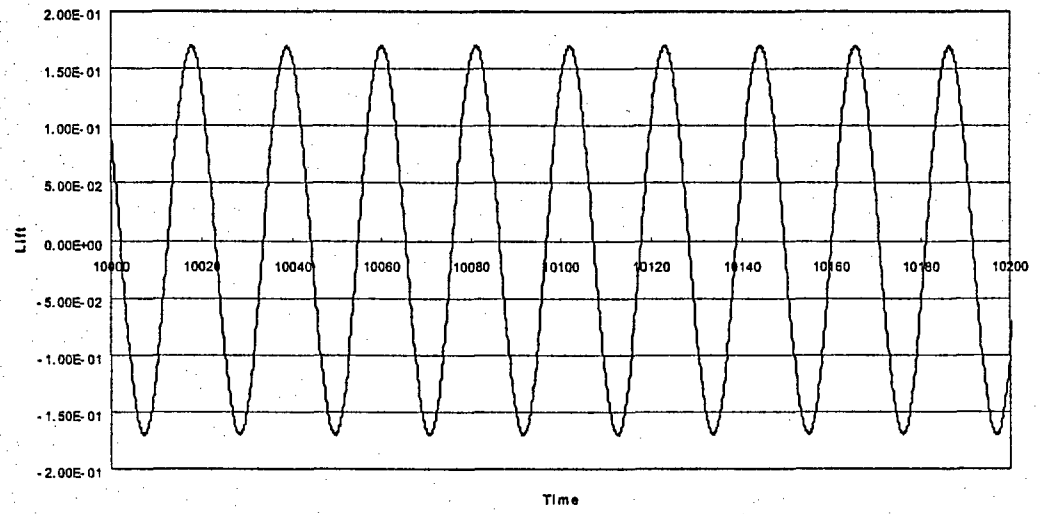

f) Time history of lift

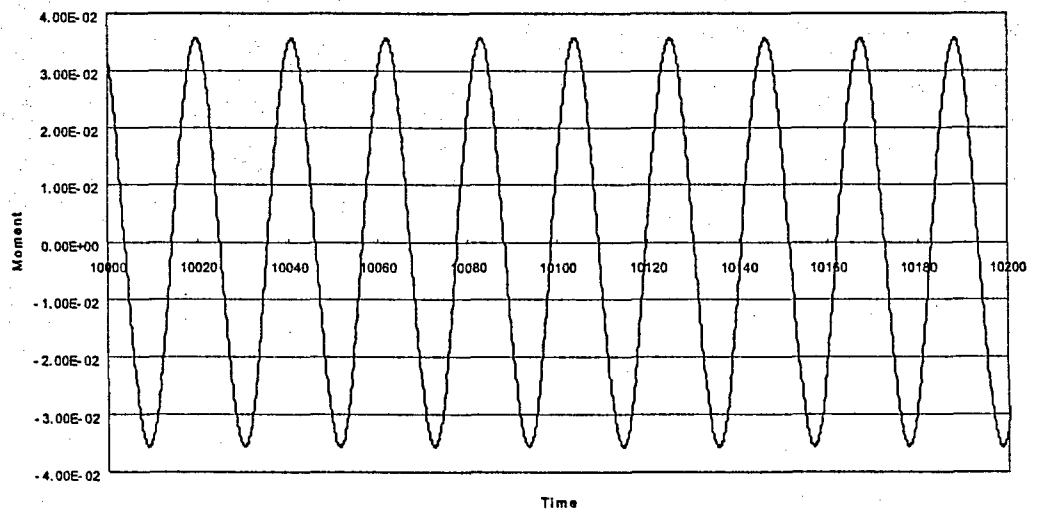

g) Time history of moment

Fig. 2.6 $\mu = 0.001$, k_d=0.0155Nm/rad, U=1.0m/s (SFSS)

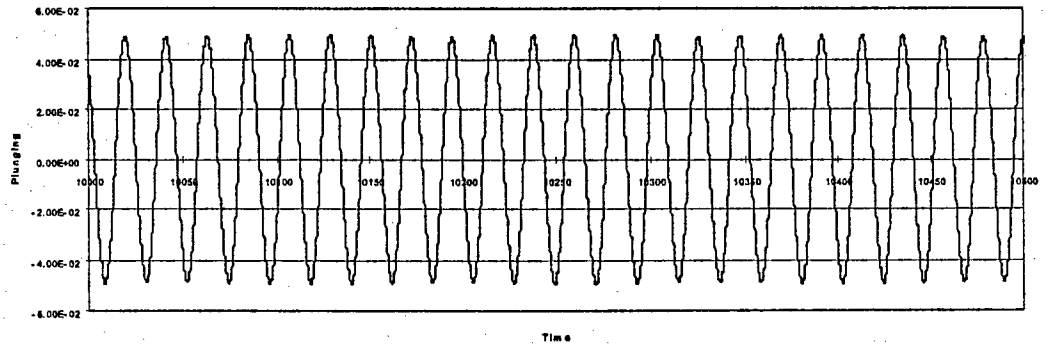

a) Time history of plunging

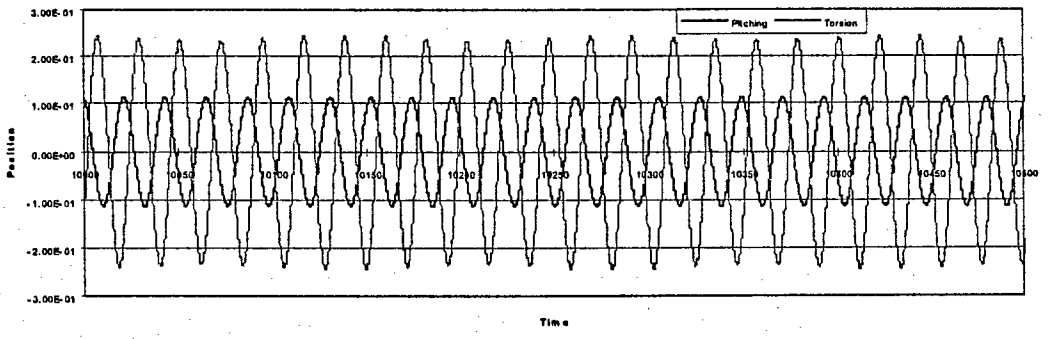

b) Time history of pitching and torsion

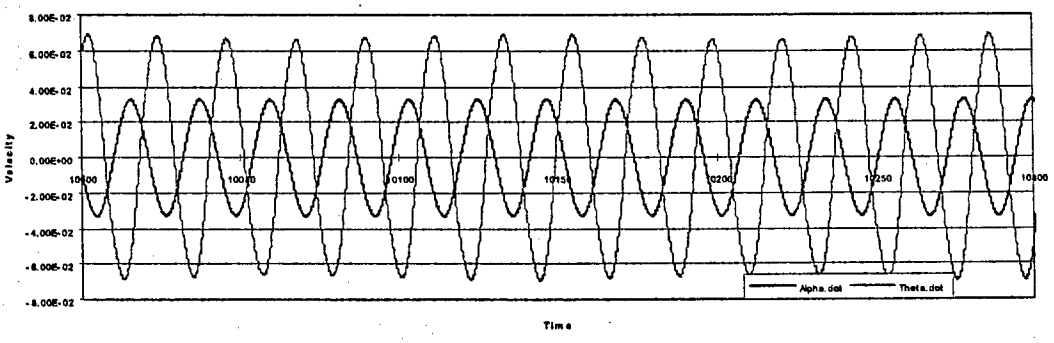

c

Time history of velocity in pitching and torsion

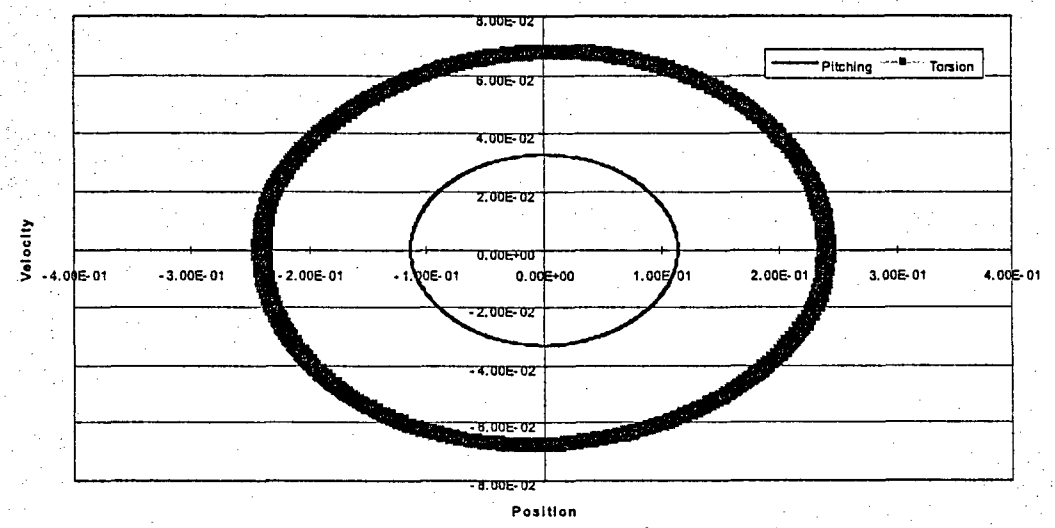

d) Phase plane plot for pitching and torsion

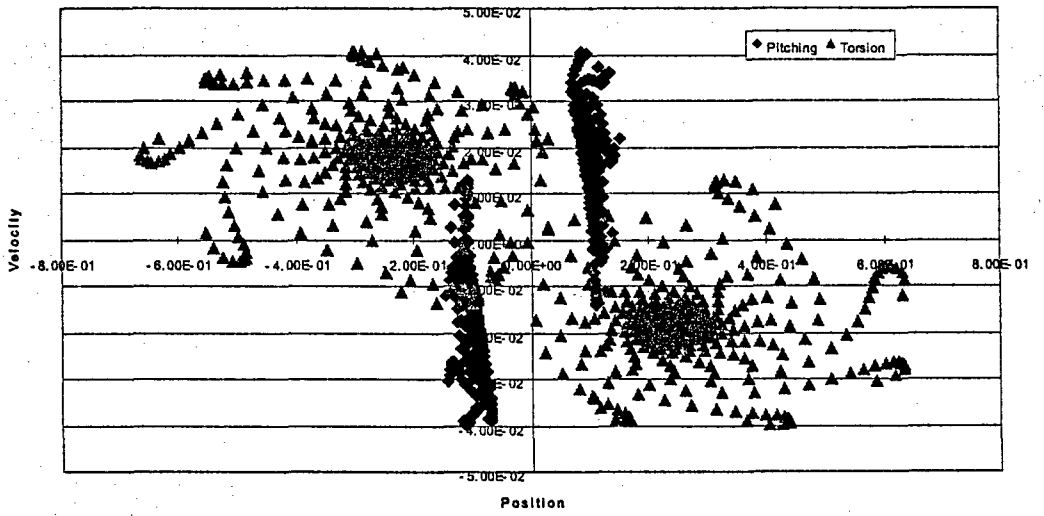

e) Sampled phase plane plot at the moment when the relative velocity becomes zero

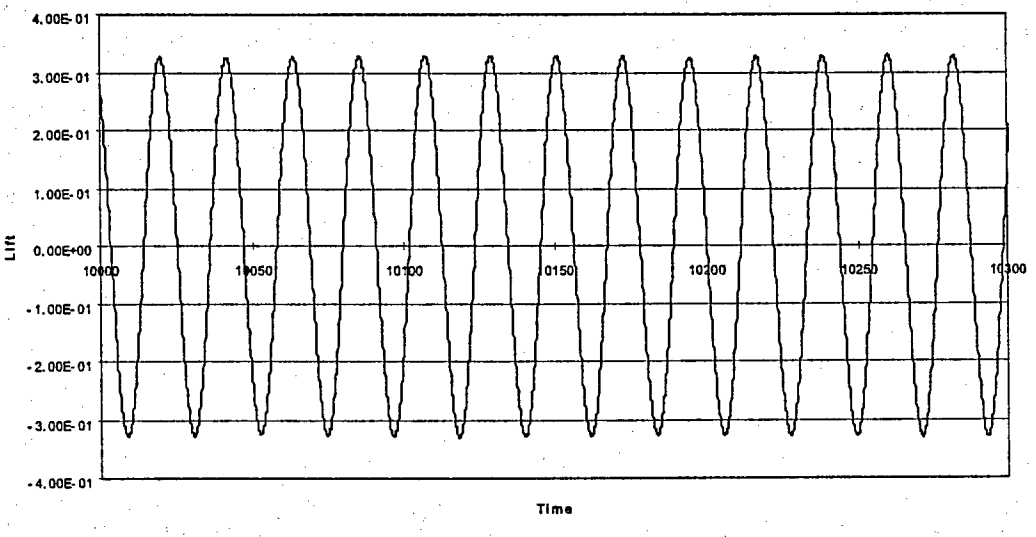

f) Time history of lift

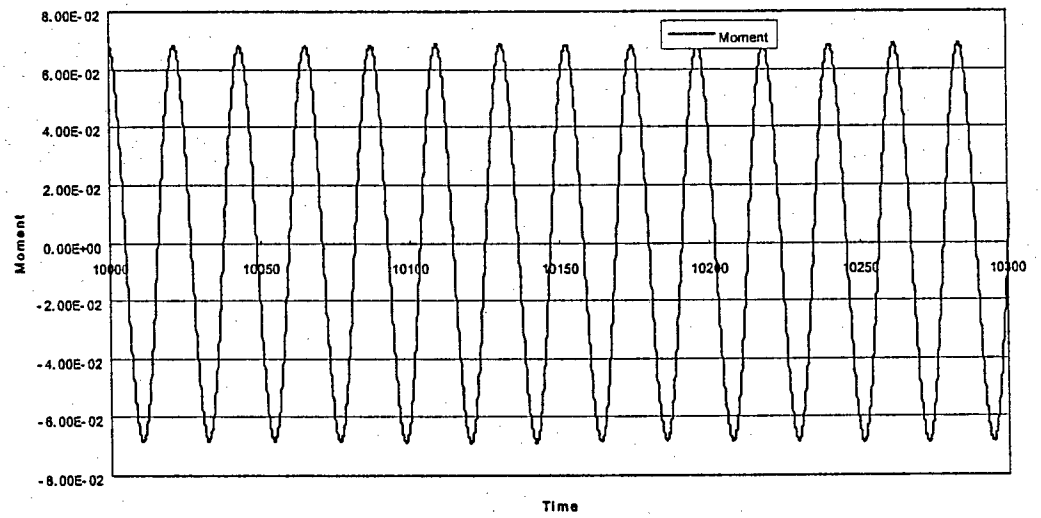

g) Time history of moment

Fig. 2.7 $\mu = 0.001$, k_d=0.0155Nm/rad, U=1.0265m/s (MFCS)

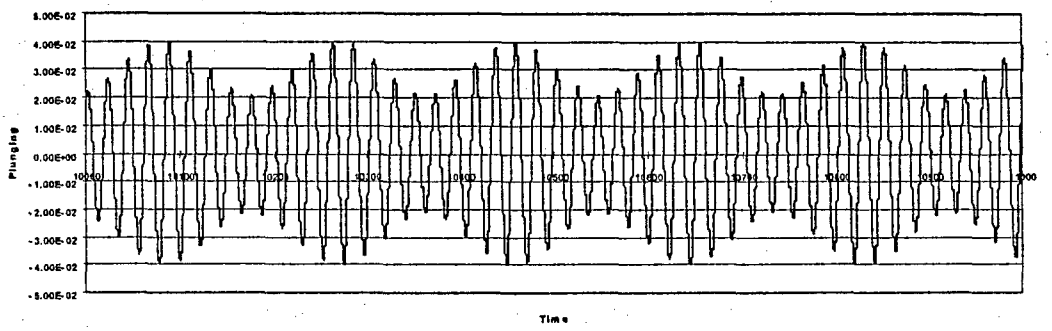

a)

Time history of plunging

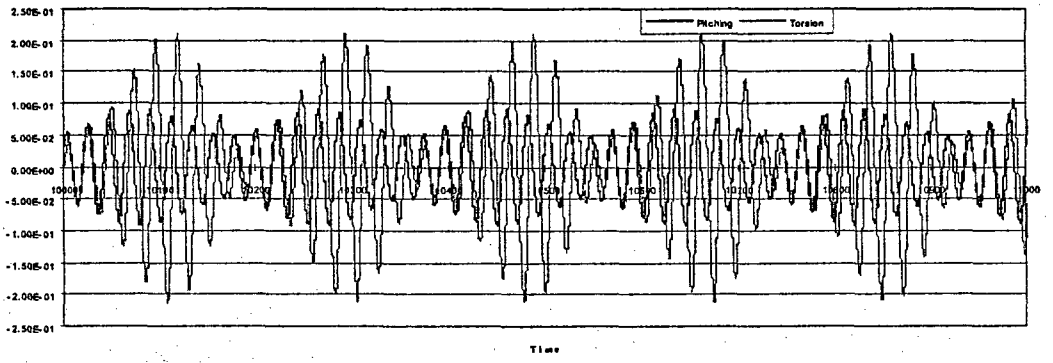

b)

Time history of pitching and torsion

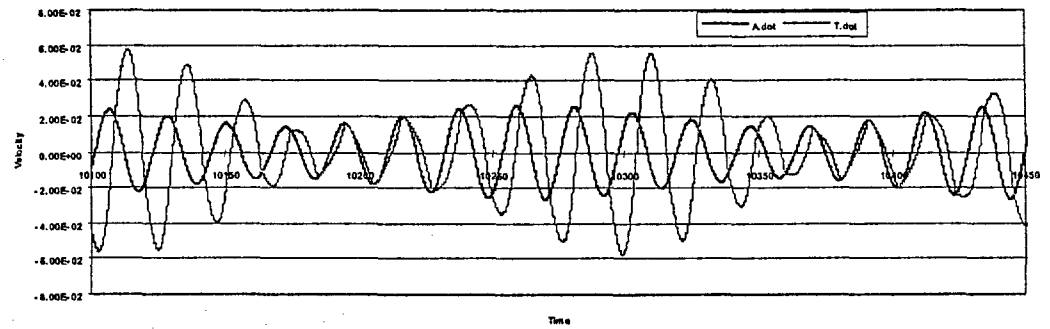

c)

Time history of velocity in pitching and torsion

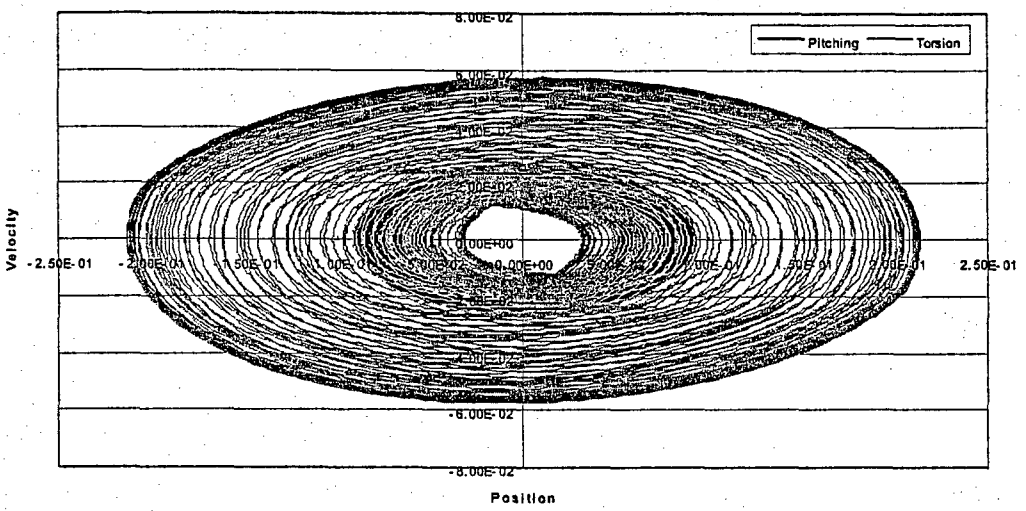

d) Phase plane plot for pitching and torsion

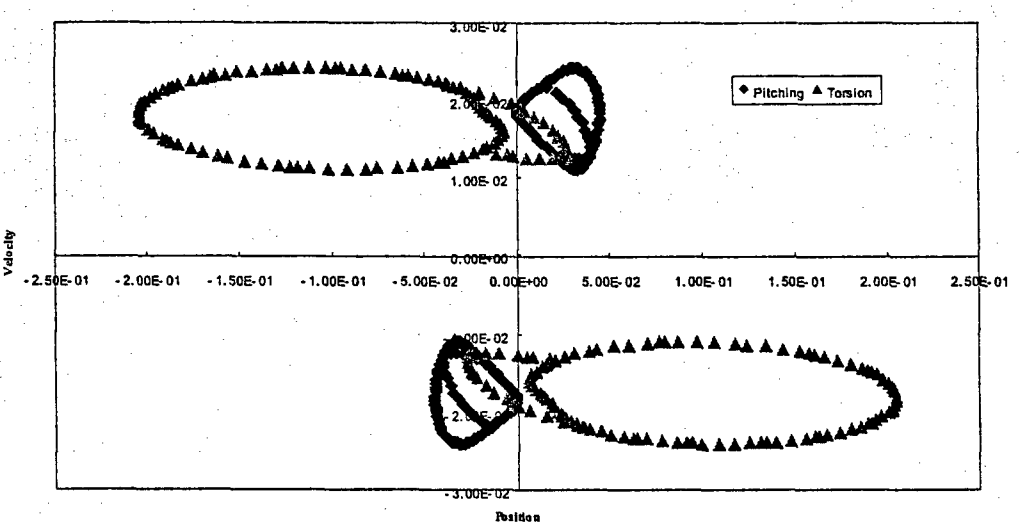

e) Sampled phase plane plot at the moment when the relative velocity becomes zero

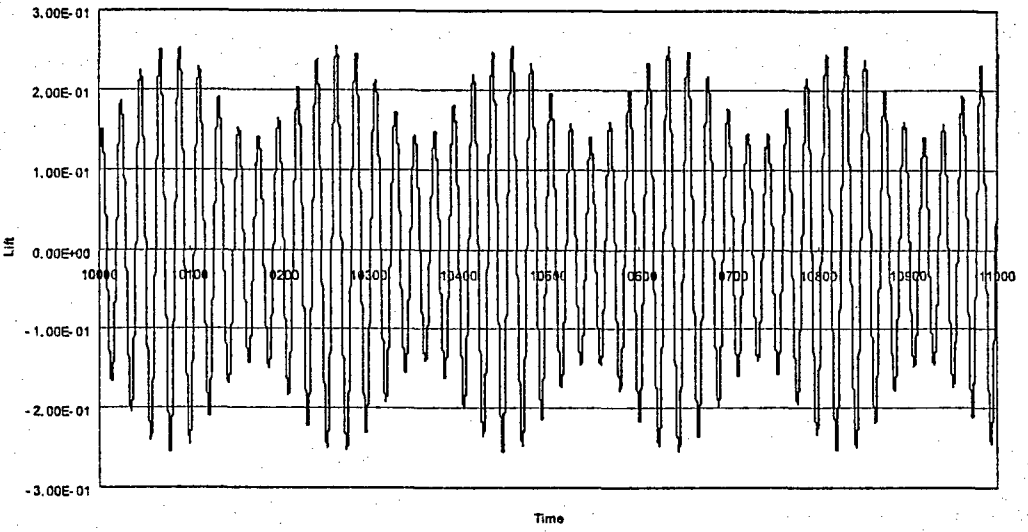

f) Time history of lift

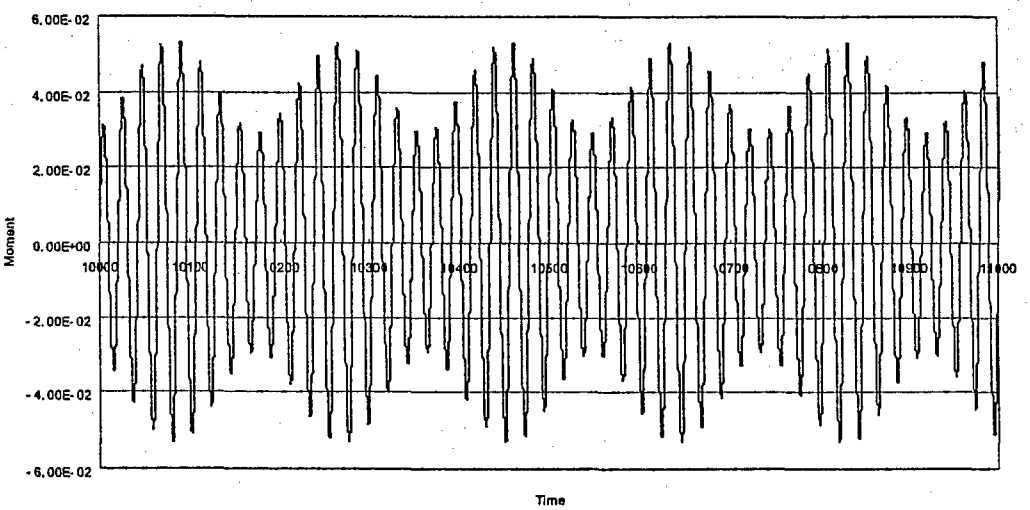

g) Time history of moment

Fig. 2.8 $\mu = 0.001$, k_d=0.0162Nm/rad, U=1.013m/s (MFSS)

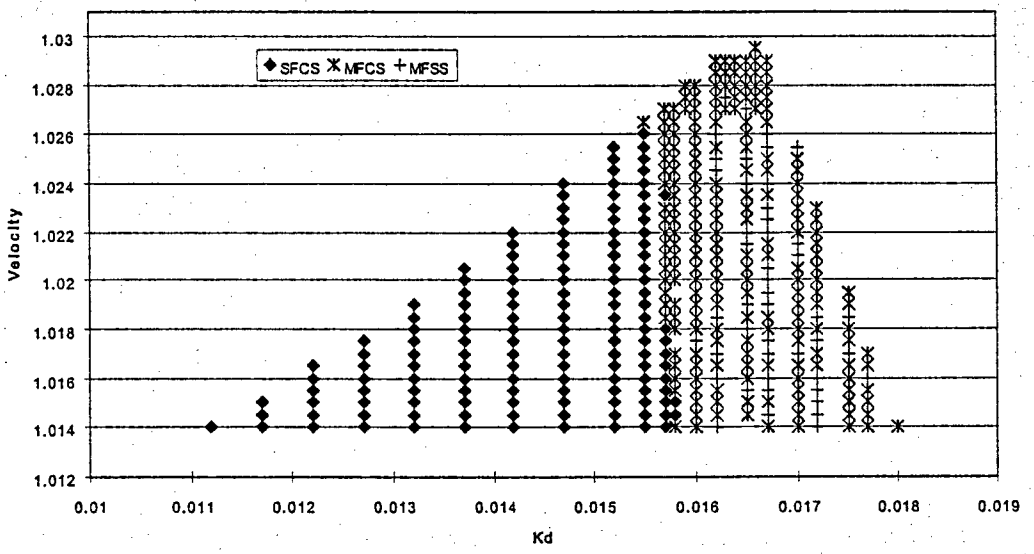

a) Characterization of the stable solutions

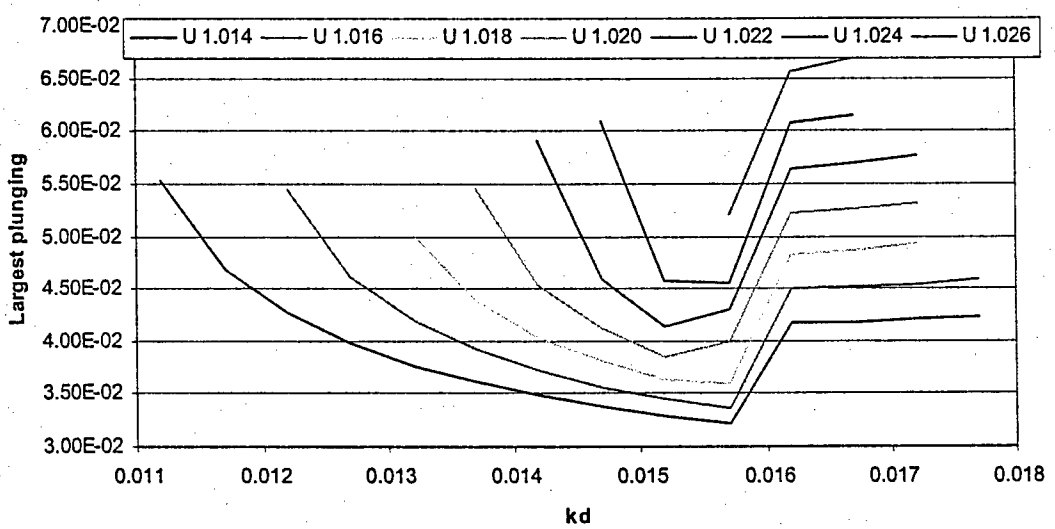

b)

Largest plunging response

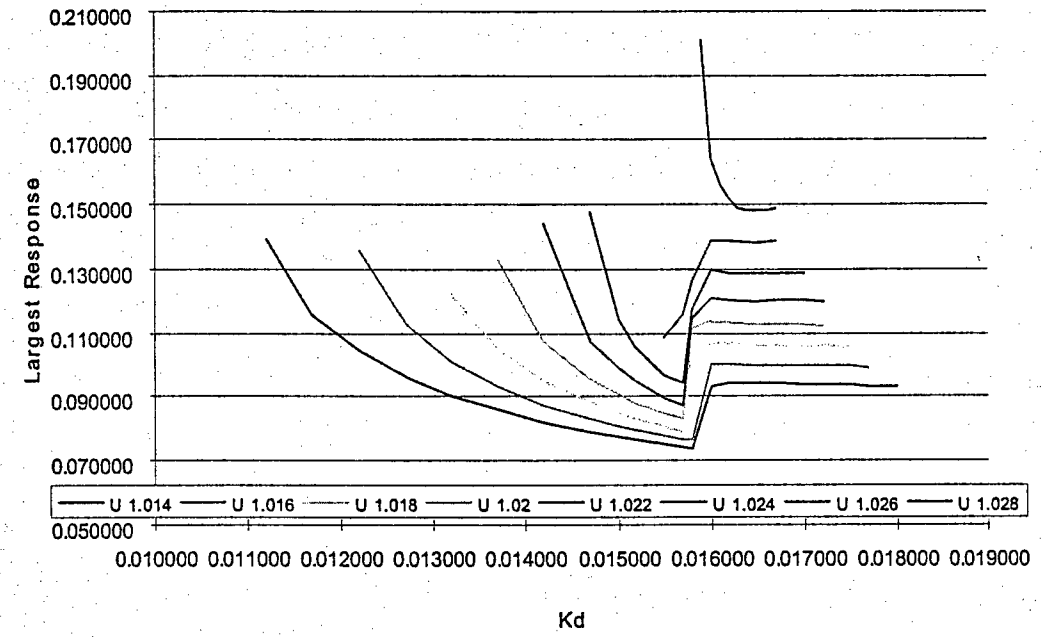

b)

Largest pitching response

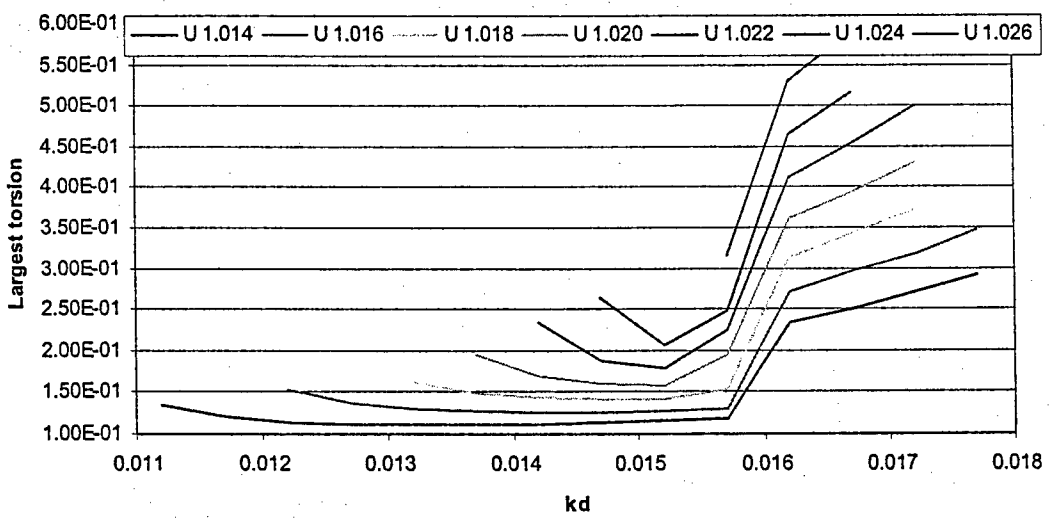

d)

Largest torsion response

Fig. 2.9 Character and largest responses as functions of U and k_d

The search for subcritical limit cycle oscillation, i.e. occurring at speeds lower than the flutter speed of the stuck system, was continued for k_d=0.016 Nm/rad in the range U=0.72 to 1.01m/s. In fact, it was found that an unstable LCO does exit for $U < U_{fl,stuck}$ and this solution is a separatrix, i.e. it separates the motions decaying to zero from those rapidly growing to infinity. In general, the instability of this separatrix renders its numerical estimation very difficult. It was nevertheless estimated here by varying the magnitude of the initial condition until a very slow decay (at first, at least) was obtained, the system response during that phase then clearly approximates the unstable LCO. On that basis, it was observed that the motions on the separatrix would be characterized as single frequency continuous slip.

For speeds larger than the flutter speed of the stuck system, stable single frequency LCOs were obtained for U in the range [0.72, 1.013]. For larger values of U, multiple frequency solutions were observed, see Fig. 2.9. Both stable and unstable LCOs pitching amplitudes are shown in Fig. 2.10. While the presence of the separatrix was not confirmed in the range $U \in [1, 1.013]$, it is conjectured that it is present and that the amplitude of these unstable motions follows the dash line of Fig. 2.10. More specifically, it is suggested that the separatrix meets the stable single frequency LCO branch at the flow speed where this solution become unstable as indicated in Fig. 2.10. The merging of stable and unstable branches has been observed in a 1.5 degree of freedom model.[6,7]

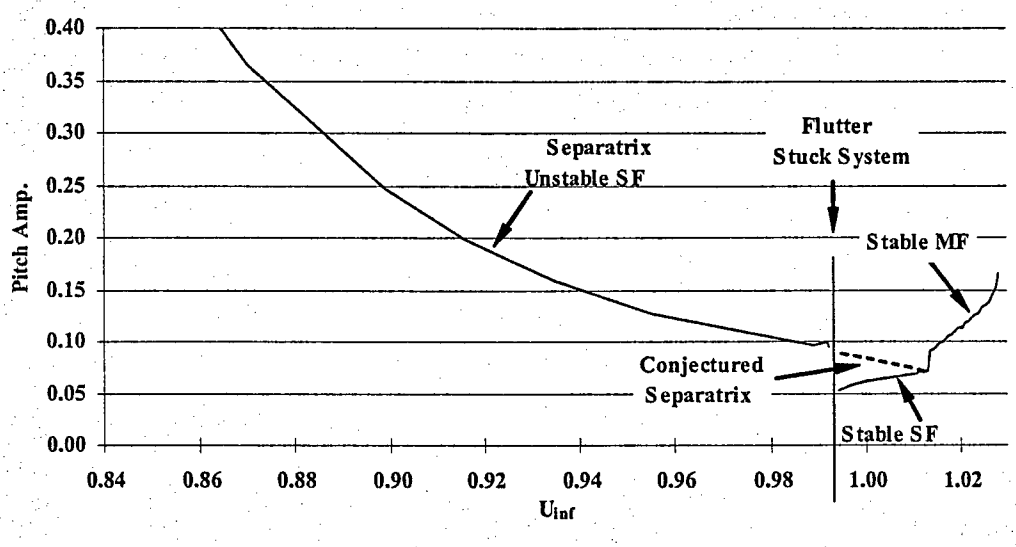

Fig. 2.10 Pitching response as a function of speed, k_d=0.0160 Nm/rad

2.3.3 Harmonic Balance Method

The results presented in the previous section have been obtained by marching in time the system response from a set of initial conditions until steady state. It would be desirable to have a procedure that allows the determination of the steady state solution without considering the transient motions. Two such approaches are possible.

An exact approach for the determination of the steady state solution can be formulated along the lines suggested by Den Hartog[11] because the system is linear except for the transition. That is, a set of yet unknown amplitudes are assumed at a time t=0 (conveniently selected as the time at which the relative velocity $\dot{\theta}-\dot{\alpha}=0$) and the

response is analytically computed for a half-cycle assuming the existence of zero, one, two.... sticking phases. Then, a periodicity condition is enforced on positions and velocities. For a continuous slip solution, this process would lead to 10 equations for 10 unknowns constituted of 9 positions and velocities at t=0 and the period. While these equations are linear in the 9 unknown initial conditions, they are extremely nonlinear with respect to the period and an iterative approach is necessary.

A simpler but approximate method to obtain the steady state solution is to rely on the harmonic balance method. This approach rests on the approximation of the response as a Fourier series of a yet unknown fundamental frequency. Inserting this representation in the equations of motion and satisfying them to the highest possible harmonic leads to a set of equations for the unknown fundamental frequency and the Fourier coefficients. This approach is most reliable when the response is closest to a series of sine and cosine terms, i.e. in continuous slip situations, and it is only in these situations that it will be investigated here.

Considering only a single harmonic, the harmonic balance approximation of the response is

$$h(t) = A\cos k\tau + B\sin k\tau = \mathrm{Re}\left[(A - iB)e^{ik\tau}\right] \tag{2-32}$$

$$\alpha(t) = C\cos k\tau + D\sin k\tau = \mathrm{Re}\left[(C - iD)e^{ik\tau}\right] \tag{2-33}$$

$$\theta(t) - \alpha(t) = E\cos k\tau \tag{2-34}$$

Note in the above equation that $\theta(t) - \alpha(t)$ does not contain both $\sin k\tau$ and $\cos k\tau$ terms. It is indeed allowed to set one of the Fourier coefficients to zero in free

response problems of time invariant systems. This assumption is in fact equivalent to imposing t=0 as a time at which the relative velocity vanishes.

Then, from Eq. (2-10) and (2-11) the lift and moment can be expressed as

$$L = (L_{hr} + iL_{hi})(A - iB)e^{ik\tau} + (L_{\alpha r} + iL_{\alpha i})(C - iD)e^{ik\tau} \tag{2-35}$$

$$M = (M_{hr} + iM_{hi})(A - iB)e^{-ik\tau} + (M_{\alpha r} + iM_{\alpha i})(C - iD)e^{-ik\tau} \tag{2-36}$$

A one term Fourier series approximation of the moment due to friction is obtained as

$$M_f = \mathrm{sgn}(\theta - \alpha)\mu M_0 \approx \frac{4\mu M_0}{\pi}\sin\omega t \tag{2-37}$$

Substituting the above expressions for all displacements and friction moment into Eq. (2.5) through (2.7) leads to the following system of equations

$$H\begin{bmatrix} A \\ B \\ C \\ D \\ E \end{bmatrix} = \frac{4\mu N}{\pi}\begin{bmatrix} 0 \\ 0 \\ 0 \\ 1 \\ 0 \\ 1 \end{bmatrix} \tag{2-38}$$

where H is the following 6x5 array

$$H = \begin{bmatrix} -Mk^2 + k_h + L_{hr} & L_{hi} & -S_\alpha k^2 + L_{ar} & L_{ai} & 0 \\ -L_{hi} & -Mk^2 + k_h + L_{hr} & -L_{\alpha i} & -S_\alpha k^2 + L_{\alpha r} & 0 \\ -S_\alpha k^2 - M_{hr} & -M_{hi} & -I_\alpha k^2 + k_\alpha - M_{\alpha r} & -M_{\alpha i} & -k_d \\ M_{hi} & -S_\alpha k^2 - M_{hr} & M_{\alpha i} & -I_\alpha k^2 + k_\alpha - M_{\alpha r} & 0 \\ 0 & 0 & -I_d k^2 & 0 & k_d - I_d k^2 \\ 0 & 0 & 0 & I_d k^2 & 0 \end{bmatrix} \tag{2-39}$$

Proceeding with linear combination of rows, it is possible to rewrite Eq. (2-39) as

$$\overline{H}\begin{bmatrix} A \\ B \\ C \\ D \\ E \end{bmatrix} = \frac{4\mu N}{\pi}\begin{bmatrix} 0 \\ 0 \\ 0 \\ 0 \\ 0 \\ 1 \end{bmatrix} \tag{2-40}$$

where $\overline{H}$ is obtained from the matrix H by replacing its fourth row by the difference between fourth and sixth row.

The determination of the 6 unknowns A, B, C, D, E and k satisfying the 6 equations of Eq. (2-36) is easily achieved by first partitioning the matrix $\overline{H}$ as

$$\overline{H} = \begin{bmatrix} \overline{H}_1 \\ \underline{\overline{H}}_2 \end{bmatrix} \tag{2-41}$$

where $\overline{H}_1$ is 5x5 and $\underline{\overline{H}}_2$ is a five component row vector. Then, introducing $\underline{\varphi}^T = [A \quad B \quad C \quad D \quad E]$, it is seen that Eq. (2-41) is equivalent to

$$\overline{H}_1 \underline{\varphi} = \underline{0} \tag{2-42}$$

and

$$\underline{\overline{H}}_2^T \underline{\varphi} = \frac{4\mu N}{\pi} \tag{2-43}$$

It is then concluded that $\overline{H}_1$ must be singular, i.e. that the fundamental frequency k must be determined so that $\det(\overline{H}_1)=0$. Once this is achieved, the vector $\underline{\varphi}$ containing the Fourier components of the response is the eigenvector of $\overline{H}_1$ corresponding to its zero eigenvalue normalized according to Eq. (2-43). This normalization condition implies that

the solution pbtained by the harmonic balance linearly scales with the coefficient of friction. In fact, this result is also valid for the exact solution following arguments developed in Ref. 8 and it is sufficient to conduct the analysis for a single value of μ as done here.

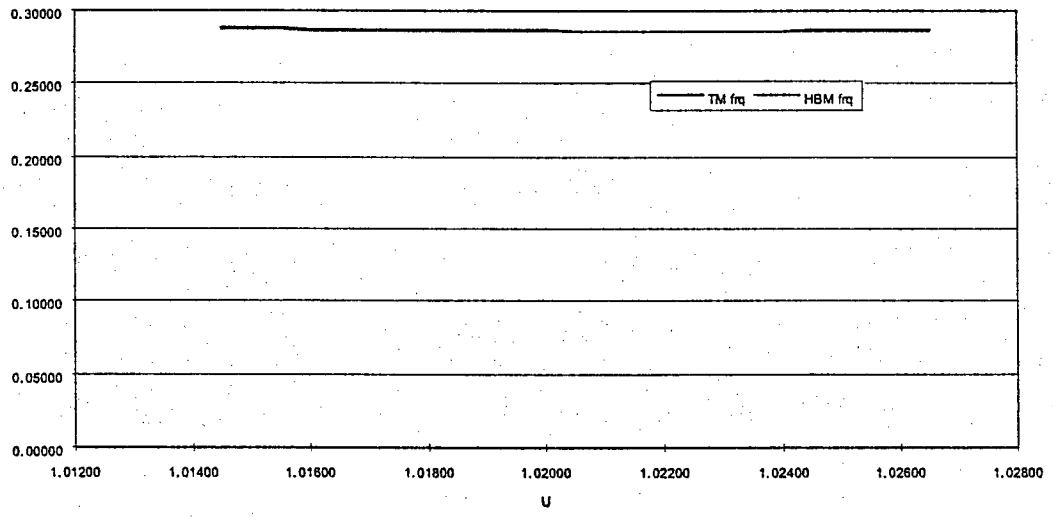

a)

Frequency comparison

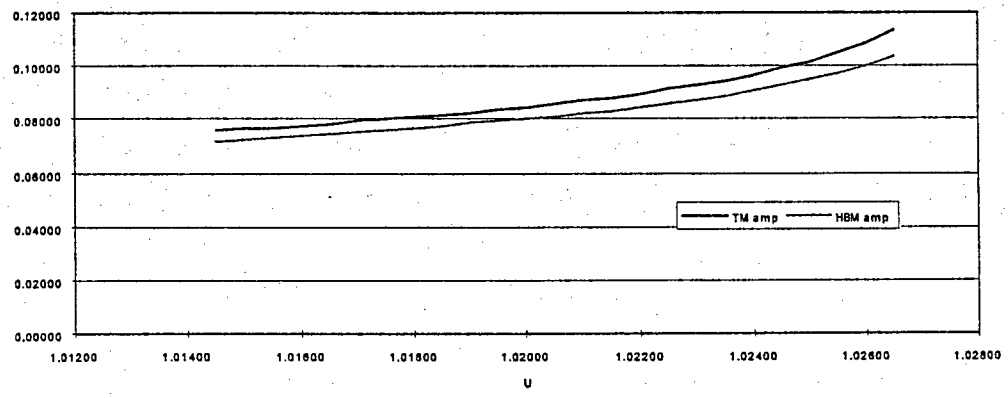

b) Maximum pitching amplitude

Fig. 2.11 Comparison of LCO frequency and pitching amplitude obtained by time marching (TM) and the harmonic balance method (HBM), k_d =0.0155Nm/rad

The above procedure was applied for k_d =0.0155 Nm/rad and $U \in$ [1.0145,1.0265] m/s. Shown in Fig. 2.11 are the frequency and amplitudes of response obtained by both the harmonic balance method and the time marching approach. Clearly, the matching is excellent for single frequency continuous slip solutions. Figure 2.12 provides a correspondence between the actual time histories for k_d =0.0155 Nm/rad and U=1.0165m/s obtained by the time marching approach and computed from Eq. (2-32) through (2-34) with the Fourier coefficients A, B, C, D, E estimated for Eq. (2-42) and (2-43). This figure demonstrates that the harmonic balance approximation represents well the solution as a function of time, not only in magnitudes.

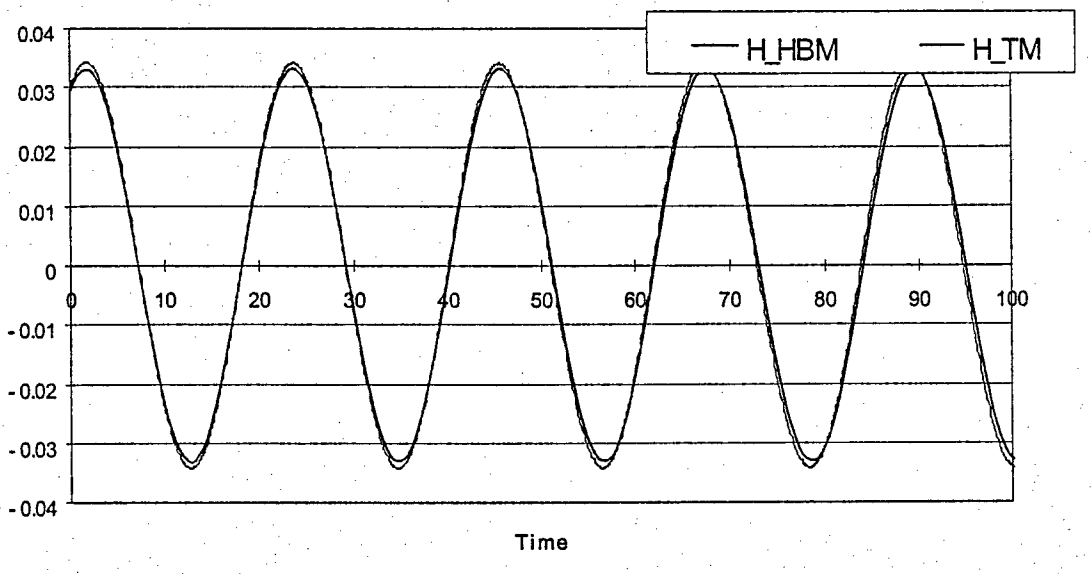

a)

Plunging

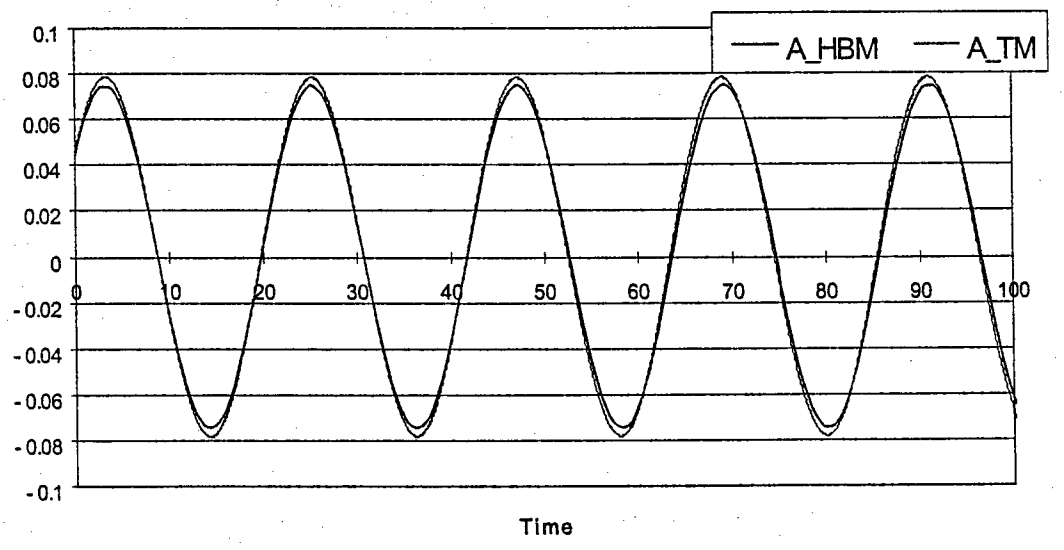

b) Pitching

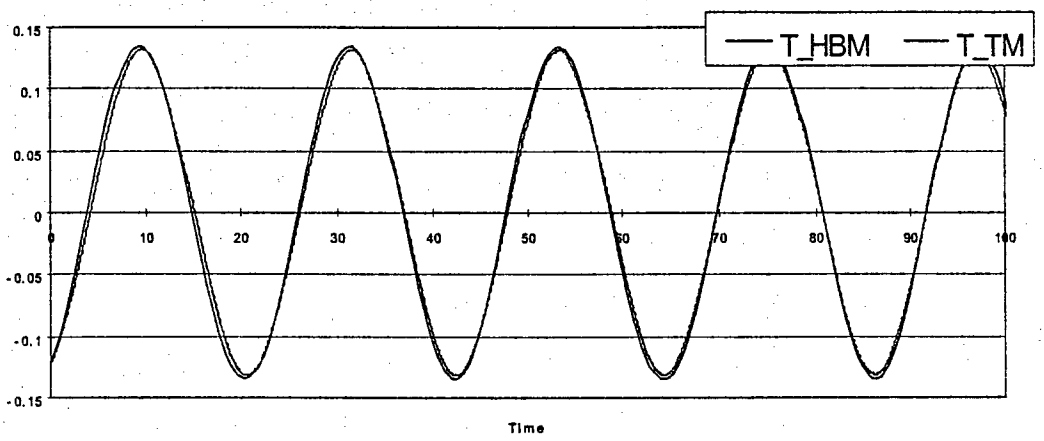

c) Torsion

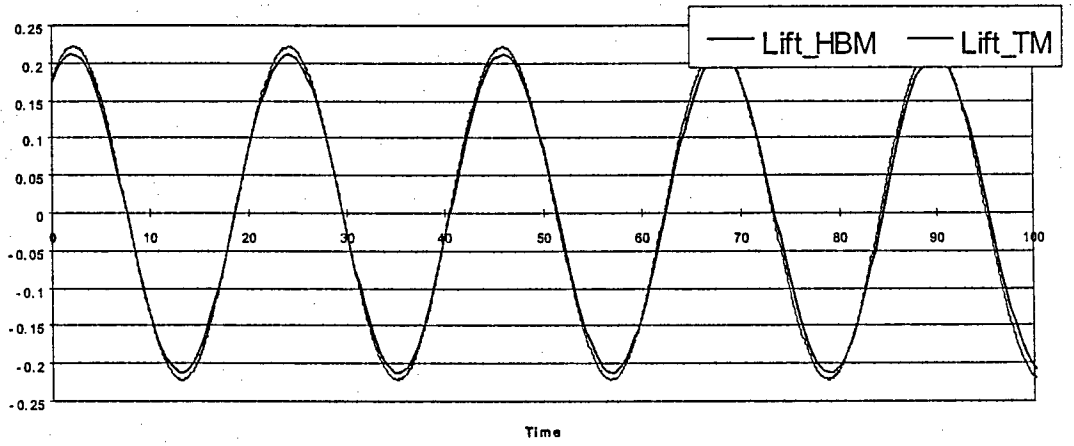

d) Lift

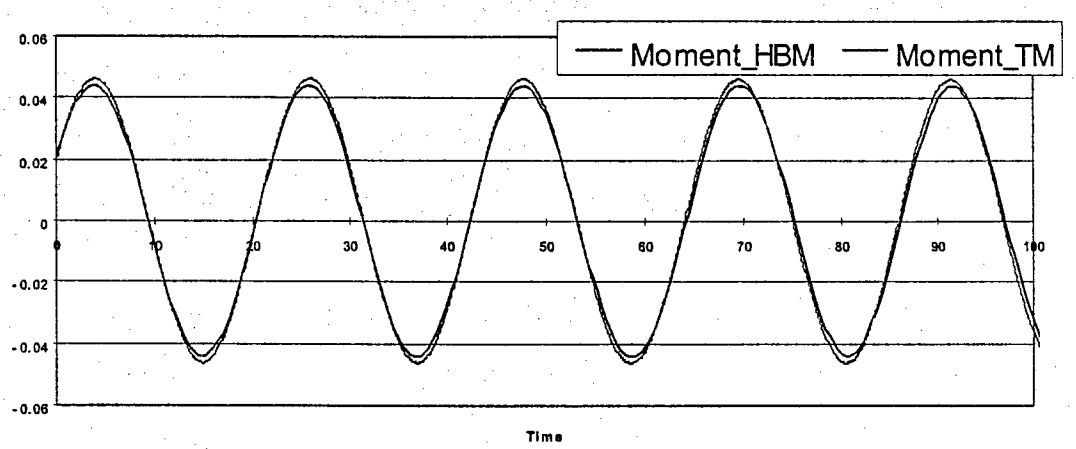

e)

Moment

Fig. 2.12 Comparison of time histories obtained by the time marching approach (TM) and the harmonic balance method (HBM).

CHAPTER 3

AIRFOIL WITH INTERNAL FRICTION

The previous chapter has focused on the assessment of friction in a system that does not exhibit a post-flutter behavior in its absence. It is desired next to evaluate the potential benefits of friction in aeroelastic systems that do exhibit aero-driven cycle oscillation. The work of Jadic et al.[12] has demonstrated that a NACA0012 airfoil in an incompressible inviscid flow may exhibit LCO behavior in a very narrow zone of speeds past the flutter point. This example will thus serve here to assess the role of friction in existing LCO and both the sliding and torsional friction models of Fig. 1.2 and 1.3 will be investigated. The aerodynamic formulation employed here is identical to the one used by Jadic et al.[12], Yao and Liu,[13] and Yao et al.[14,15] and is briefly reviewed below for completeness.

3.1. Aerodynamic formulation

The flow around the moving airfoil was assumed to be two-dimensional, unsteady, inviscid and incompressible. Accordingly, the velocity field can be expressed as

$$\underline{V} = \underline{U}_{\infty} + \nabla\phi \tag{3-1}$$

where ϕ is a pontential satisfying the Laplace equation

$$\Delta\phi = 0 \tag{3-2}$$

In addition to verifying Eq. (3-2), the potential ϕ must also satisfy the following boundary conditions

(1) The flow tangency condition

The flow is assumed inviscid and always attached on the surface of the airfoil so that

$$(\underline{V}_0 - \underline{V}_S)\cdot \underline{n} = 0 \text{ everywhere on the airfoil surface} \tag{3-3}$$

where $\underline{V}_s$ is the local velocity of the airfoil surface, and $\underline{V}_0$ is the local flow velocity on the airfoil, i.e. convection velocity, and $\underline{n}$ is the local normal to the airfoil surface.

(2) The Kelvin Theorem

The total circulation $\Gamma(t)$ of the confined flowfield is conserved

$$\frac{d\Gamma}{dt} = 0 \tag{3-4}$$

(3) The far field boundary condition

$$\underline{V}_0 = \underline{U}_\infty \text{ as } r \to \infty \tag{3-5}$$

(4) The unsteady Kutta condition

No pressure jump must take place across the wake at the airfoil trailing edge, or

$$\Delta C_p = 0 \text{ at trailing edge} \tag{3-6}$$

The current method adopts the linearized scheme developed by Kim and Mook[16].

The determination of the potential ϕ and velocity field $\nabla\phi$ satisfying the above equations was achieved through the introduction of source and vorticity distributions on the surface of the panel represented by high-order elements (cubic spline curved panels

with continuous slopes and curvatures at the joint points, see Fig 3.1) and of vortices shed from the trailing edge, see Fig. 3.2. Once shed, the vortices were assumed to convect with the local flow without dissipating thus forming an unsteady airfoil-free wake system.

While the strengths of the sources were specified by the slope of the airfoil, those of the vortices on the panel (including the one being shed) were determined at each time step to satisfy Eq. (3-3) to (3-6). More specifically, the flow tangency condition (3-3) led to the system of equations

$$A\,\underline{\gamma} = \underline{C} \tag{3-7}$$

where A is the aerodynamic influence coefficient (AIC) matrix for the vorticity distributions $\underline{\gamma} = \left[\underline{\gamma}_A \quad \Gamma_{TE}\right]^T$. Further, $\underline{\gamma}_A$ is the vector of vorticity strengths on the airfoil section and Γ_{TE} is the vortex shed to the wake at time t. Finally, $\underline{C}$ denotes the vector of net induced normal velocities at the control points due to the sources distributions, wake, vortices, and airfoil motions. Finally, the integration of the pressure on the airfoil results in the aerodynamic lift and moments, L and M_a. Further details concerning this formulation can be found in Yao and Liu[13] and Yao et al.[14,15].

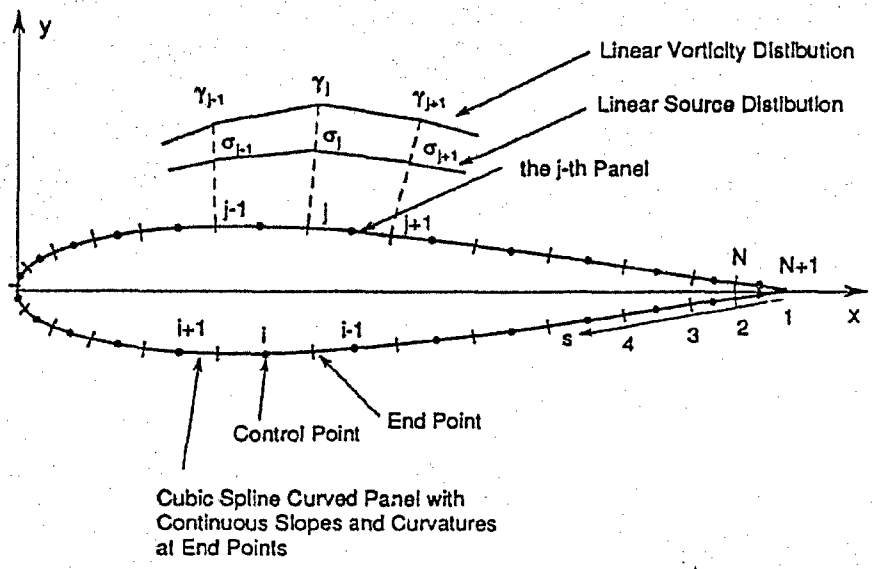

Fig. 3.1 Curved panel and linear source and vorticity distributions

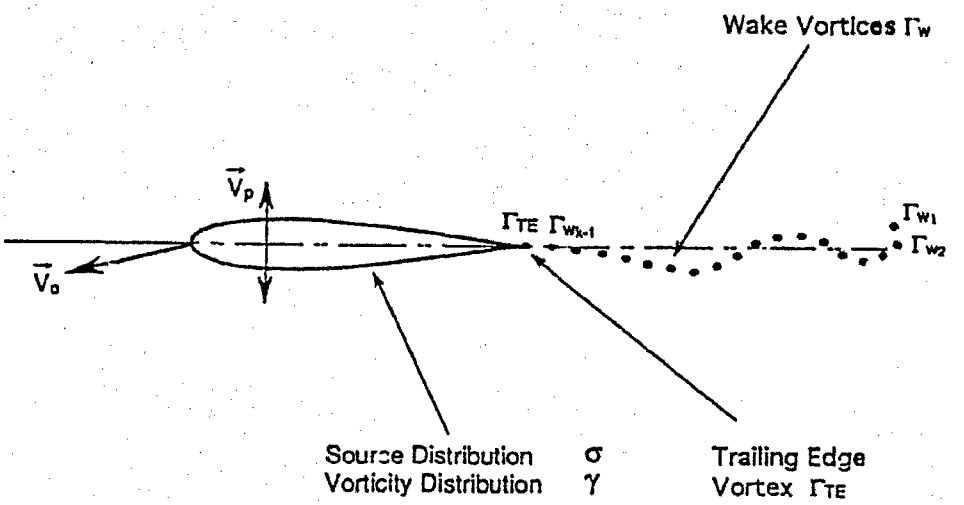

Fig. 3-2 Aerodynamic model

3.2 Airfoil with sliding block

3.2.1 Equations of motion

The structural dynamics model used in the present numerical experiment assumes that the airfoil exhibits only rigid body motion in pitching (rotation) and plunging (vertical movement). In the absence of friction, the equations of motion of this two-degree-of-freedom system are

$$M\ddot{h} - Md\cos\alpha\ddot{\alpha} + Md\sin\alpha\dot{\alpha}^2 + k_h h = L \tag{3-8}$$

$$I_\alpha\ddot{\alpha} - Md\cos\alpha\ddot{h} + k_\alpha\alpha = M_\alpha \tag{3-9}$$

where h is the plunging displacement of the airfoil, defined positive upwards, and α is the pitching displacement of the airfoil, defined positive nose up. The coefficient d is the distance between the elastic axis and the center of mass, M is the mass of the airfoil section with a unit spanwise length, I_α is the corresponding mass moment of inertia of the airfoil section. Finally, k_h and k_α are the modal stiffnesses corresponding to the plunging and pitching motions, respectively.

When an internal sliding block is present, the equations of motion become

$$\begin{aligned} &M\ddot{h} - Md\cos\alpha\ddot{\alpha} + Md\sin\alpha\dot{\alpha}^2 + k_h h - \sin(\theta-\alpha)(T_f + k_f r) \\ &-m\cos(\theta-\alpha)\left[-\ddot{h}\cos(\theta-\alpha) + r\ddot{\alpha} + 2\dot{r}\dot{\alpha} - a\dot{\alpha}^2\right] = L \end{aligned} \tag{3-10}$$

$$\begin{aligned} &Md\cos\alpha\ddot{h} - I_\alpha\ddot{\alpha} - k_\alpha\alpha - a(T_f + k_f r) \\ &-rm\left[-\ddot{h}\cos(\theta-\alpha) + r\ddot{\alpha} + 2\dot{r}\dot{\alpha} - a\dot{\alpha}^2\right] = -M_\alpha \end{aligned} \tag{3-11}$$

for the airfoil, and

$$m\sin(\theta-\alpha)\ddot{h}-ma\ddot{\alpha}+m\ddot{r}-mr\dot{\alpha}^2+(T_f+k_f r)=0 \tag{3-12}$$

for the sliding block. In these equations, θ is the fixed angle between the chord line and the track in which the block slides and a is the shortest distance between the elastic axis and the track. Further, m is the mass of the block, $r(t)$ is its displacement, and k_f is the stiffness of the spring connecting the block to the airfoil. Finally, T_f is the friction force between the block and the track. It is defined as

$$T_f=\mu_D N\cdot\mathrm{sgn}(\dot{r}) \text{ when slip occurs} \tag{3-13a}$$

and

$$|T_f|<\mu_S N \text{ when sticking occurs} \tag{3-13b}$$

where N is the normal force and μ_S and μ_D are the static and dynamic coefficient of friction, respectively.

The integration of the equations of motion broadly follows the scheme proposed by Jadic et al.[12] but modified to account for the presence and effects of the sliding block.

That is, during slip phases, Eq. (3-10), (3-11) and (3-12) can be rewritten as

$$M_1\ddot{h}+k_h h=F_1 \tag{3-14a}$$

$$M_2\ddot{\alpha}+k_\alpha\alpha=F_2 \tag{3-14b}$$

$$m\ddot{r}+k_f r=F_3 \tag{3-14c}$$

where

$$F_1 = R_1 - \frac{C_2}{C_3}R_2 - \frac{C_2}{C_3}k_\alpha \alpha$$

$$F_2 = -R_2 + \frac{C_2}{C_1}R_1 - \frac{C_2}{C_1}k_h h$$

$$F_3 = -m\sin(\theta-\alpha)\left(\frac{F_1 - k_h h}{M_1}\right) + ma\left(\frac{F_2 - k_\alpha \alpha}{M_2}\right) - T_f + m\dot{\alpha}^2 r$$

$$C_1 = M + m\cos^2(\theta-\alpha)$$

$$C_2 = Md\cos\alpha + mr\cos(\theta-\alpha)$$

$$C_3 = I_\alpha + mr^2$$

$$R_1 = -Md\sin\alpha\dot{\alpha}^2 + \sin(\theta-\alpha)(T_f + k_f r) + m\cos(\theta-\alpha)(2\dot{r}\dot{\alpha} - a\dot{\alpha}^2) + L$$

$$R_2 = a(T_f + k_f r) + mr(2\dot{r}\dot{\alpha} - a\dot{\alpha}^2) - M_\alpha$$

During sticking phases, it is not the position of the block which is an independent variable but rather the force of friction. Specifically, imposing $\dot{r} = \ddot{r} = 0$ in Eq. (3-12), it is found that

$$(T_f + k_f r) = -m\sin(\theta-\alpha)\ddot{h} + md\ddot{\alpha} + mr\dot{\alpha}^2 \tag{3-15}$$

and further that

$$M_3\ddot{h} + k_h h = F_4 \tag{3-16a}$$

$$M_4\ddot{\alpha} + k_\alpha \alpha = F_5 \tag{3-16b}$$

where

$$M_3 = C_4 - \frac{C_5^{\,2}}{C_6}$$

$$M_4 = C_6 - \frac{C_5^{\,2}}{C_4}$$

$$F_4 = R_3 + \frac{C_5}{C_6} M_\alpha - \frac{C_5}{C_6} k_\alpha \alpha$$

$$F_5 = M_\alpha + \frac{C_5}{C_4} R_3 - \frac{C_5}{C_4} k_h h$$

$$C_4 = M + m$$

$$C_5 = Md\cos\alpha + mr\cos(\theta - \alpha) + ma\sin(\theta - \alpha)$$

$$C_6 = I_\alpha + mr^2 + ma^2$$

$$R_3 = L - \left[md\sin\alpha + ma\cos(\theta - \alpha) - mr\sin(\theta - \alpha)\right]\dot{\alpha}^2$$

3.2.2 Numerical solution of the equations of motion

The numerical implementation of the above structural and aerodynamic models necessitates the careful handling of the fluid-structure interaction and of the friction related transitions, i.e. slip to stick, stick to slip and slip to slip.

In regard to the first issue, a full aero-structure feedback was desired and was accomplished in an iterative manner within each time step of the computations[12]. To

clarify this strategy, let t_i and t_{i+1} denote the beginning and end of the i^{th} time step. Then, at the first iteration of that time step, an estimate of the structural response at t_{i+1} was obtained by integrating the structural dynamics equations from t_i and t_{i+1} assuming right-hand-sides of Eq. (3-14) or (3-16) (including the aerodynamic loading) to be constant for the entire time step and with values obtained from time t_i. This estimate of the structural response was then used to update the boundary conditions for the flow field calculations which in turn provided an estimate of the aerodynamic loading at t_{i+1}. At the second iteration, these values and their counterparts at t_i were combined to yield a linear interpolation of the right-hand-sides of Eq. (3-14) or (3-16) from which the structural response at t_{i+1} was again obtained. The second iteration was completed by the updating of the aerodynamic loading at t_{i+1} and a third iteration was then started. The procedure was continued until a prescribed precision on h, α, and r (10^{-10} relative error between successive iterations) was attained. The computation at the next time step was then initiated and the process repeated until the total time was reached.

The handling of the friction induced transitions was found to fit very naturally in the above framework and was achieved by the cubic/linear interpolation strategy described in section 2.3.1.

3.2.3 Result of the sliding block study

The analysis of the system of Fig. 1.2 was carried out for $m/M = 0.1$. Further, the other system parameters were selected so that the system in sticking mode reduces to the one considered in Ref. 12. That is, $m + M = 20.0$ kg/m; $I = 1.25$ kg m, $k_h = 1.8$ N/m^2 ; $k_\alpha = 1.25$N, $d = 0.1$ m, $c = 1$ m, $\theta = 45$ deg, and a=0. The equations of motion were nondimensionalized by using the chord length and the time needed for the flow to pass through the airfoil. At time t=0, the mass m was assumed to be at the elastic axis of the airfoil. Thus, if it remained there, the airfoil properties would be identical to those considered by Jadic et al.[12] for which the flutter speed was found to be $V_\infty = 2.02$ ($V_\infty = \frac{U_\infty}{\omega_\alpha b}$) and where an LCO naturally occurs. The system was then analyzed from $V_\infty = 2.02$ to 2.4. Additionally, different stiffnesses of the internal spring were selected that yielded natural frequencies of the secondary system close to that of the LCO in the absence of friction, i.e. $k_f = 0.36$, 0.72, 1.00, and 1.20 N/m. For all cases considered, small initial velocities were given to the pitch and block degrees of freedom ($\dot{\alpha} = 0.1$, $\dot{r} = 0.1$ nondim). Limit cycle oscillations with the movable friction block were noted for nondimensional velocities up to $V_\infty = 2.2$.

The analysis of this broad set of data demonstrated the primary existence of single frequency continuous slip and continuous stick solutions, see Fig. (3.3) and (3.4), with the stuck solutions occurring at the highest coefficients of friction considered.

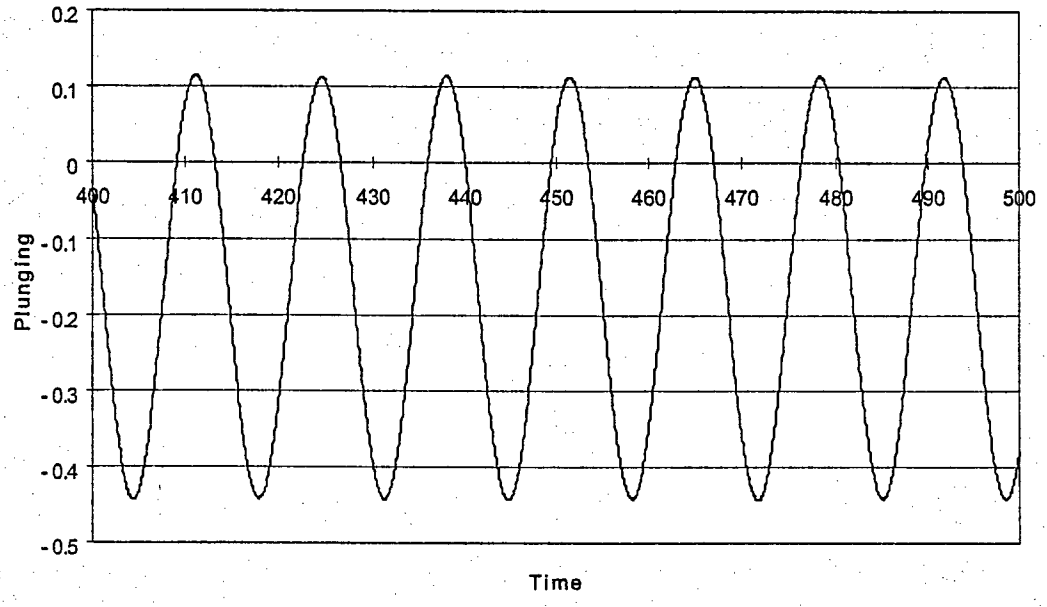

a)

Time history of plunging

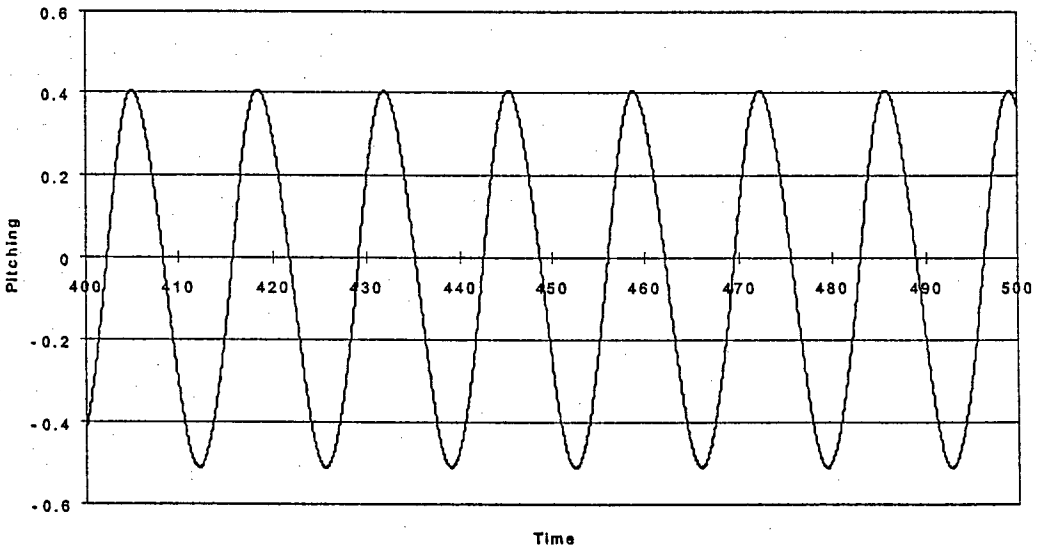

b)

Time history of pitching

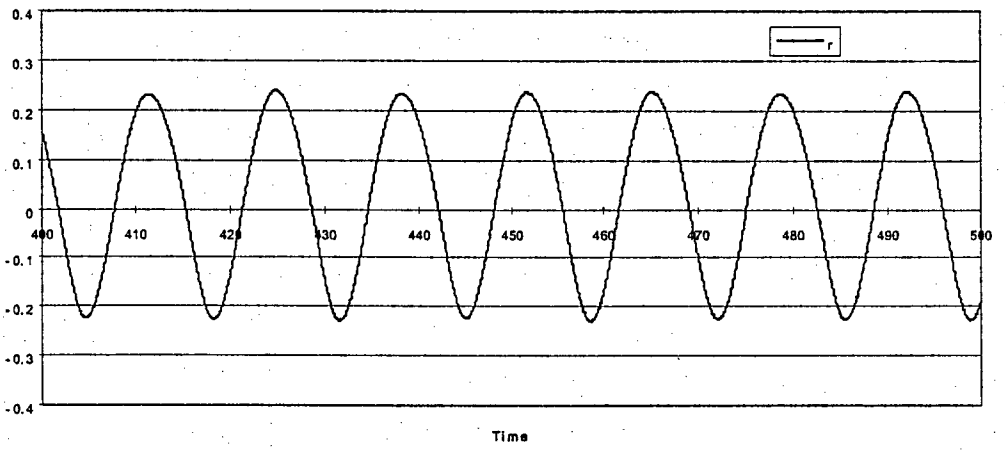

c)

Time history of the block position

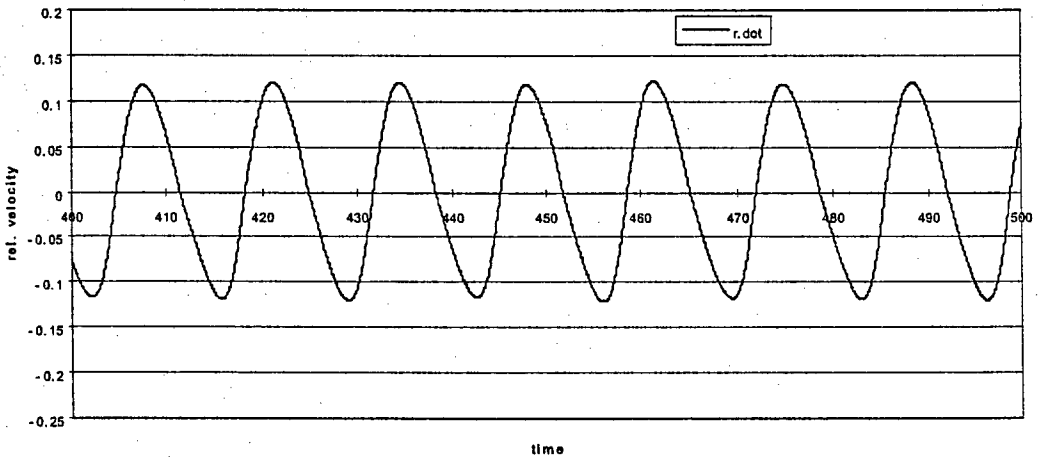

d) Time history of the relative velocity of the block

Fig. 3-3 Response of the system, μ=0.02, k_f=1.2N/m and V=2.2 (SFCS)

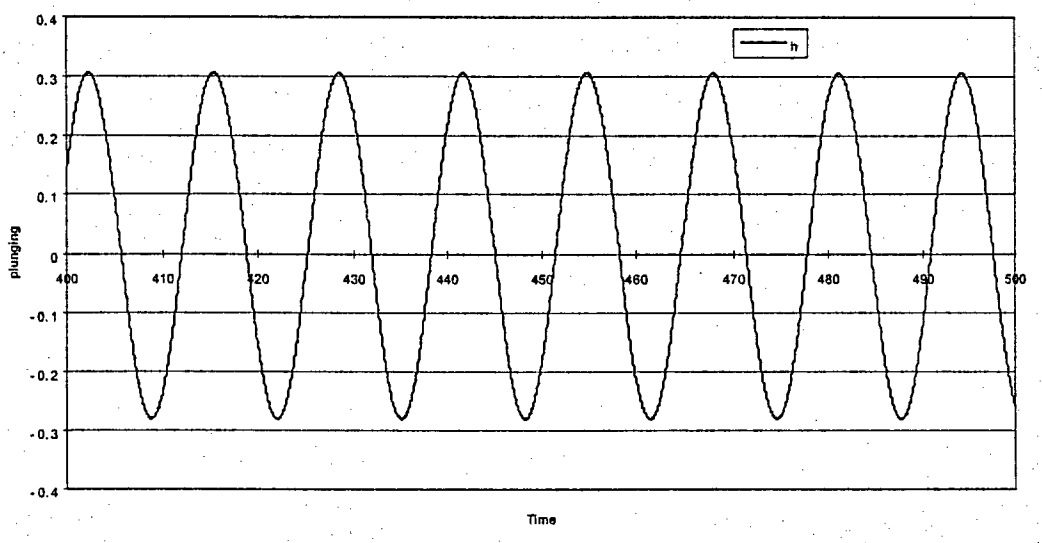

a)

Time history of plunging

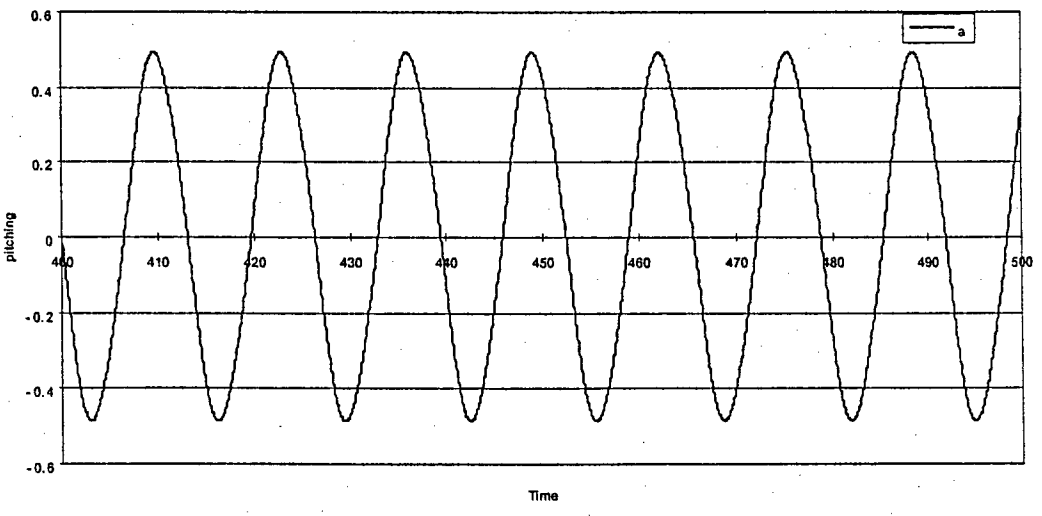

b)

Time history of pitching

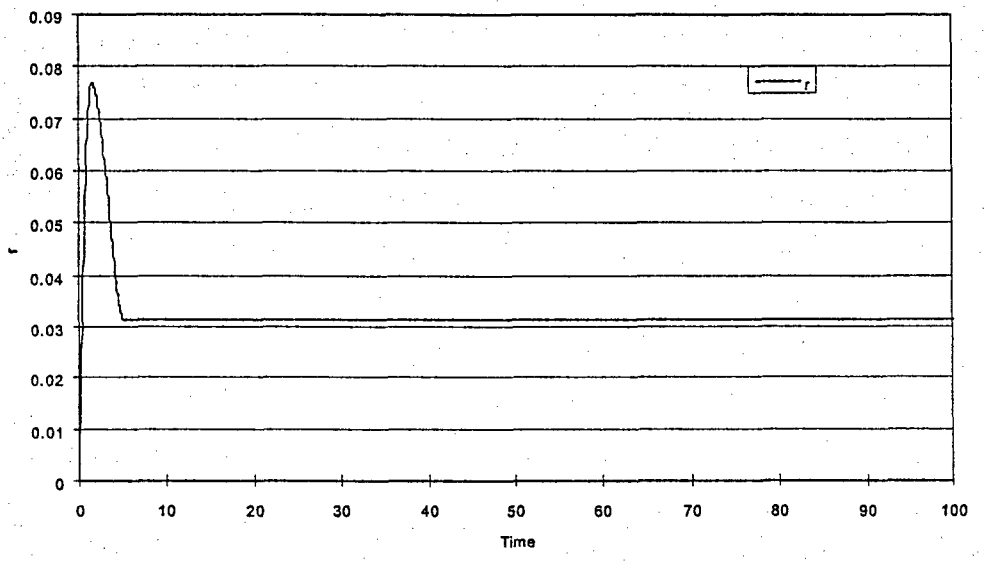

c)

Time history of the block position

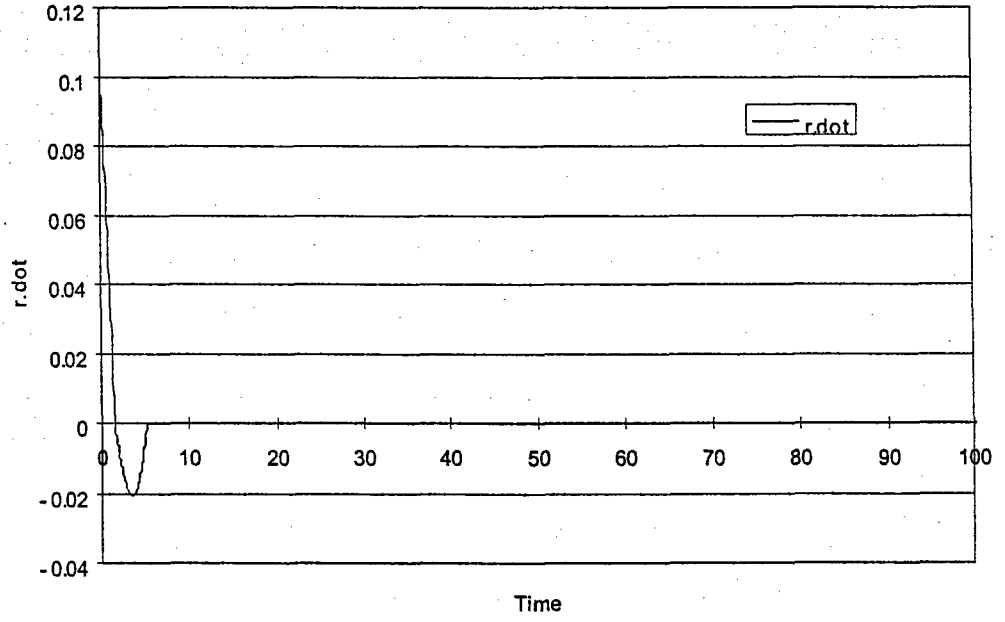

d)

Time history of the relative velocity of the block

Fig. 3.4 Response of the system, μ=0.08, k_f=1.2N/m and V=2.2 (Stuck)

The occurrence of LCO's in stuck configurations of the block was not initially expected and does as not have a counterpart in Ref. 8. This surprising result is due to the effect of the block location on the inertia of the entire airfoil. Indeed, placing the block (in a stuck configuration) away from the airfoil elastic axis increases the inertia of the system, lowers its pitching natural frequency, and increases the flutter speed. That is, placing the mass away from the center, without any motion or friction, already provides a stabilization of the system. This simple observation demonstrates that it is very difficult to assess the bonafide effects of friction on LCO amplitudes for the system of Fig.1.2. Accordingly, no further discussions of this model will take place and the airfoil with the torsional friction device of Fig. 1.3 and 1.4 will be considered instead as it does not suffer from the same issues.

3.3 Airfoil with rotating disk

Denoting by $\alpha(t)$, $h(t)$, and $\theta(t)$ the time varying pitching and plunging of the airfoil and the rotation of the internal disk, it is found that the equations of motion of the system are (the horizontal translation is assumed to be blocked)

$$M\ddot{h} - M a\cos\alpha\,\ddot{\alpha} + M a\sin\alpha\,\dot{\alpha}^2 + k_h h = L \tag{3.21}$$

$$(I - I_d)\ddot{\alpha} - Ma\cos\alpha\,\ddot{h} + (k_\alpha + k_d)\alpha - k_d\theta = M_\alpha + M_f \tag{3.22}$$

$$I_d \ddot{\theta} + k_d (\theta - \alpha) = -M_f \tag{3.23}$$

In these equations, the coefficient a is the distance between the elastic axis and the center of mass (the distance $\overline{PG}$, see Fig. 1.3), M and I are the total mass and moment of inertia of the airfoil (including the disk), I_d is the moment of inertia of the internal disk, and k_h, k_α, k_d are the stiffnesses in plunging, in pitching, and in torsion of the disk. Finally, L and M_α are the aerodynamic lift and moment acting on the airfoil, and M_f is the moment associated with friction, see Eq. (2.4).

3.3.1 Results of the rotating disk study

To echo the study of the lumped mass friction system, the analysis of the system of Fig. 1.3 and 1.4 was carried out for $I_d / I = 0.05$. Further, the other system parameter were set to m = 20.0 kg/m; $I + I_d$ = 1.25 kg m, k_h = 1.8 N/m2; k_α = 1.25 N, a = 0.1 m, and c = 1 m. Thus, the behavior of the airfoil when the disk is stuck is identical to the one obtained by Jadic et al.[12] The equations of motion were nondimensionalized by using the chord length and the time needed for the flow to pass through the airfoil. The system was then analyzed right at the flutter speed of the stuck system (nondim. $V_\infty = 2.02$), where a LCO naturally occurs.

From the time history of the response in stuck mode, it was determined that the disk would be stuck at all times if $\mu > 0.006$. Accordingly, the analysis of the airfoil with

the rotating disk was conducted for $\mu \leq 0.006$. The stiffness k_d was varied and the steady state response of the system was determined by numerically integrating the equations of motion (structural and aerodynamic) from a set of small initial conditions. Shown in Fig. 3.3-3.8 are the largest responses of the pitching, plunging, and torsional degrees-of-freedom for μ = 0.001 - 0.006. Note that the response of the system in stuck mode (or without the disk) is also shown as "h stuck" and "alpha stuck", see Jadic et al.[12]

It is seen in these figures that the responses are below their stuck levels for low values of the stiffness k_d and decrease further as k_d is increased. A minimum of both pitching and plunging responses is obtained at an intermediate value of k_d but it is immediately followed by a sharp rise (especially for the smaller values of μ) of all response amplitudes indicative of the resonance of the torsional disk system, i.e. when its natural frequency is very close to the flutter frequency. This observation is in complete agreement with the "tuned damper" discussion of Agelastos[8]. Increasing further the stiffness k_d takes the system out of resonance and all three responses decrease slowly toward their stuck configuration levels.

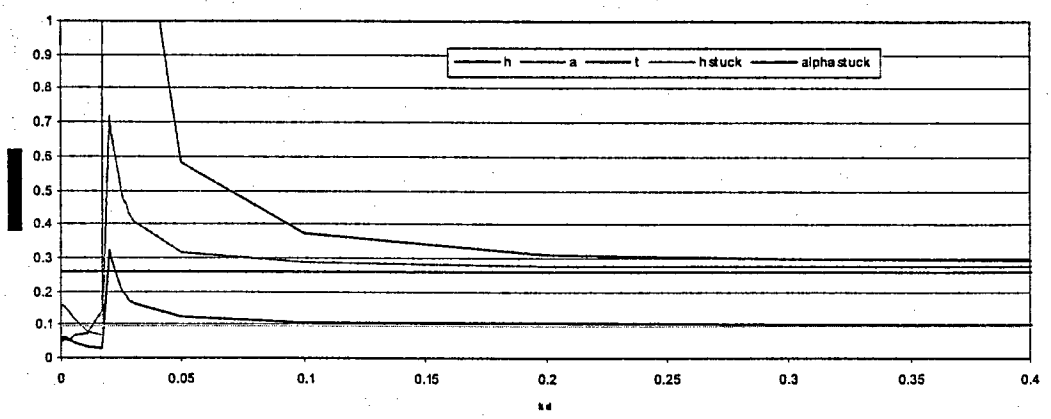

Figure 3.5. Amplitude of response in plunging, pitching, and torsion (for the disk) as a function of the stiffness k_d, μ=0.001

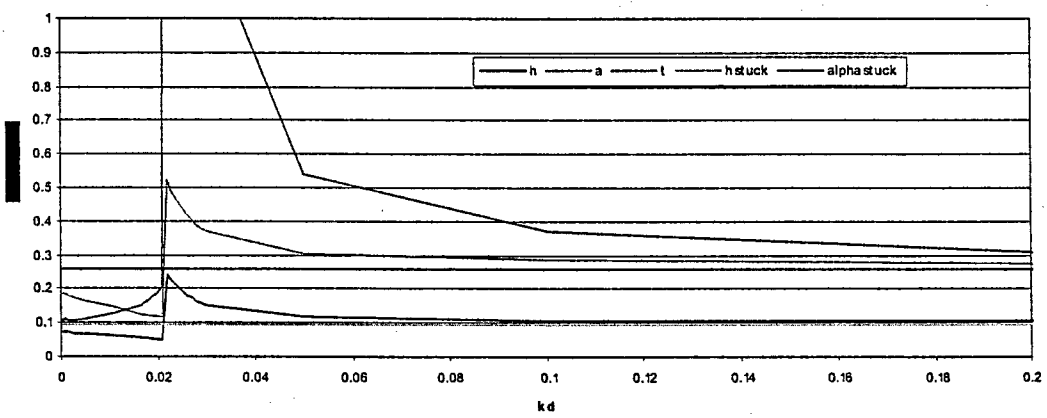

Figure 3.6 Amplitude of response in plunging, pitching, and torsion (for the disk) as a function of the stiffness k_d, μ=0.002

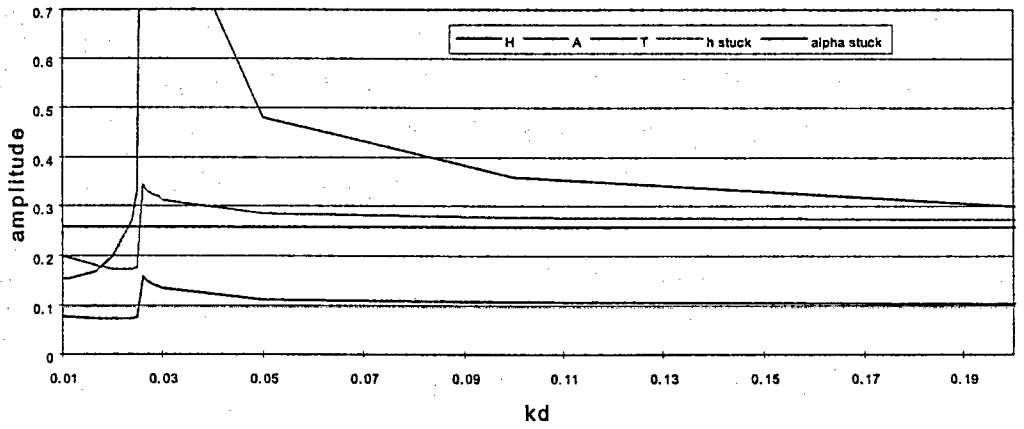

Fig. 3.7 Amplitude of response in plunging, pitching, and torsion (for the disk) as a function of the stiffness k_d, μ=0.003

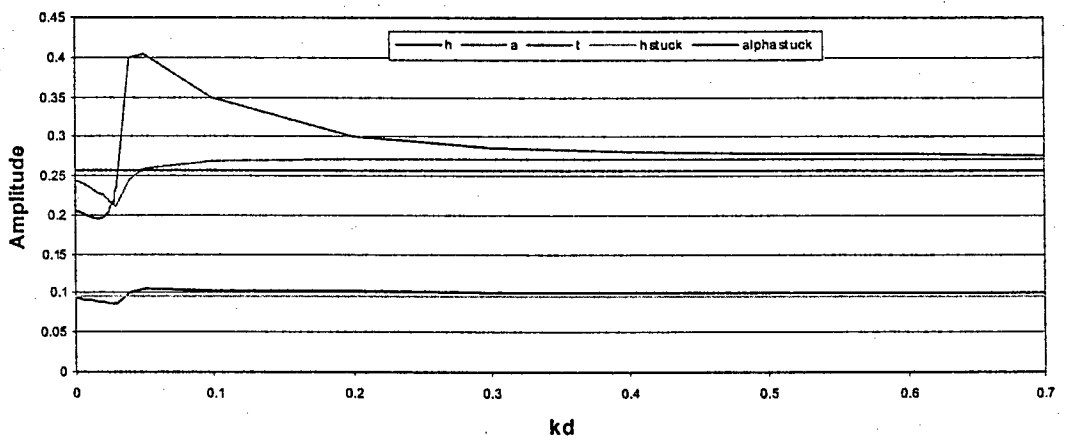

Figure 3.8 Amplitude of response in plunging, pitching, and torsion (for the disk) as a function of the stiffness k_d, μ=0.004

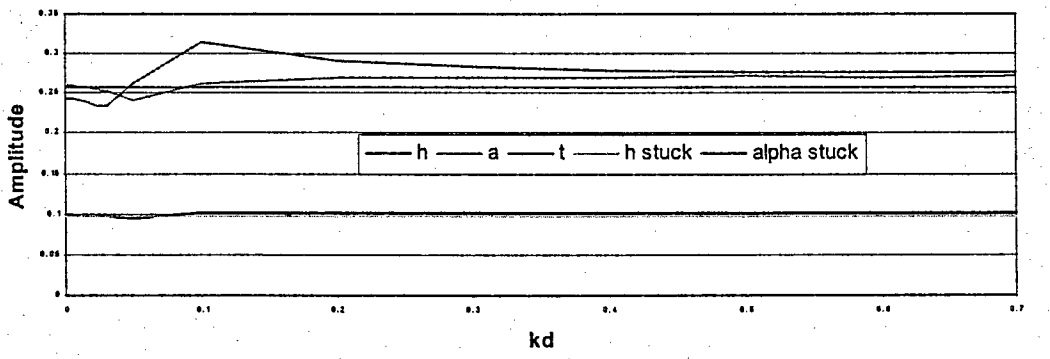

Figure 3.9 Amplitude of response in plunging, pitching, and torsion (for the disk) as a function of the stiffness k_d, μ=0.005

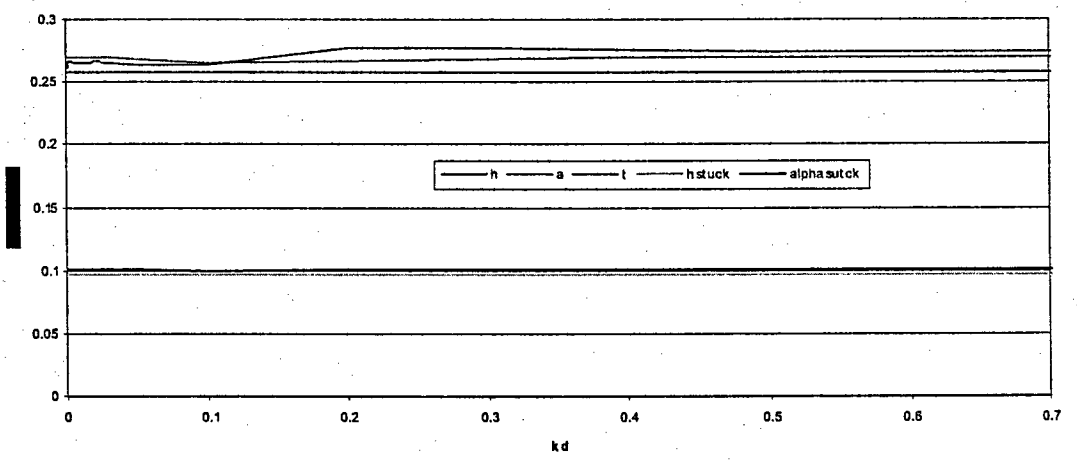

Figure 3.10 Amplitude of response in plunging, pitching, and torsion (for the disk) as a function of the stiffness k_d, μ=0.006

To condense further the results of Fig. 3.5 through 3.10, it was decided to record for each value of μ both the minimum and maximum values of the pitching and plunging amplitudes over the domain $k_d \in [0,\infty)$. The evolution of the minimum amplitude of the plunging and pitching motions with increasing coefficient of friction is shown in Fig. 3.11. It is seen that the benefit of friction is most significant for low coefficients of friction as the corresponding minimum amplitudes of response are well below the stuck values from Ref. 12. But the penalty for this choice is a risk of very high amplitudes, see Fig. 3.12 for the maximum amplitudes, as the minimum and maximum amplitudes occur within a very narrow range of k_d values.

The trend of the minimum amplitudes, see Fig. 3.11, i.e. a monotonic decrease with decreasing coefficient of friction suggests the analysis of the frictionless system, i.e. with $\mu_D = \mu_S = 0$. Interestingly, it was found that the corresponding airfoil motions converge to large amplitude LCOs when k_d is larger than 0.01685 N/m but the response appears to diverge for $k_d \leq 0.01685$ N/m. It is tentatively suggested that this behavior originates from a difference in flutter speeds of the continuously sticking and frictionless slipping systems (as discussed in connection with the flat plate in Chapter 2) and the limited domain of stable LCO of the NACA0012 airfoil in the absence of friction.

The character of the various stable limit cycle was also investigated, see Fig. 3.13. It is seen that single frequency stick slip solutions e.g. see Fig. 3.14, are found in the most of the domain with the exception of the values of k_d and μ that yield large

torsional responses. In that zone, the motions are primarily single frequency continuous slip motion e.g. see Fig. 3.15, with some rare multiple frequency solutions, e.g. see Fig. 3.16.

This characterization is expected: when a low torsional response is induced, sticking is likely to occur while continuous slip motions will be seen for large rotations of the disk. This latter situation occurs when the transfer of energy from the airfoil to the disk takes place efficiently, i.e. for low values of μ and for values of k_d that induce a torsional natural frequency close to the flutter frequency. Finally, the occurrence of multiple frequency solution at the center of the single frequency continuous slip zone is consistent with the analysis of Agelatos[8].

The pattern of the vortices forming the wake was finally analyzed. It was found that these patterns clearly parallel the steady state motions; they form a perfect harmonic arrangement for single frequency solutions, see Fig. 3.15(c) but exhibit beating when the system response is dictated by multiple frequencies, see Fig. 3.16(c).

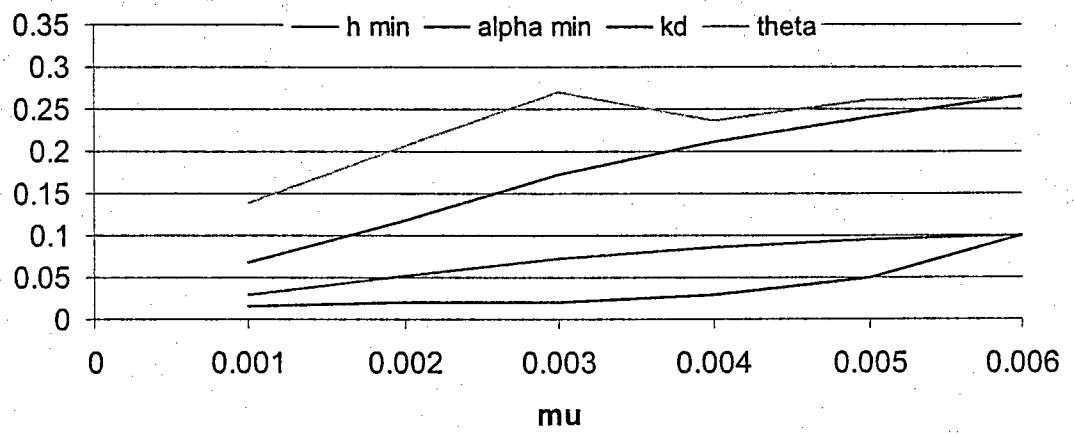

Fig. 3.11 The minimum amplitude of plunging and pitching

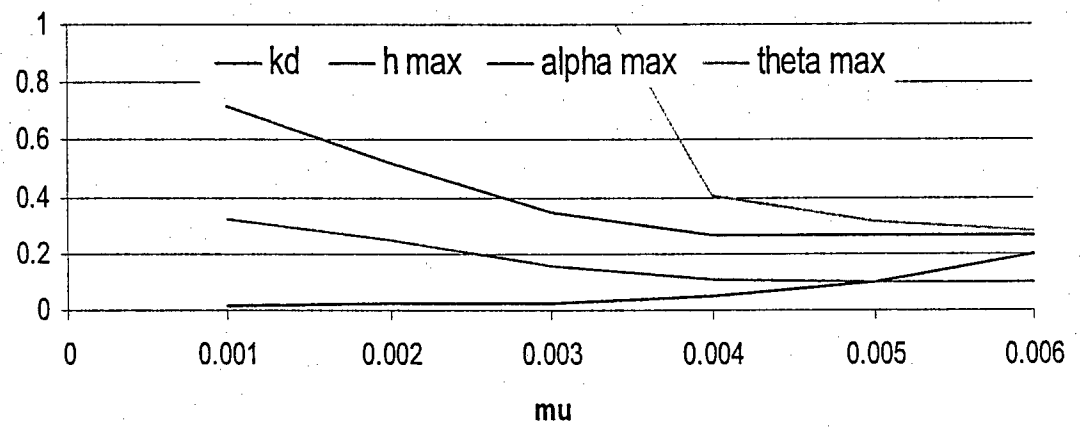

Fig. 3.12 The maximum amplitude of plunging and pitching

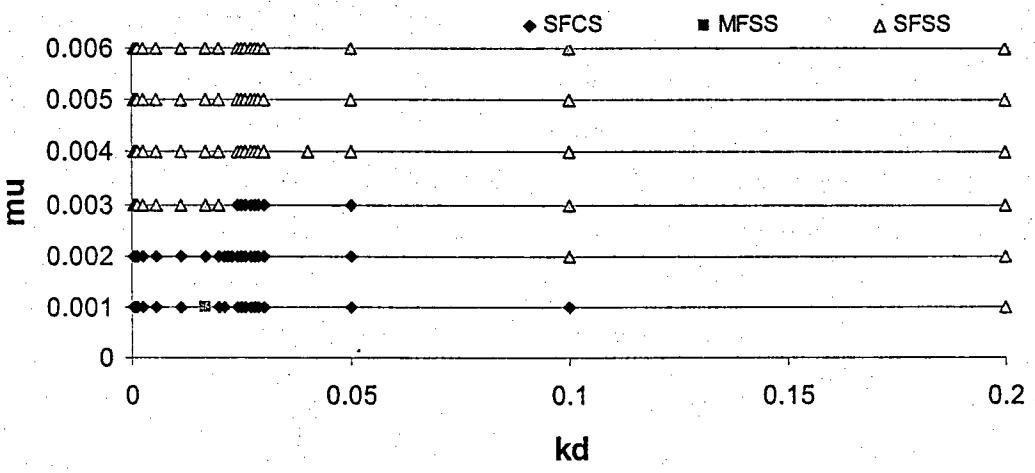

Fig. 3.13 Domain and the type of the stable solutions

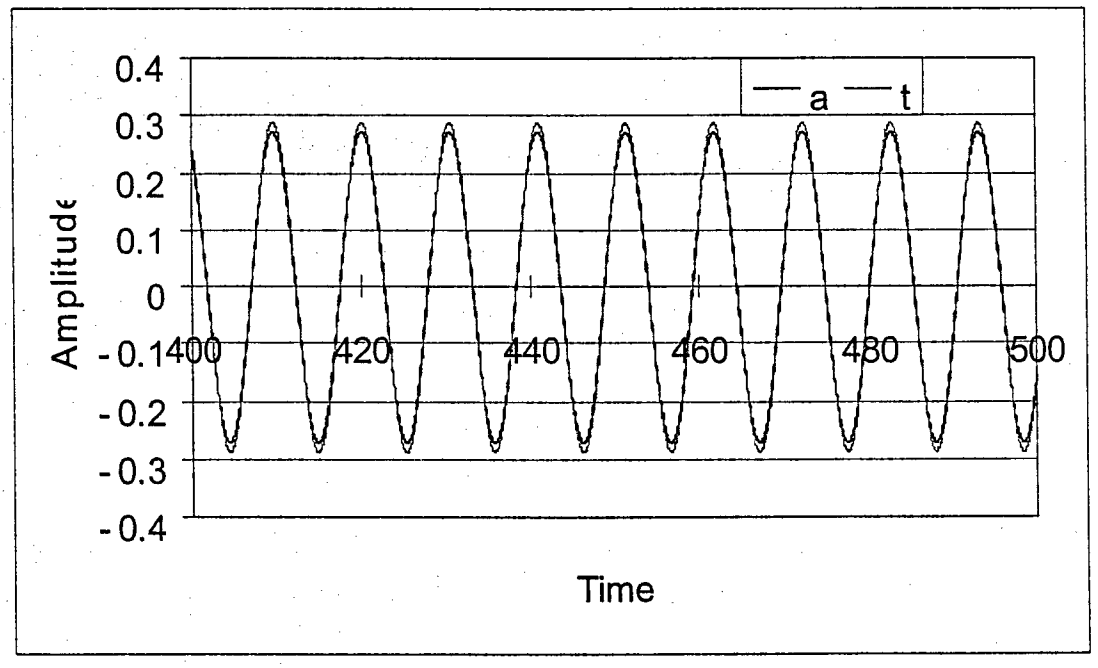

a)

Time histories of the pitching (a) and torsional (t) response

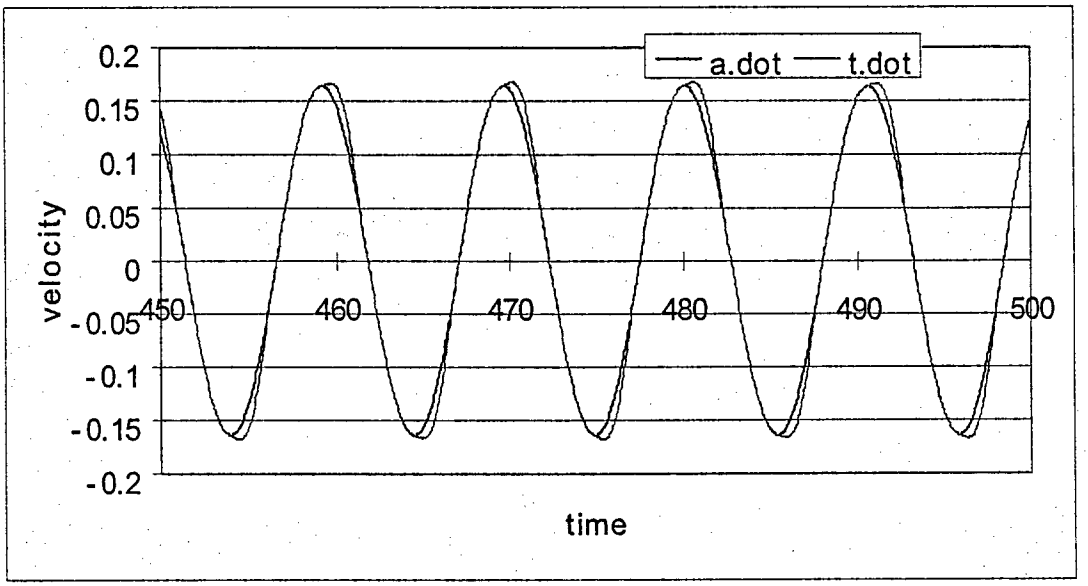

b)

Time histories of pitching (a.dot) and torsional (t.dot) velocities

Fig. 3.14: SFSS case, μ=0.004, k_d=0.3 Nm/rad

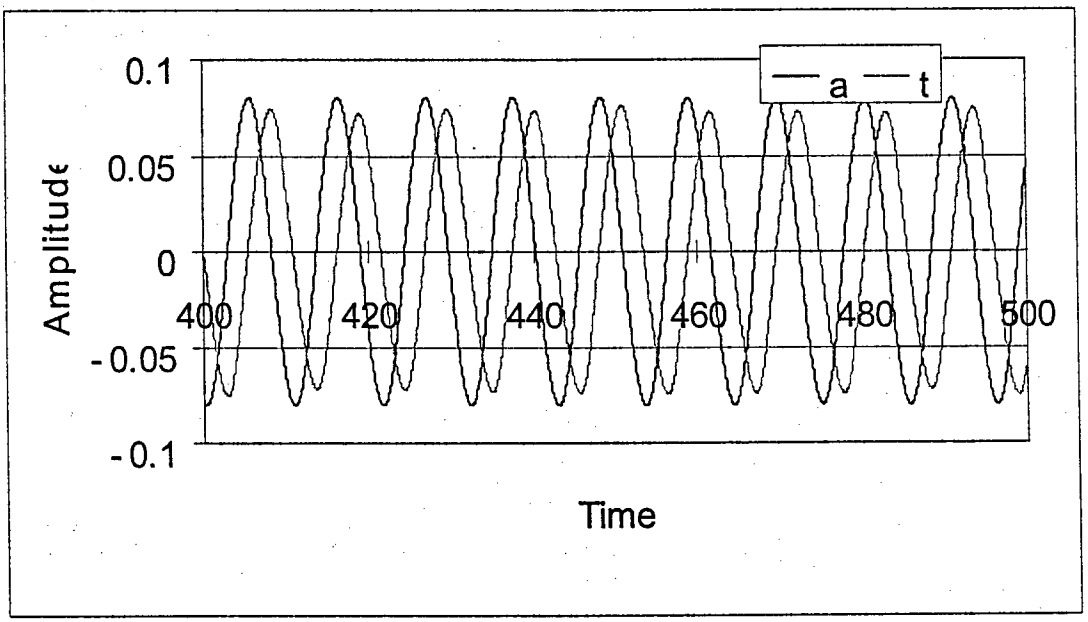

a)

Time histories of the pitching(a) and torsional (t) response

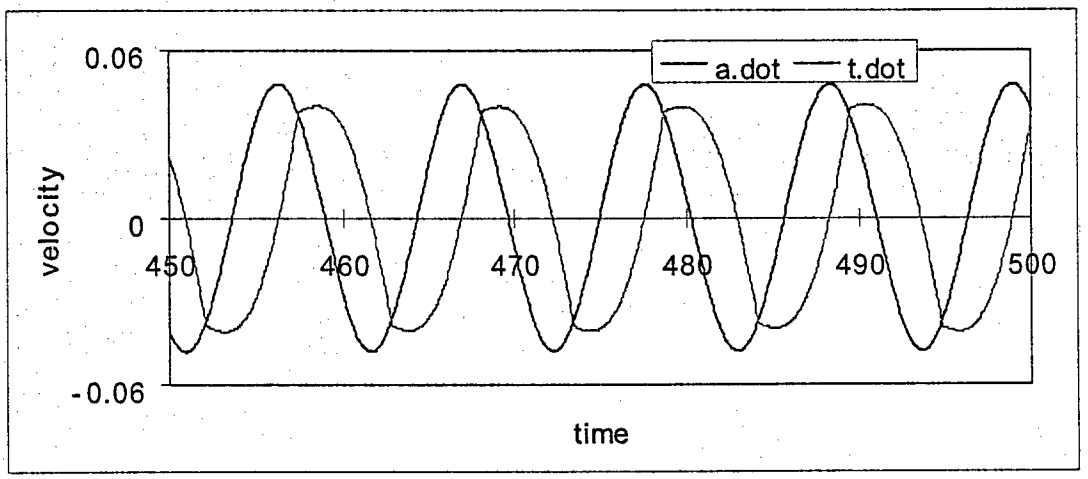

b)

Time histories of pitching (a.dot) and torsional (t.dot) velocities

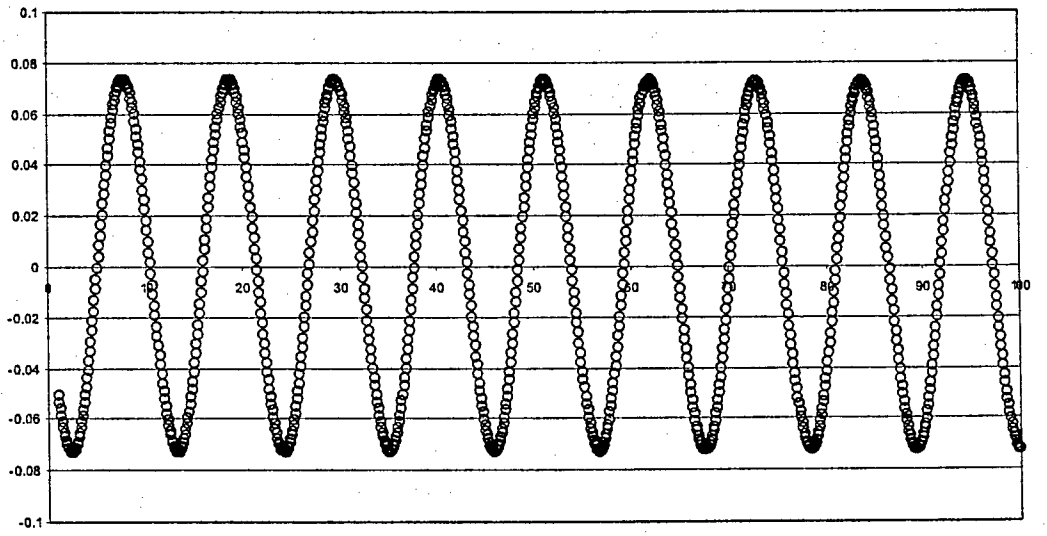

c) Position of wake vortices at nondimensionlized time t=500

Fig. 3.15: SFCS case, μ=0.001, k_d=0.01125 Nm/rad

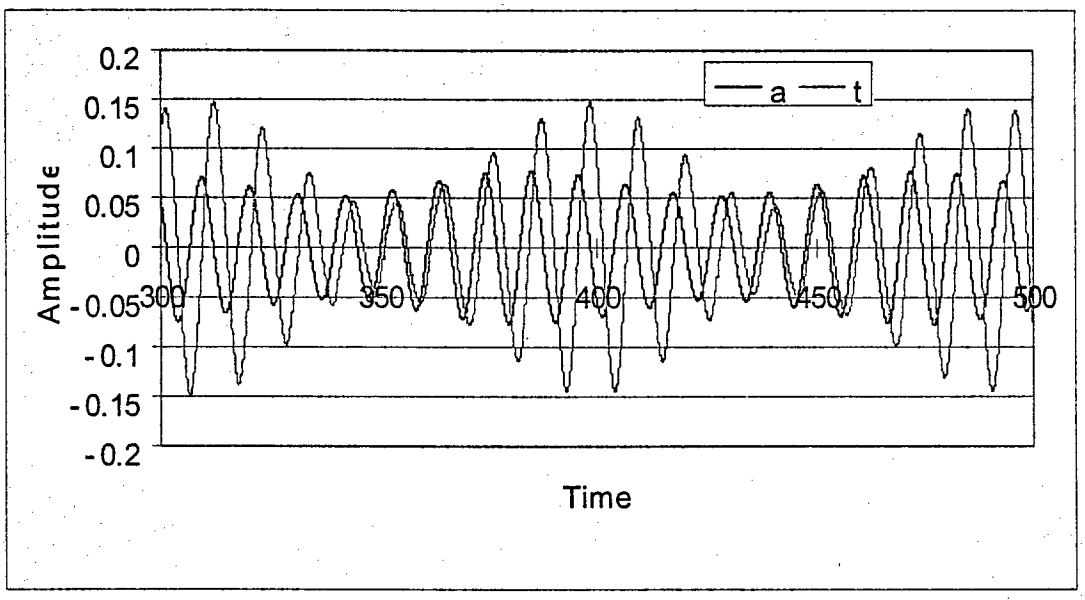

a)

Time histories of the pitching (a) and torsional (t) response

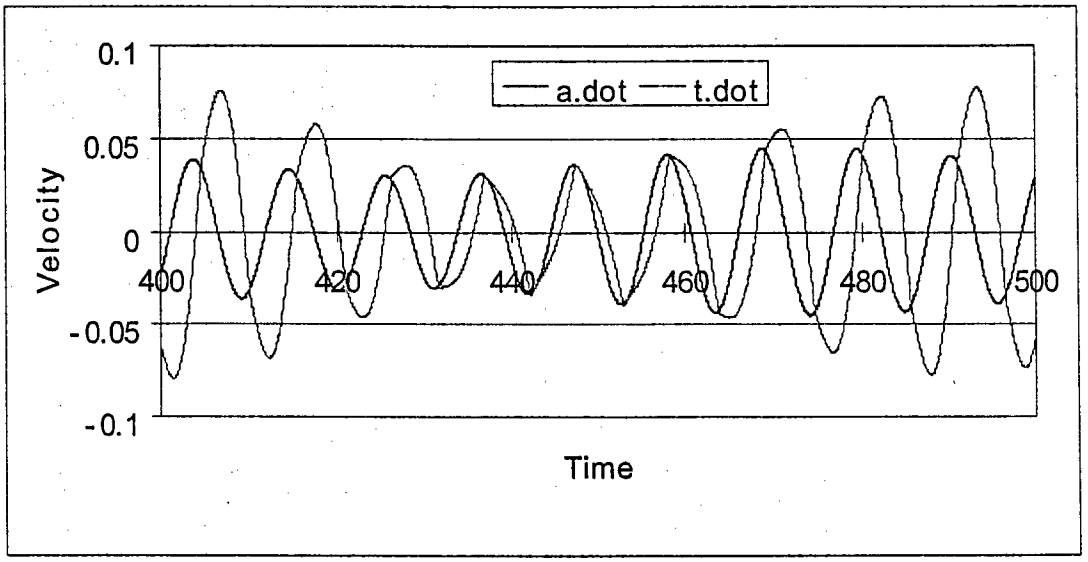

b)

Time histories of pitching (a.dot) and torsional (t.dot) velocities

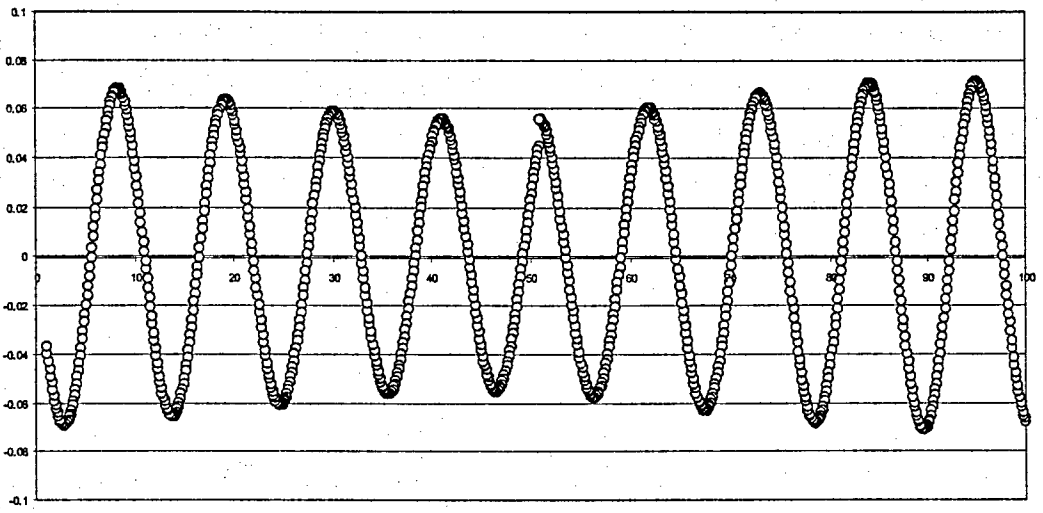

c)

Position of wake vortices at nondimensionlized time t=500

Fig. 3.16: MFSS case, μ=0.001, k_d=0.0168 Nm/rad

CHAPTER 4

CONCLUSIONS

The focus of this thesis has been on the assessment of the effects of internal friction on the response of aeroelastic systems exhibiting either explosive flutter or limit cycle oscillations.

In the first part of this thesis, a flat-plate airfoil model is considered which supports a torsional friction device composed of a disk flexibly connected to the plate by a torsional spring and squeezed between two rough surfaces. The behavior of this system is studied when placed in a uniform, inviscid and incompressible flow. A stability analysis of the system with the disk in either continuous sticking or frictionless slipping modes was carried out first to assess the expected stability domains. It was shown and justified that the system in slip mode exhibits instabilities at earlier flow velocities than its stuck counterpart. This property allows for the existence of both super- and subcritical limit cycle oscillations. While the subcritical limit cycles were observed to be unstable, a zone of stable supercritical limit cycle oscillations was found that extends about 3% past the flutter speed of the system without the friction device. This gain shows a good stabilization property since the moment of inertia of the selected friction device system is only 5% of the moment of inertia of the plate. The observed limit cycles exhibit either continuous slip or stick slip behaviors and are either single frequency (periodic) or multiple frequency (aperiodic or chaotic) with the latter ones appearing primarily at the

highest flow speeds and for the highest frequencies of the torsional friction device. The above results were obtained by time marching the plate equations of motions with a rational approximation of the Theodorsen function but a harmonic balance approach was also developed that led to very good approximations of the single frequency continuous slip limit cycle oscillations.

The second part of this thesis focused on the response of a NACA0012 airfoil placed in a uniform inviscid and incompressible air flow and supporting either the same frictional device as the flat plate or a block sliding in a rough internal track. This airfoil was shown in earlier studies to exhibit limit cycle oscillations at and slightly above its flutter speed without any frictional device. The study of this system with a frictional device provides thus a basis for the assessment of the potential effects of friction on aeroelastic systems exhibiting aero-driven limit cycles. The block moving in an internal track was first considered to model friction in the system. While limit cycle oscillations were observed, it was also shown that the block could become stuck at a position far from its original one and thus would create a change of inertia sufficiently large to stabilize the airfoil. This effect does not involve any dissipation due to friction and is thus not relevant to the present effort. Accordingly, this frictional model was not considered further and was replaced by its torsional counterpart (as in the flat plate analysis) which does not suffer from the same defect. The results of time marching computations demonstrate that friction can substantially decrease the level of the limit cycle oscillations, especially with a low coefficient of friction, but that increases in the response are also possible,

depending on the selection of the natural frequency of the torsional friction device. As in the flat plate, continuous slip and stick slip solutions were observed most of which were single frequency (periodic).

The results of this study demonstrate that friction can indeed provide a stabilization of an impending flutter and can significantly decrease the amplitude of existing limit cycle oscillations of aeroelastic systems with an appropriate selection of the friction device parameters most notably natural frequency and coefficient of friction.

REFERENCES

[1] Denegri, C.M., "Limit Cycle Oscillation Flight Test Results of a Fighter with External Stores," AIAA-2000-1394

[2] Chen, P.C., Sarhaddi, D. and Liu, D.D., "Limit Cycle Oscillations Studies of a Fighter with External Stores," AIAA-89-1727

[3] Edwards, J.W., Schuster, D.M., Spain, C.V., Keller, D.F., Moses, R.W., "MAVRIV Flutter Model Transonic Limit Cycle Oscillation Test," AIAA-2001-1291

[4] Cunningham Jr., A.M. and Meijer. J.J., "Semi-Empirical Unsteady Aerodynamics for Modeling Aircraft Limit Cycle Oscillations and Other Nonlinear Aeroelastic Problems," International Forum on Aeroelasticity and Structural Dynamics, Manchester, U.K., Jun. 1995.

[5] Mignolet, M.P., Liu, D.D., Chen, P.C., "On the Nonlinear Structural Damping Mechanism of the Wing/Store Limit Cycle Oscillation," AIAA-99-1459

[6] Sinha, A., and Griffin, J.H., "Friction Damping of Flutter in Gas Turbine Engine Airfoils," *Journal of Aircraft*, Vol. 20, 1983, pp. 372-376.

[7] Sinha, A., and Griffin, J.H., "Effects of Friction Dampers on Aerodynamically Unstable Rotor Stages," *AIAA Journal*, Vol. 23, 1985, pp. 262-270.

[8] Agelastos, A.M., *Effects of Coulomb Friction on Flutter and Limit Cycle Oscillations According to a Structural Dynamic Model*, M.S. Thesis, Arizona State University, May 2005.

[9] Fung, Y.C., "An Introduction to the Theory of Aeroelasticity", Dover Publications, 2002.

[10] Jones, R.T., "The Unsteady Lift of a Wing of Finite Aspect Ratio," *NACA Rept.* 681, 1940.

[11] Den Hartog, J.P., "Forced Vibrations With Combined Coulomb and Viscous Friction," Trans. of the ASME, APM-53-9, 1931, pp. 107-115.

[12] Jadic, I., So, R.M.C., and Mignolet, M.P., "Analysis of Fluid-Structure Interactions Using a Time Marching Technique," Journal of Fluids and Structures, Vol.12, No.6, pp. 631-654, 1998.

[13] Yao, Z.X., and Liu, D.D., "Vortex Dynamics of Blade-Blade Interactions," *AIAA Journal*, Vol. 36, No.4 pp 497-504, April, 1998

[14] Yao, Z.X., Garcia-Fogeda, P., Liu, D.D. and Shen, G., "Vortex/Wake Flow Studies for Airfoils in Unsteady Motions," AIAA Paper 89-2225, 1989.

[15] Yao, Z.X., Jadic I., So R.M.C., Liu, D.D., and Tang W., 1995, "Flow-Induced Vibrations On A Turbine Blade In a Blade Row Using A Vortex Dynamics Model," *presented at the international forum on Aeroelasticity and Structural Dynamics*, June 26-27, Manchester, United Kingdom.

[16] Kim, M.J., and Mook, D.T., "Application of Continuous Vorticity Panels to General Unsteady Incompressible Two-Dimensional Lifting Flows," *Journal of Aircraft*, Vol. 23, pp.464-471, 1986